A Hydrodynamic Analysis of Deep-Water Moorings

by

Zi Lin

A thesis presented in fulfilment of the requirements for the degree of Doctor of Philosophy
2015

Department of Naval Architecture, Ocean and Marine Engineering

University of Strathclyde, Glasgow

Declaration

This thesis is the result of the author's original research. It has been composed by the author and has not been previously submitted for examination which has led to the award of a degree.

Zi Lin

Signature: Date:

ACKNOWLEDGEMENTS

First, I would like to thank my first supervisor Dr Philip Sayer for his excellent supervision and continuous instruction throughout this research. I am full of respect for his expertise and patience, from the supervision and discussion on the project to the proof reading of the thesis.

I also would like to thank my second supervisor Prof. Atilla Incecik for his encouragement and valuable advice on my project. Without his advice, I could not finish my PhD.

I also want to thank the financial support from the department of Naval Architecture, Ocean and Marine Engineering (NAOME) and the Faculty of Engineering, University of Strathclyde, Glasgow and China Scholarship Council (CSC).

I acknowledge with the assistance from Dr Jason Jonkman from NREL on FAST and the assistance from Orcina on OrcaFlex.

I appreciate my master degree's supervisor Prof. Bin Teng, from whom I have benefited the basic knowledge of wave-structure interaction problems.

I am grateful to Mrs Thelma Will, the graduate secretary and Mr David Percival, the senior technical programmer from the department of NAOME for their assistance during my PhD. Many thanks are due to Dr Zhengqiang Xu and other colleagues in the department of NAOME for their assistance during my PhD.

Finally, I would like to express my gratitude for my parents, for their support.

Contents

LIST OF FIGURES

LIST OF TABLES

NOMENCLATURE

General symbols

A	Projected area
A_e	Aranha scaling factor
A_{ij}	Added mass matrix
B	Additional viscous damping
B_{ij}	Radiation damping matrix
C	Drag coefficients (for current force)
C_A	Added mass coefficients
C_D	Drag coefficients
C_M	Inertia coefficients
DoF	Degrees of Freedom
$F_{current}$	Current force
F_{drift}	Wave drift exciting force
F_e	External force
F_{ext}	Wave exciting force
$F_{mooring}$	Mooring force
F_v	Viscous damping force
F_{wd}	Wave drift damping
f	Frequency
f_m	Peak frequency
g	Gravitational constant
H_S	Significant wave height
K_{ij}	Hydrostatic restoring matrix
T_E	Effective tension
M	Mass matrix, including floating body added mass
M_a	Infinite frequency added mass
R	Retardation function
T_P	Peak period
V	Current velocity
X	Floating body motion response
X_{LF}	Floating body low frequency motion response

β_e	Encounter heading
τ_e	Encounter period
ε	Elongation of mooring line
ζ	Wave elevation
ρ	Water density/rod mass per unit length
r'	Unit tangent vector to the space curve
$r' \times r''$	Bi-normal vector
r	Position vector
r''	Principal normal vector
$\vec{u}$	Floating body velocity
ω	Circular frequency

Abbreviations

API	American Petroleum Institute
BEM	Boundary Element Method
BV	Bureau Veritas
BVP	Boundary Value Problem
CFD	Computation Fluid Dynamics
DDF	Deep Draught Floater
DNV	Det Norske Veritas
EWEA	European Wind Energy Association
FAST	Fatigue, Aerodynamics, Structures, and Turbulence
FEM	Finite Element Method
FOWT	Floating Offshore Wind Turbine
FPSO	Floating, Production, Storage and Offloading
JIP	Joint Industry Project
JONSWAP	Joint North Sea Wave Observation Project
LF	Low Frequency
LR	Lloyd's Register
NREL	National Renewable Energy Laboratory
Op	Operating
QTFs	Quadratic Transfer Functions
OTRC	Offshore Technology Research Centre
RAOs	Response Amplitude Operators
SBFEM	Scaled Boundary Finite Element Method
Sd	Shutdown
SPH	Smooth Particle Hydrodynamics
TLP	Tension Leg Platform
WF	Wave Frequency

ABSTRACT

The move by the offshore oil & gas industry to deep water has an impact on the selection of mooring system configuration and design method. Methods of analysis need to be re-evaluated as water depth increases. The primary purpose of this thesis is to study the hydrodynamics of deep water moorings and the nonlinear dynamic response of the mooring line, which is representative of a Spar platform and a floating offshore wind turbine (FOWT). Emphasis is placed on the coupling effects between the floating body and mooring line and the nonlinear dynamic response of elastic mooring line.

For a Spar platform, this thesis studied the behaviour of a 4-point mooring system in water depths from 300m to 3000m, using an indirect time-domain method. A panel method was applied for the hydrodynamics of the floating structures and a lumped mass and spring method for the dynamic response of the mooring lines. Coupled analysis results for intermediate water depth were compared with experimental data to check the validity of the numerical modelling. The results from coupled low frequency (LF) and fully coupled analysis are compared and discussed. Results from parametric studies are compared to offer guidance to mooring system designers on the suitability of particular approaches.

For a floating wind turbine, three water depths-300m 600m and 900m were simulated in the time domain under both operational and shutdown conditions. A fully-coupled analysis was carried out to study the motion response of the FOWT under wave only and wave-plus wind condition. The aerodynamic modelling was based on the blade element momentum theory, while the mooring system global performance was simulated by the indirect time-domain method. By performing a comprehensive parametric study, the effects of the second-order wave drift force and the aerodynamic turbine thrust force on the motion response of the FOWT are studied and discussed.

The performance of a polyester mooring line is non-linear and its elongation plays a significant role in the dynamic response of an offshore moored structure. Unlike chain, the tension-elongation relationship and the behaviour of elastic polyester ropes are

complex. In this thesis, by applying a new stiffness model of the mooring line, the traditional elastic rod theory is extended to allow for large elongations, which are appropriate for simulating the static and dynamic response of both polyester lines and traditional chains. Galerkin's method was applied to discretise the equation of motion for the rod. One beneficial feature of the present method is that the stiffness matrix is symmetric; in non-linear formulations the element stiffness matrix is often non-symmetric. The static problem was solved by Newton-Raphson iteration whereas a direct integration method was used for the dynamic problem. The mooring line tension based on the enhanced model was validated against the proprietary software OrcaFlex. Results of mooring line top tension predicted by different elongation conditions were compared and discussed. The present method was then used in a time-domain simulation of a Spar-type platform, typical of those used for offshore wind turbines, moored by three taut lines in waves and currents. From a comparison between linear and non-linear formulations, it is seen that a linear spring model under-estimates the mean position when the turbine is operating, but over-estimates the amplitude of the platform response at low frequencies when the turbine has shut down.

KEY WORDS: fully coupled analysis, coupled LF analysis, motion response, mooring line dynamic response, mooring system, **finite element analysis, elastic rod theory, polyester mooring line, water depth variation**

1. Introduction

1.1. Background

1.1.1. Oil and gas exploration moving to deeper water

The offshore industry has seen an increasing number of moored structures in recent years, reaching ever-deeper water. Initially, fixed platforms were used for oil & gas exploitation while floating platforms become increasingly popular in deep water. The first offshore platform was installed in 1947 with a water depth of 6.4m (21ft) while today the water depth of platforms being installed is over 2438m (8000ft, Barton, 2014). Figure 1.1 shows the evolution of maximum water depth for offshore drilling and production industry from 1940s. As for 2014, world's record deepest drilling has reached as deep as 3174m. The currently deepest platform in 2014 is 2500m. In the 1980s it was less than 300m. Figure 1.2 presents the ranges of water depth for each type of platforms, including currently used, qualified and conceptual designed. From the figure we can see that for deep and ultra-deep water depth, the overall trends of offshore units are floating ones.

Floating platforms mainly rely on mooring system to resist environmental loading. The effects of deep-water oil & gas exploration have an impact on the selection of mooring system configuration and design method. With the increasing of water depth, the coupling effects between floating body and mooring lines are varied, leading to different assumptions and run time between deep-water and shallow-water mooring system analysis. Analysis methods suitable for shallow water depth need to be re-evaluated as the water depth increases.

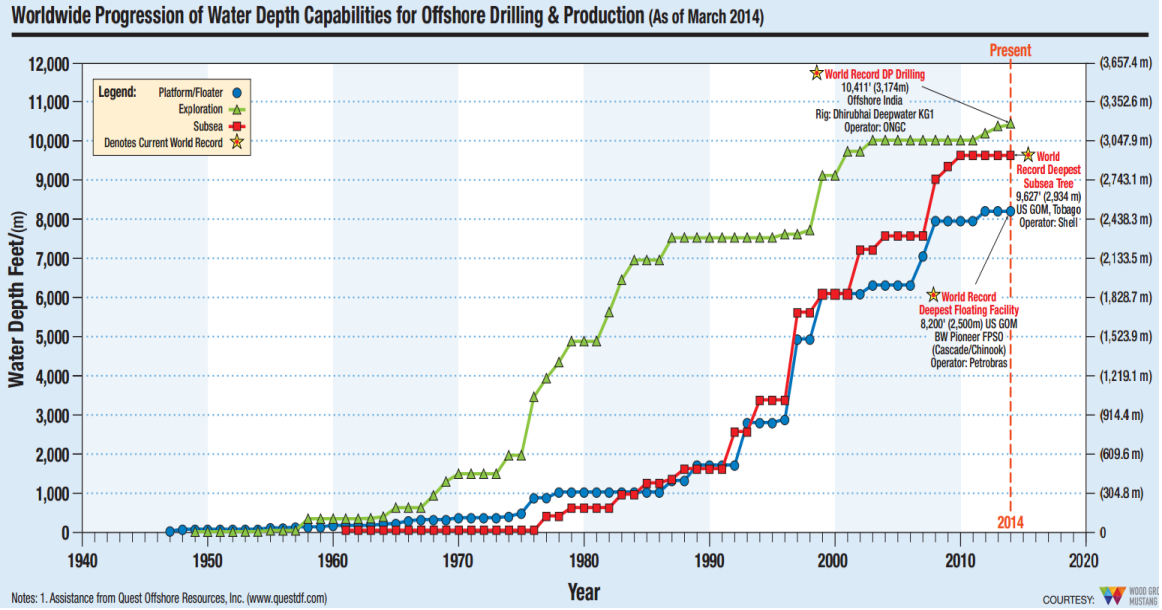

Figure 1.1 Worldwide Progression of Water Depth Capabilities for offshore Drilling & Production (Source: Offshore Magazine)

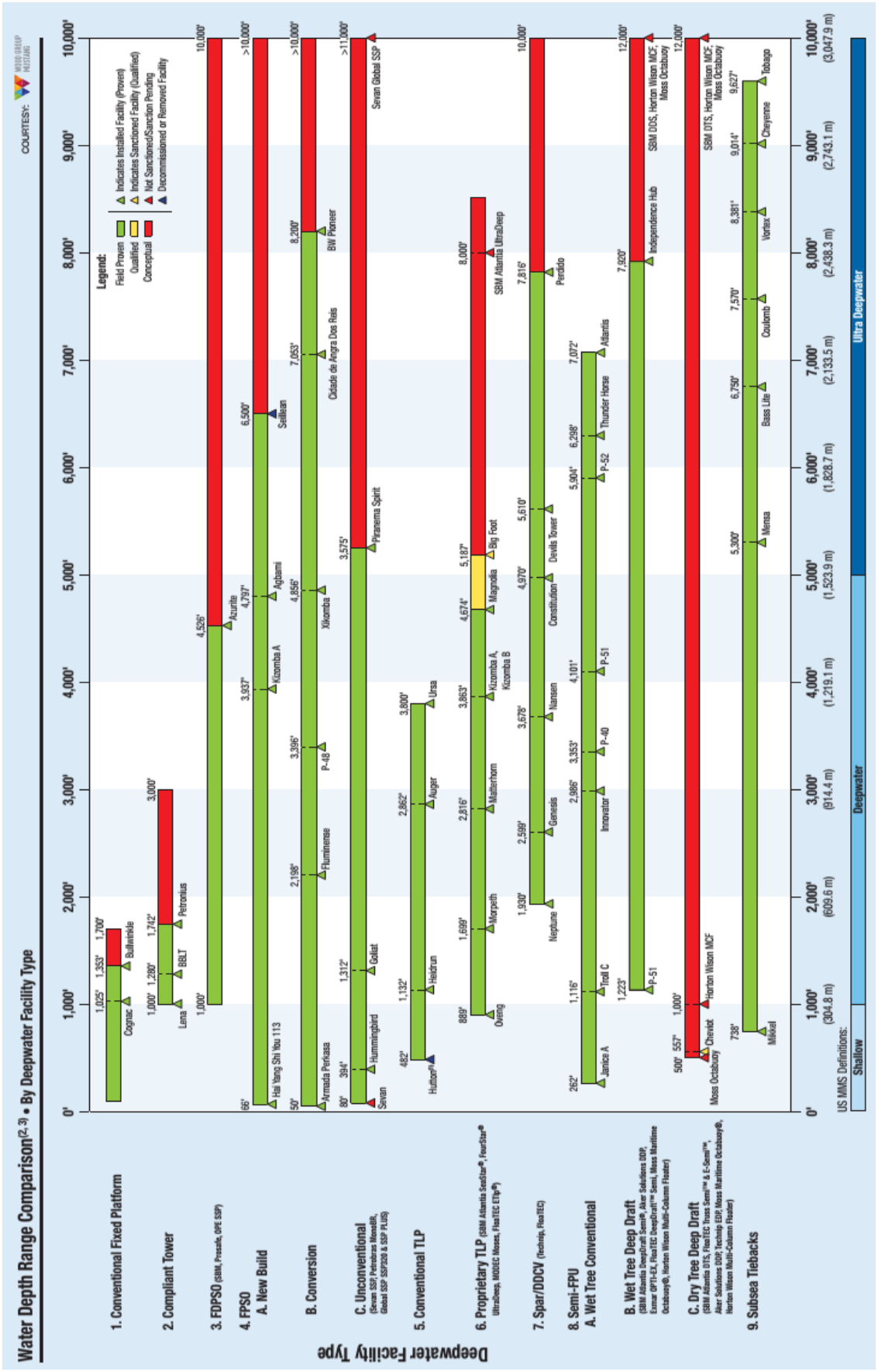

Figure 1.2 Water depth range comparison, by deepwater facility type(source: Offshore Magazine)

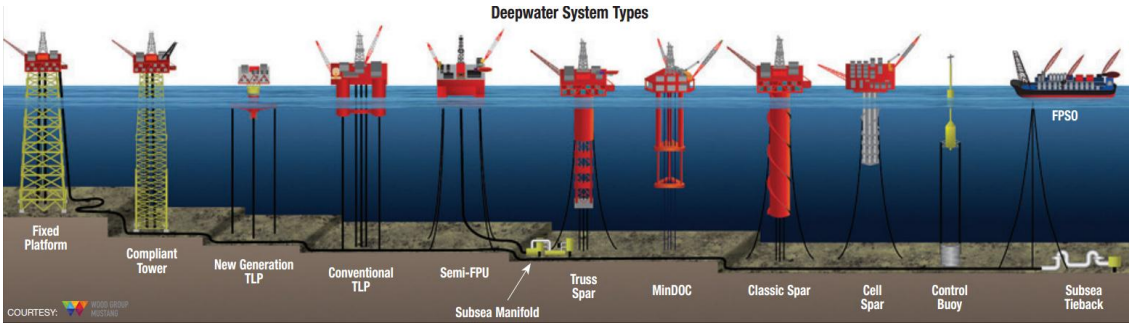

Figure 1.3 Different types of deep water platforms (source: Offshore Magazine)

TLPs, Spars, Semisubmersibles and FPSOs are four popular types of offshore floating platforms. Each types of floating platform can be further divided into some sub-types. For example, there are Classic Spar (a bare cylinder), Truss Spar (with heaving plates) and Cell Spar (multiple columns), etc. Table 1.1 illustrates the natural periods for four typical types of offshore floating bodies. The natural periods in surge, sway and yaw are because of the restoring effects from the mooring system. TLP has a very small pitch/roll motion but its vertical mooring line requires suction anchor, which is very expensive. Spar platform is very suitable for deep-water circumstance but may not be suitable for water depth between 30m and 60m, due to its large draft (Mercier, OTRC). Semisubmersible has a relative low installation costs but requires special optimization of the column diameter (Mercier, OTRC), otherwise the slowly varying and mean drift motion would be very large. FPSOs have the ability of providing field storage, eliminating the use of long pipelines (McCaul, 2006). But FPSOs have a large water plane area, especially for the ship-shaped ones, which may experience very large slowly varying and mean drift motion. These second-order effects have negative effects on the designing of mooring system.

Table 1.1 Typical natural periods of deep water floaters (DNV-RP-F205)

	Natural periods (seconds)			
Floater Mode	FPSO	DDF	TLP	Semi
Surge	> 100	> 100	> 100	> 100
Sway	> 100	> 100	> 100	> 100
Heave	5 – 12	20 – 35	< 5	20 – 50
Roll	5 – 30	50 – 90	< 5	30 – 60
Pitch	5 – 12	50 – 90	< 5	30 – 60
Yaw	> 100	> 100	> 100	> 100

Based on different structures and water depth, the mooring systems can be classified by several different ways. Figure 1.4 shows a schematic of single point and spread mooring. Spars and Semisubmersibles use spread moorings to resist environmental loading from all directions. FPSOs could use spread mooring in relative mild weather while for severe weather conditions turret moorings are used because of its weathervane ability.

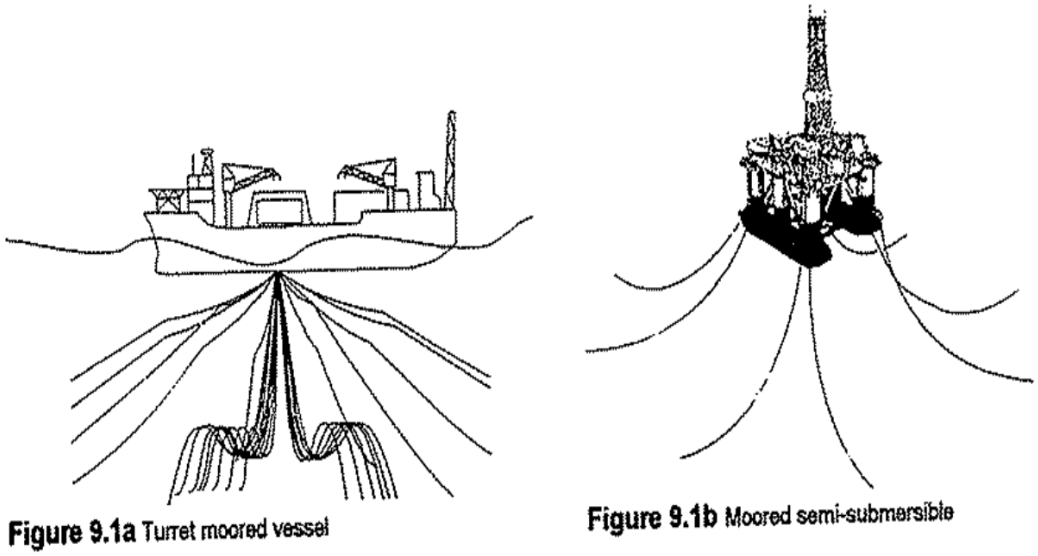

Figure 1.4 Single point and spread mooring (Barltrop,1998)

In relative shallower water depth, catenary chains are widely used for the station-keeping. The horizontal restoring force provided by the changing of chain weight is the main force to counter the drift off-station. But with increasing water depth the

chain becomes very long and heavy and so is neither practical nor economic. In contrast, taut mooring lines, which are light and have large strength to weight ratio, are appropriate for deep water. In the industry, a multi-compound mooring line is often used. Figure 1.5 shows an example of a multi-compound mooring line consist of chain and polyester rope. Figure 1.6 shows a sketch of slack and taut mooring systems and their key attributes. Compared with slack mooring system, taut mooring system has the advantage of lighter weight, shorter mooring line length and a smaller mooring radius, which are more suitable for deep water mooring, compared with slack mooring. But taut mooring system usually requires an expensive suction anchor to resist the mooring line vertical tension at the anchor point, while for slack mooring lines there is almost no vertical force at the anchor point.

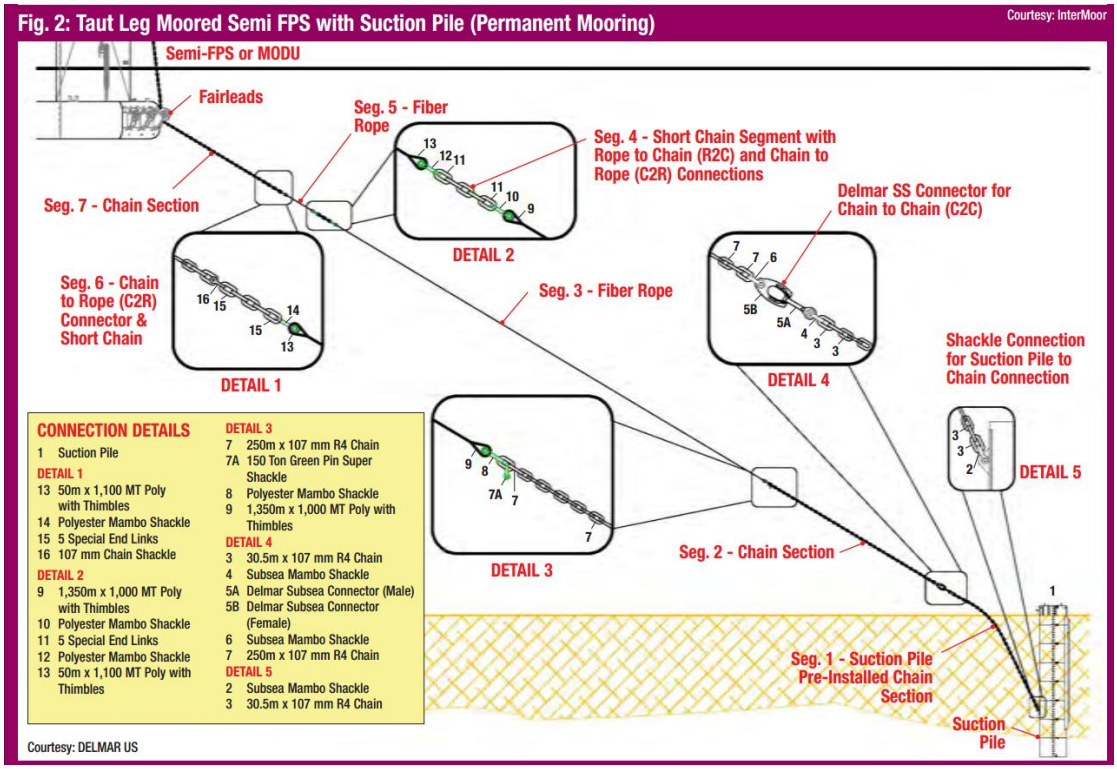

Figure 1.5 Properties of a multi-compound mooring line (Source: Offshore Magazine)

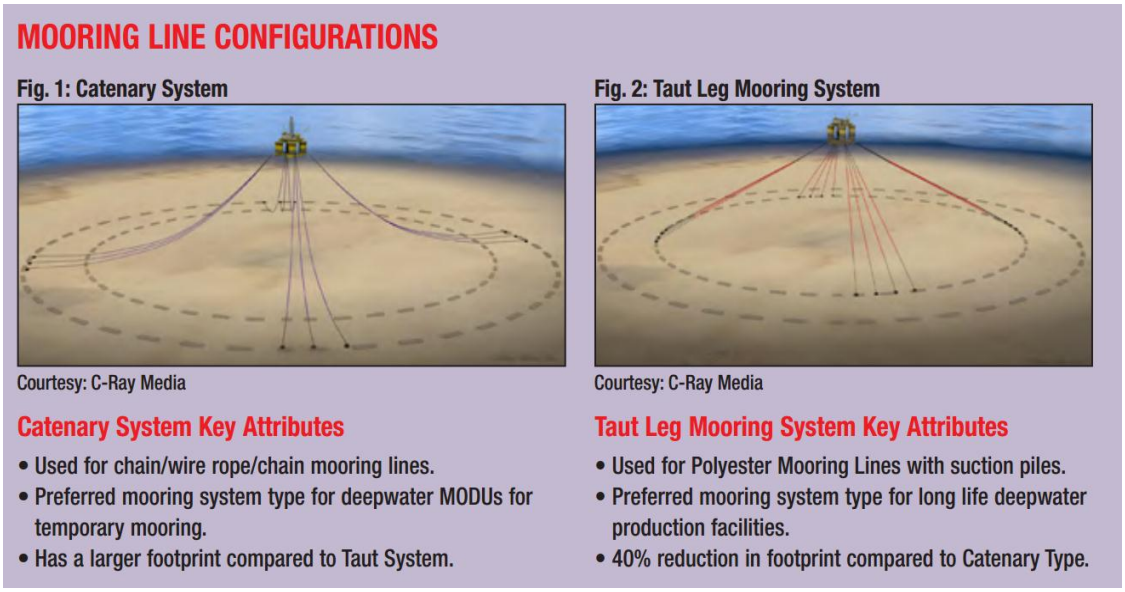

Figure 1.6 Mooring line configurations (source: Offshore Magazine)

A group of mooring lines, consisting of 3-4 lines at each anchor point, is often used, as illustrated in Figure 1.7. This can increase the performance of the station-keeping ability of the system as an increased number of mooring lines decrease the average mooring line tension per line, as well as allowing some redundancy in case of line breakage or anchor pull-out.

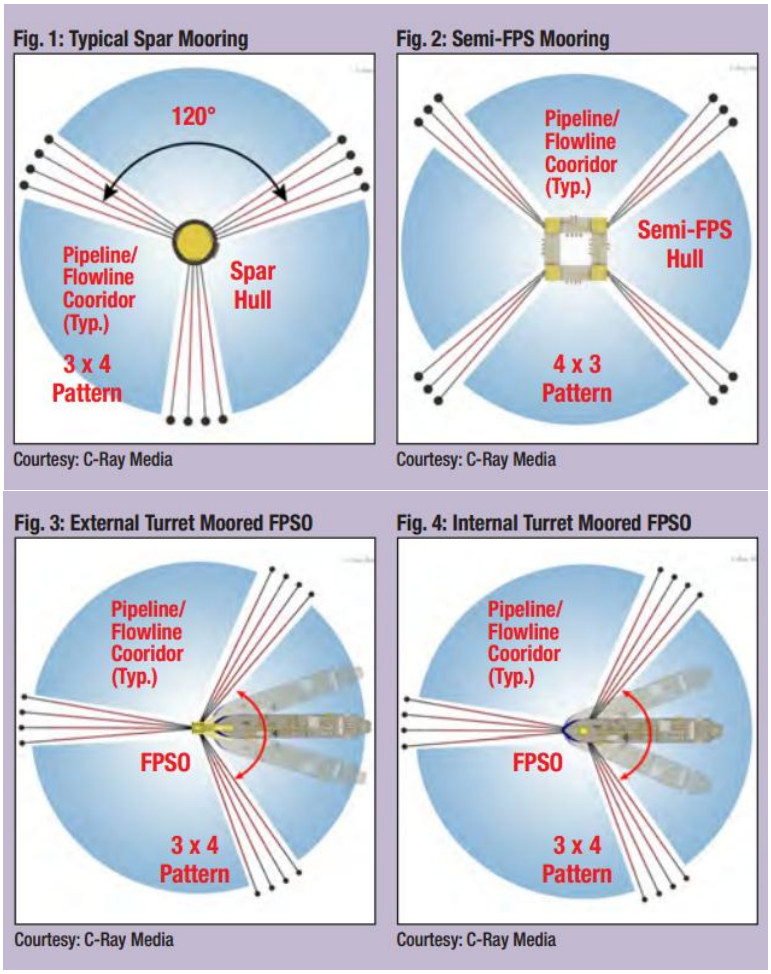

Figure 1.7 Offshore mooring patterns (source: Offshore Magazine)

1.1.2. Development of offshore wind energy

The capture of offshore wind energy plays a key role across the maritime industry (EWEA, 2013). Offshore wind turbines are becoming larger and more powerful, and are being deployed in ever-deeper water depths. They can be mounted on a fixed or floating base, but the former starts to lose its economic advantage for water depths larger than 60m (Goupee et al, 2014). The advantages for offshore wind turbine include a long distance from the density populated area and much more potential, compared with land-based wind turbine. Although most of current installed wind turbines are fixed ones, as we can see from Figure1.8, the overall trend of the wind turbine industry is increasing the distance to shore and increasing water depth (Figure 1.9). The concept of FOWT was investigated intensively in recent years. Hywind, developed by Statoil, is the first offshore floating wind turbine installed in the world

(till 2012). It's a Spar-type FOWT with three catenary lines with a design water depth of 320m. The present study therefore has direct relevance to installation in ever deeper waters.

As with offshore platforms, floating wind turbines often use mooring lines to resist environmental loading. Although the mooring system design for a floating offshore wind turbine (FOWT) has benefited from the experience of offshore oil and gas platforms, there are still several unknowns for a specific type of floating bodies, e.g. size and environmental loading, etc. From a report of EWEA (2013), it is recommended that more research must be done on mooring and anchoring systems for wind turbines.

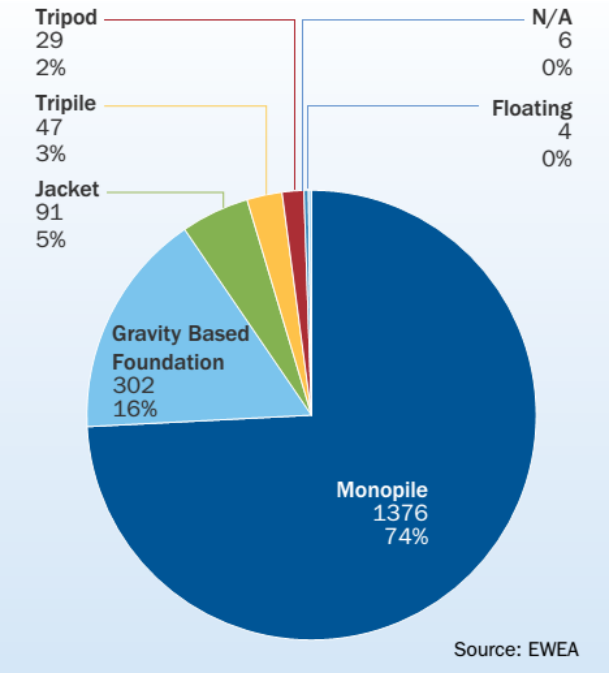

Figure 1.8 Share of substructure types for online wind farms, end 2012 (UNITS), EWEA (2013)

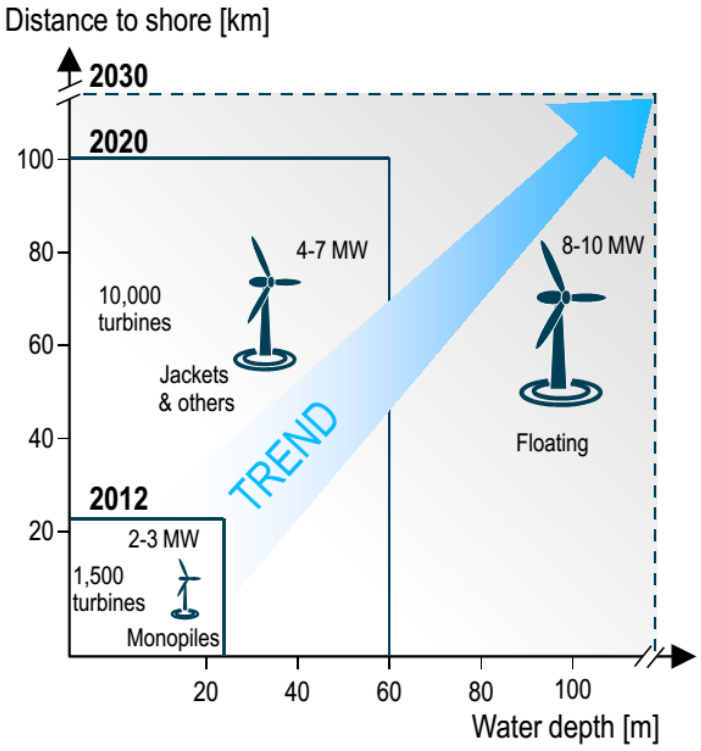

Figure 1.9 Development of wind turbine size and location (EWEA, 2013)

1.2. Existing problems

Water depth has long been considered as one of the most significant design factors in mooring system design. When changing water depth, the mooring line length, material and configuration, etc. are required to modify to satisfy design criteria. The inherent coupling effects between the floating body and mooring line also vary with the changing of water depth.

1.2.1. Re-evaluation of traditional methods of analysis for deep water moorings

Coupled analysis has long been considered for large water depth. It is general believed that in deep water the mooring line becomes very long and the total weight of chain is comparable with the upper floating body. So the heavy chain may have a larger effect on the motion response of the floating body. To this end, fully coupled analysis is necessary to get the accurate motion response and mooring line tension.

Ormberg and Larsen (1998) showed that under large water depth, the percentage of LF response becomes dominant and a non-coupled analysis failed to predict the motion response correctly. However fully coupled time-domain simulation often require a very long running time, which is not possible for the designing purpose. Nowadays, there are still a large number of floating platforms designed with the quasi-statically coupled method. Apart from the fully coupled methods, some simplified methods with certain approximations could also get satisfied results, but requires less running time. The accuracy of these simplified methods may vary according to different water depths. Due to today's overall trend of going deeper water, it is necessary to re-examine and quantify the methods of analysis considering water depth variation.

1.2.2. Examination of traditional methods of analysis for moored floating wind turbines

Similar to offshore oil platforms, offshore floating wind turbines often keep station by mooring lines. Owing to the successful experience from offshore oil & gas platforms,

the design and modelling of the FOWT has applied almost the same theory and process as offshore platforms, e.g. the hydrodynamic analysis of floating body, mooring design and the types of FOWTs (Spar, TLP and Semisubmersible, etc). The methods of analysis for the hydrodynamic aspects of a FOWT and its mooring system are almost the same as offshore platforms. However, the geometry and operational water depth are different from offshore oil & gas platforms, leading to different hydrodynamic performances. Figure 1.10 shows a schematic of a TLP-type FOWT and a TLP. Plus, the effect of the turbine thrust force may have an effect on the motion response of the floating body and mooring line tension and vice versa. These difference leads to the importance of examination of traditional mooring system methods of analysis for a FOWT.

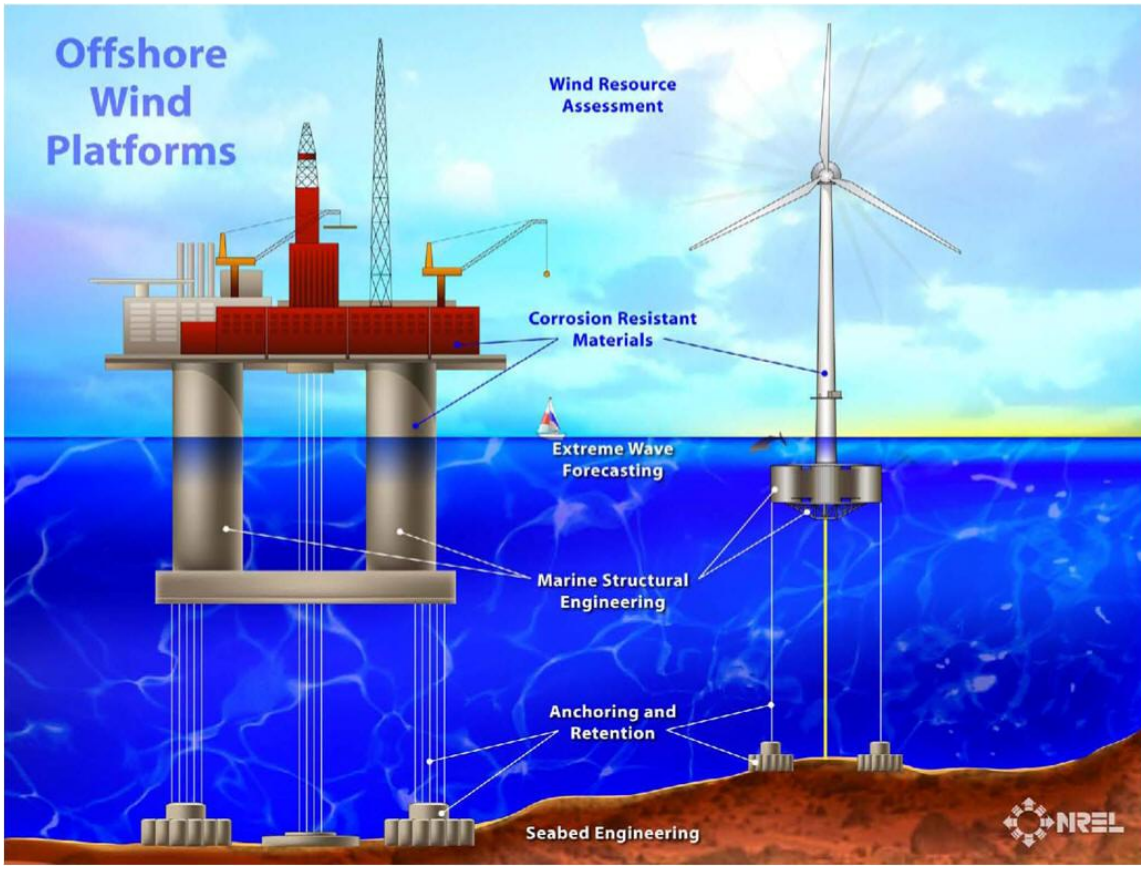

Figure 1.10 Schematic of an offshore platform and a FOWT (Source: NREL)

1.2.3. Rules and regulations: appropriateness for deep water mooring?

Water depth has long been considered as a key parameter in mooring system design. Sensitivity studies of mooring system have been undertaken by many researchers for a range of environmental conditions (Kim, et al, 2001; Guedes Soares, et al, 2001), mooring line hydrodynamic coefficients (Wichers and Devlin, 2001), mooring line configurations (Qiao, et al. 2012) and different methods of analysis (Ormberg and Larsen 1998; Astrup, et al, 2001; Kim, et al, 2001; Kim and Sclavounos, 2001;Tahar and Kim, 2003; Low and Langley, 2006). These particular studies have tended to focus on just one water depth, even though water depth is considered a significant parameter in mooring system design. Chen, et al (2001) used a hybrid wave model and Morison's equation for a JIP Spar moored by four slack chains in three water depths (318m, 618m and 1018m). The results from the case study show that for slack mooring system with catenary chain, the dynamic response becomes increasingly important under larger water depth, as the chain for larger water depth becomes very long. Comparison between coupled and uncoupled analysis has been widely studied, but only a few attempts to quantify the water depths effect on the coupled LF analysis, a hybrid time and frequency domain analysis. Luo and Baudic (2003) compared coupled and coupled LF methods for a turret-moored FPSO in 900m, 1800m and 3000m, respectively. Sensitivity studies against water depth found that polyester mooring was attractive for deep-water moorings because of the large strength to weight ratio. But in Luo and Baudic's method, the LF response was solved using a 3-DoF formulation. The results predicted by coupled LF method need to allow the simulation of 6-DoF and other types of floating structures.

A major concern in today's mooring system design is to improve the accuracy of the methods of analysis but requiring fewer running time. There are existing design codes for a mooring system design from the classification societies, e.g. API, BV, DNV and LR. However, less guidance focuses on the effects of water depth variation. One existing one is from DNV-OS-E301, a dynamic analysis has to be carried out for water depth larger than 100m. However, considering the water depth range for

currently installed offshore platforms (up to ~3000m), this number is incomplete and needs to be further studied and quantified.

2. Project outline

2.1.Objectives

Based on the background and motivation of current research, the main objectives are as follows:

1) To review methods of analysis for modelling the hydrodynamic response of a moored floating body.
2) To analyse, propose and compare procedures for analysing a deep water mooring system.
3) To develop a method for modelling the nonlinear response of an elastic mooring line.

2.2. Scope of the project

- **Single floating body**

For different types of structures, the number of floating body may include just one body or multiple bodies. However, in order to limit the number of parameters, only single body circumstance will be studied in current project.

- **Deep-water**

The term *deepwater* has different interpretations within the offshore industry. In the early years of oil & gas development, 100m water depth was considered as very deep water, while nowadays the industry has reached approximates 3000m. So, in this study, considering the operating water depth for different floating bodies, the term *deepwater* refers to a water depth larger than 300m, the same as the definition in Figure 1.2.

- **Mooring line only**

Mooring system is just one effective way of station-keeping methods for offshore floating structures. In some larger water depths, a combination of mooring system and dynamic positioning system is widely used for the purpose of safety and efficiency. It is well known that there are a very large number of parameters affecting the designing of a mooring system, for example, risers also contribute a lot on providing damping of the whole system. So, in order to limit the number of parameters, the mooring line only circumstance is considered.

2.3. Thesis layout

Chapter 1 gives a brief introduction and background of the project, explaining the reason and motivation for current research.

Based on the background and motivation described in chapter 1, the objective and scopes of this project are shown in chapter 2.

Chapter 3 reviews the widely used mathematical and numerical modelling for mooring line response, floating body hydrodynamic analysis and a combination of mooring line and floating body (mooring system) response method, respectively. Advantages and disadvantages of each method are discussed briefly.

A classic Spar and a Spar-type offshore floating wind turbine are analysed in chapter 4 and chapter 5, respectively.

Based on the traditional elastic rod theory, chapter 6 introduces a new stiffness model, simulating the static and dynamic response of polyester mooring line. Chapter 6 also gives examples of the application of the elastic mooring line model, including mooring line broken condition and a comparison between the developed method and linear spring method for a taut moored Spar-type FOWT under both wave only and wave plus wind condition.

Discussion and conclusions are shown in chapter 7 and chapter 8, respectively.

3. Literature review

3.1. Mooring line static and dynamic analysis

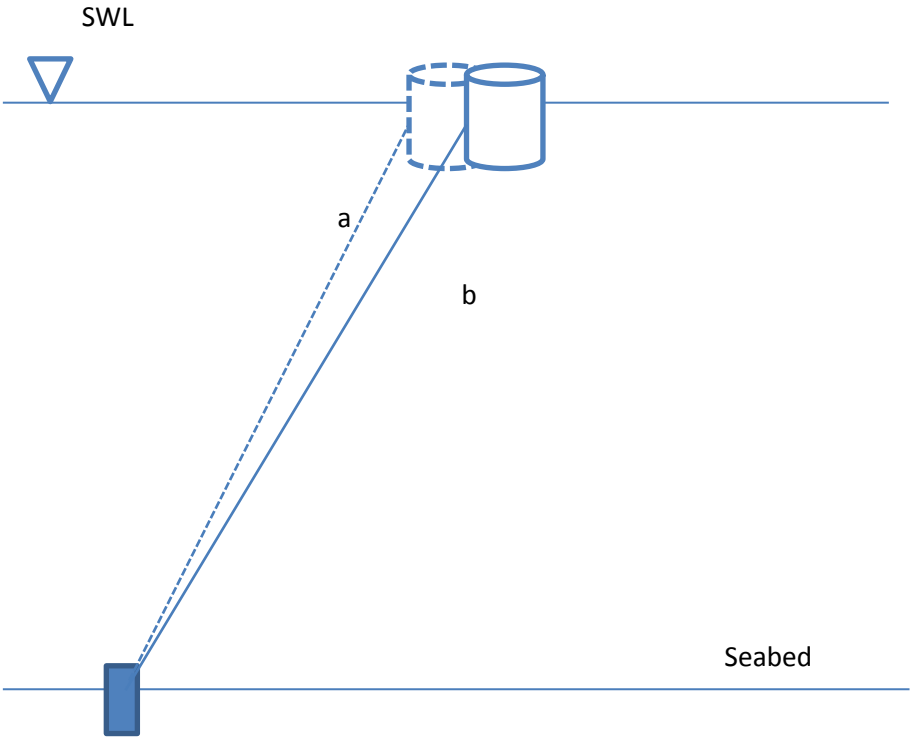

Figure 3.1(a) Taut mooring line

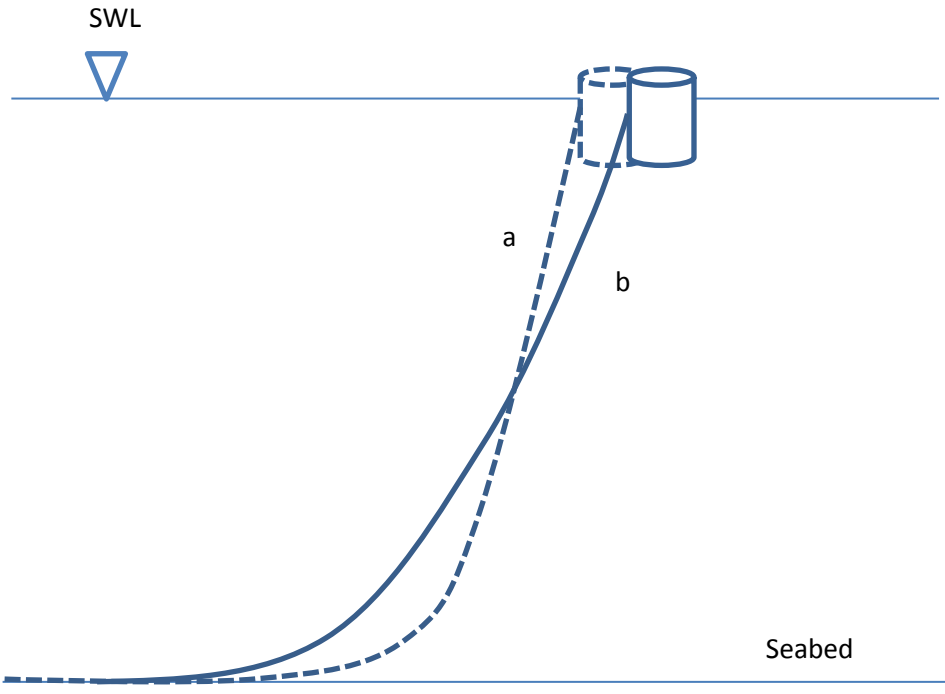

Figure 3.1(b) Slack mooring line

The motion response of mooring lines is sometimes highly nonlinear and depends on water depth. Taut mooring lines rely on the changes of elongation to provide restoring force while chains rely on the changing of weight. For a taut mooring line, as we can see from Figure 3.1(a), the mooring line geometry (*line a* and *line b*) before and after the horizontal offset does not vary significantly, even in deep water. But how to model the line's elongation from *line a* to *line b* is very important. However, for a slack mooring line, as we can see in Figure 3.1(b), the geometry of *line a* and *line b* varies a lot compared with the taut mooring line, but the elongation can be ignored.

The modelling of a single line is of great complexity, especially for polyester mooring lines. Numerical simulation of the dynamic response of mooring line has been studied during the past few decades, be it extensible or non-extensible. However, for polyester mooring lines, the nonlinear material behaviour and dynamic response are still not well studied, which are real challenges faced by the researchers in developing the methods of analysis for mooring line. Based on different assumptions, focusing on various modelling aspects, some widely applied mooring line models, including advantages and disadvantages are described as follows:

- **A massless spring**

This is the most straight forward method of mooring line modelling and is widely used in the traditional design of offshore structures. The spring can be linear or nonlinear, time-dependent or time-independent. This method ignores the dynamic behaviour of mooring line. Plus, the friction between seabed and mooring line is also difficult to model by this massless spring method. Current and wave loading on the mooring lines also cannot be included in this modelling. The general approach of this method is to generate the spring stiffness, either from the catenary equation (e.g. Kurian et al, 2010, Agarwal and Jain, 2003) or the static restoring force curve. Kim et al (2001a) and Kim et al (2001b) compared massless spring and fully coupled dynamic method for a TLP and a Spar, respectively. From the comparison they showed the damping from mooring lines and risers, which was not included in the massless spring model, was a main contribution for the difference. Kim et al (2013)

compared linear spring and nonlinear FEM in dynamic analysis of two structures: a semisubmersible and a turret-moored ship. Results and comparisons from the above two examples showed that the difference between massless spring method and nonlinear FEM method was not large when the effect from mooring line was small. In other words, the weight of mooring line was negligible compared with the weight of floating body. But when the weight of mooring line became larger, the linear massless spring method, ignored the coupling stiffness effect of surge-pitch or sway-roll in the mooring system, failed to generate the same results as FEM analysis.

- **Catenary equation**

In the initial preliminary design stage, static analysis of mooring line is widely applied for its fast calculation feature. One of the widely used analysis approach is the catenary equation, which offers a simple analytical solution but based on many assumptions, e.g. ignoring the effect of current and the mooring line moves quasi-statically. In other words, the dynamic response of mooring line is not accounted for. Elasticity of mooring line can be considered in the catenary equation (Faltinsen, 1998), but the effect from the seabed friction and dynamic responses are ignored in the catenary equation. In the industry, the mooring line often includes a couple of segments, e.g. a chain-wire rope-chain multi-compound line. The dynamic response of a multi-compound line is difficult to model by the catenary equation.

- **Finite difference method**

The finite difference method discussed in this section is a series of partial differential equations developed by Godman & Berslin (1976). Following Godman & Berslin's equations, many developments of the finite difference method were investigated, (Tjavaras et al, 1998. Chatjigeorgiou et al, 2001. Chucheepsakul et al, 2003) mainly aiming at enhancing the numerical stability and /or including some nonlinear characteristics, as the FDM method requires special treatment of the numerical model to avoid the numerical instability.

- **Multi-body system dynamic method**

Multi-body system dynamics discretize the mooring line into several rigid bodies. Similar to the widely used FEM, the multi-body method divides the mooring line into several segments. But unlike FEM or the lumped mass and spring method, the multi-body discretization results in a large number of degrees of freedom for a single line, because each segment of the mooring line is treated as a rigid body with 6 DoF. Thus, the multi-body method results in numerous of equations, which requires a very long running time. Nonlinear dynamic response and non-linear material behaviour of mooring line and seabed friction can be simulated with the multi-body method. In order to solve the multi-degree problem, a sub system technique was applied by Kreuzer and Wilke (2002), simulating a moored pontoon in random sea.

- **Lumped mass and spring method**

The lumped mass method considers the mooring line as a series of nodes connected with springs. Mass of the continual line is lumped equally on each node. It is considered as a special case of FEM, for which the shape function becomes a single line (Low, 2006). The lumped mass method introduced by Von de Boom (1985) is a development of the original lumped mass method by Walton and Polacheck (1959), improving the model to include elastic behaviour. Liu and Lars (1997) presented a mooring cable response model, simulating the influence of current and seabed friction based on a simple lumped-mass model. A comparison was made between the frequency and time domain method and results from the two methods compared well. Leonard & Nath (1981) compared lumped mass model and finite element method for oceanic cables. Some important conclusions from the comparison showed that both methods could generate accurate results, but the efficiency depended highly on the discretization. The lumped mass and spring method requires the transformation between local and global coordinate, which could increase the total running time if there is a large number of segments.

- **Nonlinear FEM**

In linear finite element analysis, the derived stiffness element matrix is constant as the displacement of structures is small, which means the stiffness matrix remain unchanged during the whole simulation. But for mooring lines, having large displacement, the above assumption tends to generate totally wrong results. This can be accomplished by means of the nonlinear finite element analysis, which is categorized into material nonlinearity and geometry nonlinearity (Bathe, 1996). If we assume constant EA of mooring line, analyzing mooring line static and dynamic becomes geometry nonlinearly problem with cable element (Bathe, 1996). Kim et al (2004) developed a computer program based on geometry nonlinear with iso-parametric curved element. Nonlinear FEM has proved to be an effective way of modelling mooring line response. Due to the widely used and developed of commercial finite element analysis software, this method is still widely applied in both design and research. But one problem is the inherent character of finite element analysis, requiring the transforming between local and global coordinate, resulting in a longer running time.

- **The elastic rod theory**

Unlike the nonlinear finite element analysis described in last paragraph, the elastic rod theory is a global coordinate based method. That is to say, no transformation between local coordinate and global coordinate is required. In other words, the transformation between local and global coordinate is dealt within the element stiffness matrix. So to some extent, it is considered as less time-consuming than the traditional nonlinear finite element method. Following by the classical rod theory from Love (2003), Nordgren (1974) and Garrett (1982) developed the rod theory and solved the nonlinear governing equation with finite difference method and Galerkin's method, respectively. Love (2003), Nordgren (1974) and Garrett (1982)'s rod theory are based on inextensible and equal principal stiffness assumption. Following by the pioneer work of Garrett's inextensible elastic rod theory, many researchers developed the rod theory (Chen et al, 2001; Ma & Webster, 1994; Tahar, 2001; Kim, et al, 2010, Tahar et al, 2012), including elongation of mooring line, seabed friction and non-linear

stress-strain relationship. Pauling & Webster (1986) applied Garrett's elastic rod theory on the large amplitude analysis of a TLP under wind, wave and currents, extending the stretch condition to allow small elongation. Ran (2000) developed finite element formulation for mooring line and risers based on Garett's rod theory both in frequency domain and time-domain. The stretch of mooring line is considered in Ran's method but the extension is still assumed linear and small. A considerable amount of research has been done, but these researches do not pay much attention to the elongation of mooring line and nonlinear material characteristics. Some important studies on polyester mooring line can be found by Tahar (2001), Chen et al (2001), Chen (2002), Tahar and Sidarta (2013) and Kim, et al (2011), but still requires further investigation.

3.2. 3-D floating body hydrodynamic analysis

Water waves are often considered as non-rotational, non-viscous and non-compressible. With these assumptions, the potential theory is widely applied in the field of wave-structure interaction. Although some viscous flow theory or CFD are popular in predicting response and analysing forces in fluid-structure interaction, the running speed is not suitable for the designing purpose. So potential theory, featured as fast and accurate, still widely used in designing a mooring system. In this section, categories and methods discussed mainly based on the potential flow theory.

- **Time or frequency domain analysis**

Time domain and frequency domain method are two types of widely applied method in predicting the body motion in waves. In the early days, due to the limitation of computer running speed, a frequency-domain method (e.g. Lee and Sclavouns, 1989 Molin, 1979, Ogilvie, 1983) was used. However, the conception of time-domain analysis was initiated earlier than frequency-domain method. Frequency-domain method is capable of dealing with some weakly nonlinear problems, but some highly nonlinear problems or transit problems, etc. have difficulty in using frequency-domain analysis. Fully nonlinear problems can only be solved with time-domain method. The most famous time domain analysis method is Cummins's impulse response function

method (Cummins, 1962). In this method, the frequency dependent added mass and radiation damping are calculated in the frequency-domain. Then, the generated hydrodynamic coefficients are transformed into time domain using Fourier transformation. Time series of wave loads are generated by Voltera model, be it first-order, second-order or even higher order. Due to its fast running speed and accuracy, almost all of the commercial software in mooring system analysis use this method in evaluating wave forces and body motions (e.g. Table 3.2). However, this method is still based on frequency-domain method and the damping coefficients on high frequency are difficult to obtain. Plus, the frequency-domain method fails to consider the effect of body motion on the calculation of diffraction problems. Another disadvantage of the impulse response function method is its inaccuracy on higher order problems, e.g. the springing and ringing problems of TLP. An alternative direct time-domain method was initiated by Isaason and Cheung (1992), solving the forces and motion of bodies totally in the time domain. By a perturbation method with Taylor series expansion in the time domain, the diffraction potential and radiation potential were no longer separated but considered together, as the scattered potential. This method can solve most of the non-linear problems but one problem is the running speed when calculating second order (or even higher order) wave forces. Together with the equation of motion of mooring line in the time domain, the efficiency of this direct time-domain method is less satisfied compared with the indirect time domain method. So in this project, considering of the types floating body- Spar and FPSO and the real problems in the designing process, e.g. running speed, an indirect time domain method was applied.

- **Mathematical modelling**

Potential flow theory for solving wave-structure interaction problem includes solving the Laplace equation plus boundary conditions. For simple structures, for example a bottom-mounted or a truncated cylinder, there are analytical or semi-analytical solutions, using eigenfunction expansion (e.g. Garrett, 1971) or diffraction theory initiated by MacCamy & Fuchs (1954) which is capable for larger scale structures. Real offshores structures often include some arbitrary geometry, instead of cylinder-

shaped bodies. The boundary condition for water wave-structure interaction problems is often very complicated and almost no analytical solution exists. To this end, there are some simplifications, e.g. linear free surface condition, linear body surface condition, etc.

- **Numerical methods**

The linearized problem based on the potential flow theory mainly follows the following two assumptions (Folley, 2012):

(1) The ratios of wave height to wavelength (i.e. wave steepness) and wave height to water depth must both be much smaller than 1.

(2) The motions of the body are small and around a fixed mean position: the ratio of the typical amplitude of motion to the typical dimension of the body is much smaller than 1.

The linearized free surface and body surface condition may generate satisfied results under mild weather condition and steady state problems, but failing in dealing with the transit or nonlinear phenomenon. To this end, many attempts have been investigated in the nonlinear problems, which can be further be divided into 1) free surface non-linear 2) body surface non-linear 3) fully non-linear.

Due to the complexity of the floating structures, there are no analytical solutions, except for some simple structures, e.g. a vertical cylinder. To this end, some numerical methods such as BEM (Bai & Teng, 2013), FEM (Renzi et al, 2014), FDM and SBFEM (Tao, et al, 2009), or meshless method (e.g. SPH) are widely applied. Compared with discretizing the whole body for FEM method, BEM method only requires surface mesh generation. But unlike FEM, the generated matrix in motion equation is not sparse matrix. Using Green's second theory, the volume problem can be transferred to a surface problem. In other words, for BEM the mesh generation only requires on the surface of the domain, instead of the whole domain.

3.3. Mooring system analysis

Table 3.1Comparison of mooring system methods of analysis

	Floating body and mooring line interaction	Current loading	Mooring line damping	Seabed friction	Accuracy	Run time
Uncoupled	×	×	×	×	Not satisfied	Low
Quasi-statically coupled	Partly considered	In static analysis	×	√	Sometimes satisfied	Low
Enhanced decoupled	×	√	√	√	OK	Medium
Coupled LF	In LF range	√	√	√	OK	Medium
Fully coupled (Indirect time domain)	√	√	√	√	Good	High
Fully coupled (Direct time domain)	√	√	√	√	Good	High
Fully coupled (Fully nonlinear problem)	√	√	√	√	Good	Highest

As for a mooring line and floating body analysis, that for a mooring system, be it coupled or non-coupled, can also be done in either the frequency domain or time domain. See, for example, the design rules and regulations of API or DNV. Due to the nonlinearities and interaction between floating body and mooring line, the time domain approach, by incorporating the inherent nonlinearities and coupling effects of

the mooring system characteristics, is considered to be the only reliable method for mooring analysis. But because of the large number of load cases, some simplified methods, partly or fully ignoring the coupling effects, are still widely used in mooring design. Table 3.1 shows a comparison of different methods of analysis for a mooring system (Focusing on the time-domain method.). The advantages and disadvantaged of each method will be explained and discussed briefly. The run time in Table 3.1 and current research are based on a PC with a processor of Intel® Core™ i7-2600 CPU@3.40GHz (8Cores).

- **Uncoupled method**

The process of uncoupled analysis includes two steps. First, floating body hydrodynamic analysis is done with any of the specific method discussed above. Then, the generated floating body motion time history is input as a top motion of mooring line (e.g. Ormberg and Larsen, 1998).

Uncoupled method often utilised a massless spring when performing floating body hydrodynamic analysis, as described in section 3.1. Non-coupled method ignores both of the coupling effects between floating body and mooring line, treating the floating body and mooring line as completely two separated parts. Because of the damping from mooring line is ignored, uncoupled method usually generates larger platform motion response compared with fully coupled or other semi-coupled methods. Consequently, a relative large safety factor is used, and as such is considered a conservative design method. When performing mooring line static/dynamic analysis, current forces can be considered when using some advanced mathematical modelling as described in section 3.2, but as the generated top motion response failed to consider the interaction between floating body and mooring line, the output is still not very accurate. Ormberg and Larsen (1998) showed that for deep-water circumstance, the two-step method might generate severally wrong results by a comparative study of a turret-moored vessel.

- **Quasi-statically coupled method**

For floating body moored by catenary chains, the main restoring force is from the weight of the chain. It is often considered that the oscillation of mooring line is out of the range of WF frequencies. Assuming the chain moves very slowly compared with the upper floating body, mooring line dynamic response and line shape are replaced by the static results. A quasi-static approach was applied by Nava et al (2013) for modelling a point absorber, studying the effects of different mooring system and mooring line materials. For each time instant, an innovative iterative procedure was applied.

Figure 3.2 shows the mooring line shape predicted by dynamic method and quasi-static method. The quasi-static method may give a motion of floating body and mooring line top tension correctly, but failing in the evaluation of fairlead horizontal force. The reason is when using quasi-static method WF response of mooring line is not accounted for. This simplification results in an inaccurate evaluation of mooring ling top angle, as we can see the difference between the dotted line and the solid line in Figure 3.2. So the quasi-static method may not predict the horizontal and vertical components of mooring line tension correctly.

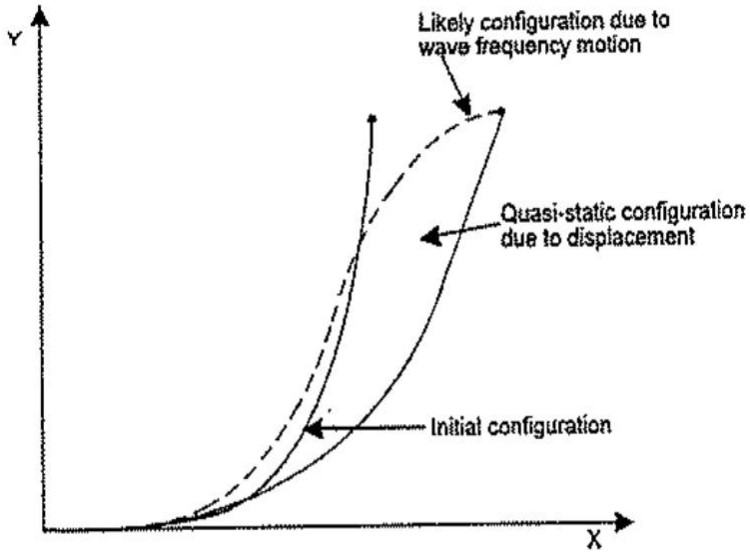

Figure 3.2 Differences in mooring line behaviour (Bartrolp, 1998)

- **Enhanced decoupled method**

The decoupled analysis refers to the analysis of mooring system utilising a two-step method. Effects from the mooring line are considered as simplified restoring force, e.g. static restoring force curve (e.g. Kim, et al ,2001a). The simplified method discuss above may generate sever inaccurate results. One key problem is the ignorance of mooring line damping. The floating body's instant position at each time interval is highly determined by the interaction between floating body and mooring line. But if the LF damping is correctly accounted for, this enhanced decoupled method can also generate satisfied vessel motion response (Ormberg, et al, 1998).

- **Coupled LF method (Hybrid method)**

Solving the coupled equations in time domain is strongly recommended in mooring system design, at least as a tool of checking some important design cases (Ormberg and Larsen, 1998). But due to the low run speed of time-domain coupled analysis, some simplified analysis methods are still popular. Coupled LF method solves floating body LF motion response, excited by LF range environmental loading in time domain while solving WF motion response in frequency domain. Low (2006) developed a hybrid method, solving WF response in frequency domain while LF response in time domain. The method considered the coupling effects between WF and LF response, which is a good simplification even for large LF motions, but only required less time compared with running coupled analysis. Though the application of the hybrid method has been studied by some researchers, the effort in analysing of the hybrid method for a variety of water depths is lacking. Plus the real world wave – structure interaction problem do not always fit well with this separation of WF or LF parts. Whether the WF or LF parts of floating body motion response is dependent of the mooring line or not still need further investigation.

- **Fully-coupled method**

Fully coupled methods, analysing the floating body and mooring system simultaneously, have long been recognized as having the capability to capture the coupling effects but requiring fewer simplifying approximations. When offshore

industry continually moves into deep water, the traditional uncoupled method is not accurate and a coupled method should be applied, at least for a check of design cases (Ormberg and Larsen, 1998). Ran et al (2000) presented a spar moored by a multi-compound line in 780m water depth by a coupled dynamic approach. A comparison between time domain and frequency domain method showed a larger wave-frequency and slowly varying responses and mooring tensions for the frequency domain results. Here the coupled analyses are based on the same mathematical model: 1) calculating floating body's hydrodynamic coefficients in the frequency domain without consideration of mooring line or body motion. 2) Solving system equation of motion simultaneously in time domain. Almost all the commercial mooring system analysis software uses this indirect time-domain method, as can be seen from the examples in Table 3.2. This fully coupled method has one simplification: assuming the wave exciting force and hydrodynamic coefficients are independent of the motion of floating body. This approximation may not be accepted for higher-order problems. To this end, an enhanced fully coupled model was given by Yang et al (2011). They developed a new coupled dynamic analysis method where the analysis of floating body was based on direct time-domain method. With the perturbation in the time domain to second-order, the wave forces were evaluated with the consideration of motion of floating body. A truss spar in 1500m water depth was studied based on the above method and a comparison between quasi-static and dynamic method was carried out, showing the importance of mooring line dynamic response and coupling effects in deep water. However, considering the aim of current project, an indirect time domain method was applied in this study, because the direct time domain method requires a very large running time, which is not suitable for designing purpose. The term fully coupled in the following paragraph refers to the indirect time domain analysis.

The key findings from the literature review suggest that the following require further study, particular so that there can be greater confidence in the guidance offered for deep water installations:

- The accuracy and efficiency of the hybrid (coupled LF) method in deep water

- The nonlinear dynamic response of polyester mooring line

Table 3.2 Commercial software for mooring system analysis

	Floating body hydrodynamic analysis	Mooring line static and dynamic analysis	Ability of running time domain mooring system analysis	System equation of motion
SESAM (DNV)	WAMIT and Morison's equation	FEM	√	Fully-coupled
HARP (Texas A&M University and Offshore Dynamics, Inc.)	WAMIT	Elastic rod theory	√	Fully-coupled
Ansys-AQWA	Frequency-domain diffraction theory (panel method)	Nonlinear cable element(described by a polynomial of up to fifth order or 2-D load extension database)	√	Fully-coupled
OrcaFlex (Orcina)	Morison's equation/Input from other hydrodynamic software	Lumped-mass method	√	Fully-coupled

4. Time-domain analysis for a classic Spar platform in waves and currents

4.1. Introduction

An increasing number of floating structures are being designed to operate in ever deeper water, for which there can be marked differences in the characteristics of currents. The effects of these and the wind-generated waves have an impact on the selection of mooring line configuration and design method.

Generally, mooring system dynamic response is determined by two coupling effects (Low and Langley, 2008): (i) coupling effects between floating body and mooring line/riser (type 1 coupling); (ii) coupling effects between mean offset, WF response and LF response (type 2 coupling). Both effects require a coupled or so called 'integrated' analysis, treating the floating body and mooring line together. But with the increase of water depth, each coupling effect plays a different role in determining the global performance of mooring system. So, some simplified methods, partly or fully ignoring the coupling effects, are still widely used. Non-coupled or quasi-static coupled methods ignore both of the above coupling effects, usually resulting in larger floating body motion response. Ormberg and Larsen (1998) studied a turret-moored FPSO: it was shown that the traditional two-step or non-coupled method failed to produce accurate results in comparison with a fully coupled analysis and with experimental data. Obviously, however, fully coupled methods are much more computationally intensive and time consuming.

In this chapter, the first step was to understand better the key parameters in mooring system design, comprising a detailed sensitivity study against water depth (~300-3000m) under a wave-only condition, with and without current, using WAMIT and OrcaFlex. Due to the complexity of mooring system response and the associated large number of parameters, risers were not modelled in our study. Various conditions were considered, including mooring line configuration. The quasi-static method, coupled

LF method and fully-coupled analysis were compared, focusing on the level of coupling between the floating body and mooring lines. Results from parametric studies are here compared to give guidance on the suitability of particular approaches.

4.2. Description of the mooring system

The mooring system used in our case studies comprises a large-diameter deep-draft cylinder (a classic Spar platform) and four mooring lines. Figure 4.1 shows a schematic of the four-line mooring system. The main particulars of the cylinder are shown in Table 4.1.

Table 4.1 Main properties of the platform (Chen, et al, 2001)

Parameters	Values
Diameter (m)	40.54
Draught (m)	198.12
Mass (kg)	2.592×10^8
Centre of gravity (m)	-105.98
Pitch radius of gyration (m)	62.33
Mooring point beneath mean still water level (m)	-106.62
Surge natural period (s)	331.86
Surge damping coefficient	0.0526
Heave natural period (s)	29.03
Heave damping coefficient	0.0053
Pitch natural period (s)	66.77
Pitch damping coefficient	0.0086

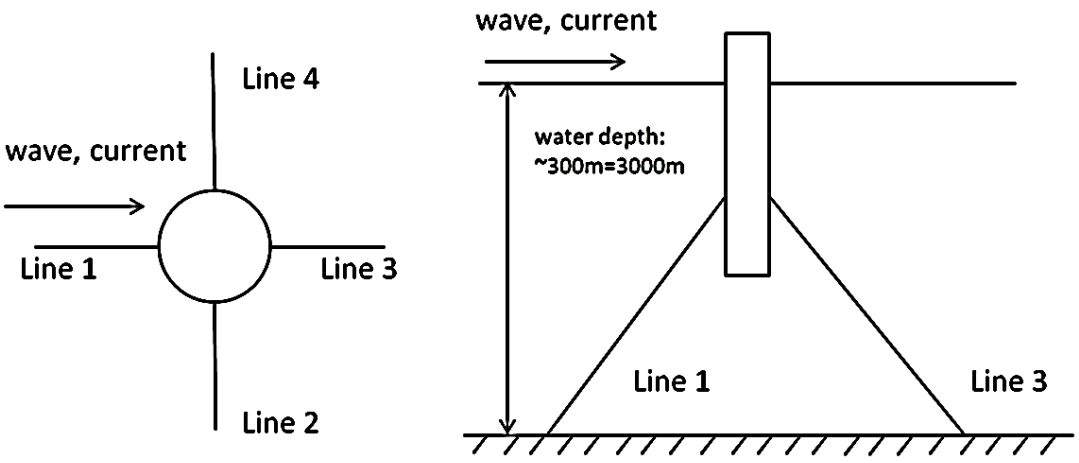

Figure 4.1 Schematic of the mooring system (Chen, et al, 2001)

4.3. Methods of analysis

4.3.1. Floating body hydrodynamic analysis

For wave-structure interaction problem, assuming non-viscous, non-rotational and incompressible flow, the velocity potential Φ satisfies the following equations in the fluid domain

$$\nabla^2\Phi=0 \tag{4.1}$$

The free surface condition

$$\frac{\partial^2\Phi}{\partial t^2}+g\frac{\partial\Phi}{\partial z}+\frac{\partial}{\partial t}\left|\nabla\Phi\right|^2+\frac{1}{2}\nabla\Phi\left|\nabla\Phi\right|^2=0 \text{ , on } z=\zeta \tag{4.2}$$

and the body surface condition

$$\frac{\partial\Phi}{\partial n}=\vec{u}\bullet\boldsymbol{n} \tag{4.3}$$

where *n* denotes the normal component.

For the frequency-domain method, the velocity potential can be divided into two parts. One is the time independent part φ (*x*,*y*,*z*) and another one is the harmonic oscillation part $e^{i\omega t}$

$$\Phi=\mathrm{Re}(\varphi e^{i\omega t}) \tag{4.4}$$

where Re denotes the real part of the complex value.

By further dividing the velocity potential into diffraction φ_d and radiation φ_r potential, where $\varphi_s=\varphi_d+\varphi_r$, φ_0 denotes the incident velocity potential, a linearized free surface condition and body surface condition were applied in current study as the mean wave drift force, the seconder-order effect can be derived and calculated directly from the linear BVP.

The velocity potential in the field satisfies the following BVP (WAMIT)

- **Diffraction problem**

1) In the domain

$$\nabla^2\varphi_d=0 \tag{4.5}$$

2) Linearized free surface condition

$$\frac{\partial \varphi_d}{\partial z} - \frac{\omega^2}{g}\varphi_d = 0 \text{ , on } z=0 \tag{4.6}$$

3) Body surface condition

$$\frac{\partial \varphi_d}{\partial n} = -\frac{\partial \varphi_0}{\partial n} \tag{4.7}$$

4) Seabed condition

$$\frac{\partial \varphi_d}{\partial z} = 0 \text{ , on } z=-h \tag{4.8}$$

- **Radiation problem**

1) In the domain

$$\nabla^2 \varphi_r = 0 \tag{4.9}$$

2) Linearized free surface condition

$$\frac{\partial \varphi_r}{\partial z} - \frac{\omega^2}{g}\varphi_r = 0 \text{ , on z=0} \tag{4.10}$$

3) Body surface condition

$$\frac{\partial \varphi_r}{\partial n} = -i\omega\xi \bullet \boldsymbol{n} \text{ , on body surface} \tag{4.11}$$

4) Seabed condition

$$\frac{\partial \varphi_r}{\partial z} = 0 \text{ , on } z=-h \tag{4.12}$$

4.3.2. Time domain mooring system analysis

- **Quasi-static method**

This is the traditional method for mooring system design. The system equilibrium position is determined first, using the mean environmental loading, followed by a static analysis of the whole system. Environmental forces, including mean drift forces, are included, but only considered as static forces acting on the floating body. All the dynamic coupling effects, including those between floating body and mooring system and the coupling effect between WF/LF motions, are ignored. In this thesis, the quasi-static method applied aims at offering a comparison for the mean value between coupled LF and fully coupled analysis.

- **Coupled LF method**

In the coupled LF analysis, or called coupled slow drift analysis, the global motion is split into WF and LF parts, and each part is solved separately. The coupling effects between floating body and mooring lines are considered only in the LF range. More specifically, in the LF range, the floating body motion response is solved in the time domain. Compared with a fully coupled analysis, because of WF motion response is evaluated in frequency domain, a relative larger time step is needed due to the large period of slow drift motion responses. Thus a coupled LF model is less time consuming than a fully coupled approach. A flowchart of coupled LF analysis is presented in Figure 4.2.

The LF motion of the floating body is calculated by solving the following equation in the time domain:

$$[M + M_a(\infty)]\ddot{X}_{LF} + \int_0^\infty R(t-\tau)\dot{X}_{LF}d\tau + KX_{LF} = F_{drift} + F_{current} + F_{mooring} + F_{wd} \tag{4.13}$$

For the WF responses, displacement RAOs were used to impose the WF motion on the floating body total motion response. The displacement RAOs were calculated in WAMIT by solving the equation of motion in the frequency domain:

$$\sum_{j=1}^{6}[-\omega^2(M_{ij} + A_{ij}) + i\omega B_{ij} + K_{ij}]X = F_{ext} \tag{4.14}$$

- **Fully-coupled method**

Based on the method of Cummins (1962), the retardation function is transferred from the frequency domain using an Inverse Fourier Transform. The floating body motion is then solved in the time domain:

$$[M + M_a(\infty)]\ddot{X} + \int_0^\infty R(t-\tau)\dot{X}d\tau + KX = F_{wave} + F_{current} + F_{mooring} + F_v \tag{4.15}$$

There is no need to divide the whole motion response into WF and LF parts, and so the fully coupled output will be a combination of WF, LF and mean drift response. As

in the fully-coupled method, coupling effects are included automatically. The equation of motion of the whole system is solved iteratively for each time interval. Since the range of WF motion is smaller than that the LF motion, a relatively small time step is required. A flowchart of fully coupled analysis is shown in Figure4.3.

Figure 4.2 Flowchart of mooring system coupled LF analysis

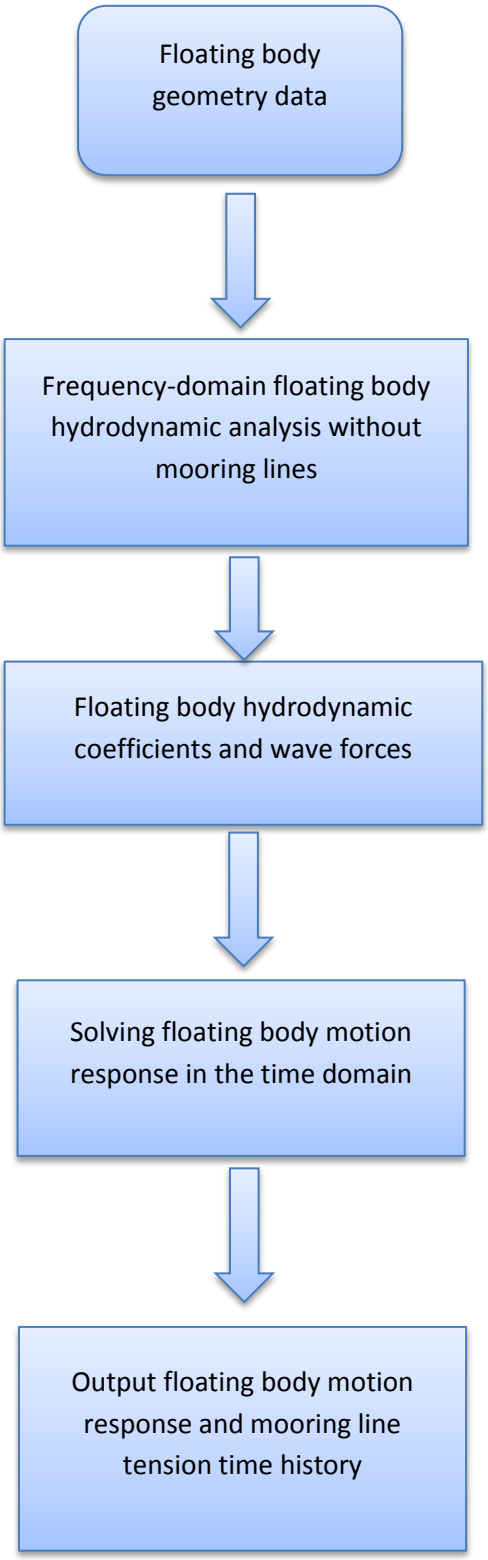

Figure 4.3 Flowchart of mooring system coupled analysis

4.4.Numerical modelling

Floating body hydrodynamic analysis was simulated using the diffraction/radiation computing package WAMIT. In WAMIT, two types of Boundary Element Method (BEM) 1) lower order method and 2) higher order method (based on B-spline function) are applied for solving the integral equation. In this chapter, considering of the large volume of the cylinder, the higher order BEM method was applied for solving the integral equation (see Appendix 2). By solving the linear BVP, the added mass, radiation damping and wave exciting forces were calculated with different frequencies. Considering the long simulation time for calculating full QTFs, only mean drift force was calculated. The second-order difference-frequency component of wave loading was calculated with Newman's Approximation (Newman, 1974), which is considered as a good and efficient method of approximation under deep-water circumstance.

4.4.1. Cylinder mesh

Figure 4.4 shows the mesh generation of the cylinder. The cylinder was divided into two patches, one was the side and the other one was the bottom of the cylinder. Because of the symmetry of the cylinder, meshes were generated only on a quarter of the cylinder.

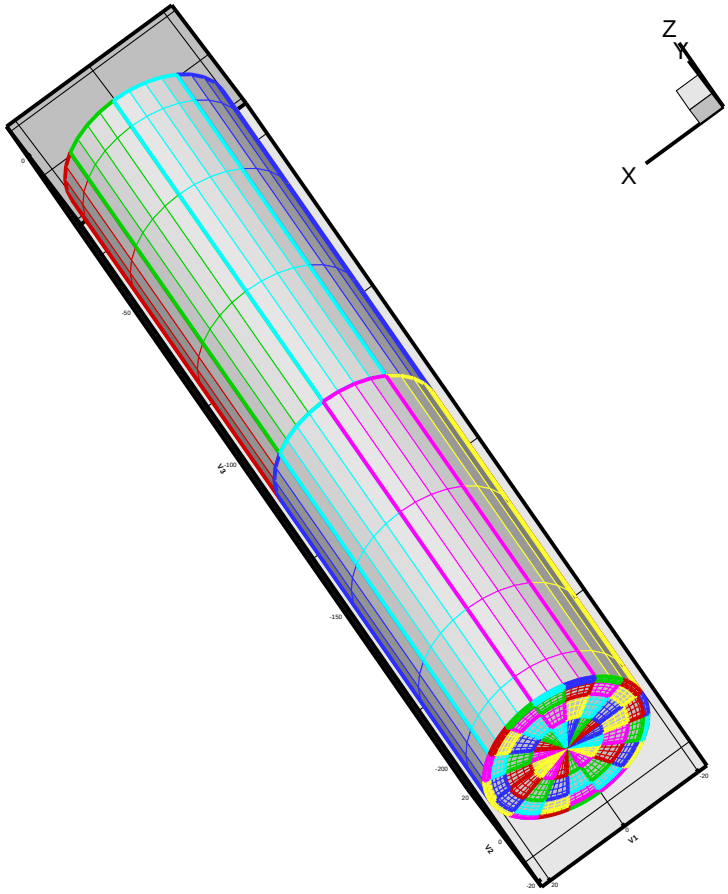

Figure 4.4 Cylinder mesh

4.4.2. Validation of mean wave drift force

Wave drift forces are important in the mooring system design because the mean position of the mooring system is partly determined by the mean wave drift forces. Although mean drift forces can be evaluated by solving the first-order BVP, it is beneficial to check the values of mean drift force, comparing with available experimental data. So, in this chapter, a specific mooring system and a specific water depth were selected because of the availability of experimental data.

In order to check the accuracy of mean drift forces, a comparison of current results and available experimental data (Spar Model Test Joint Industry Project, 1995) is provided in Figure 4.5. The test was conducted in 1994, including a total of 305 tests

comprising random wave, regular wave and 14 combinations of bi-chromatic waves. Current study used the mean drift force results, as shown in Figure 4.5. From the comparison we can see that a good agreement is shown between numerical results and available experimental data for frequency under 0.6 rad/s. The difference in wave range larger than 0.6 rad/s is less important for the LF response. The good trend in comparison offers good and accurate preparation for the time domain whole system dynamic response simulation.

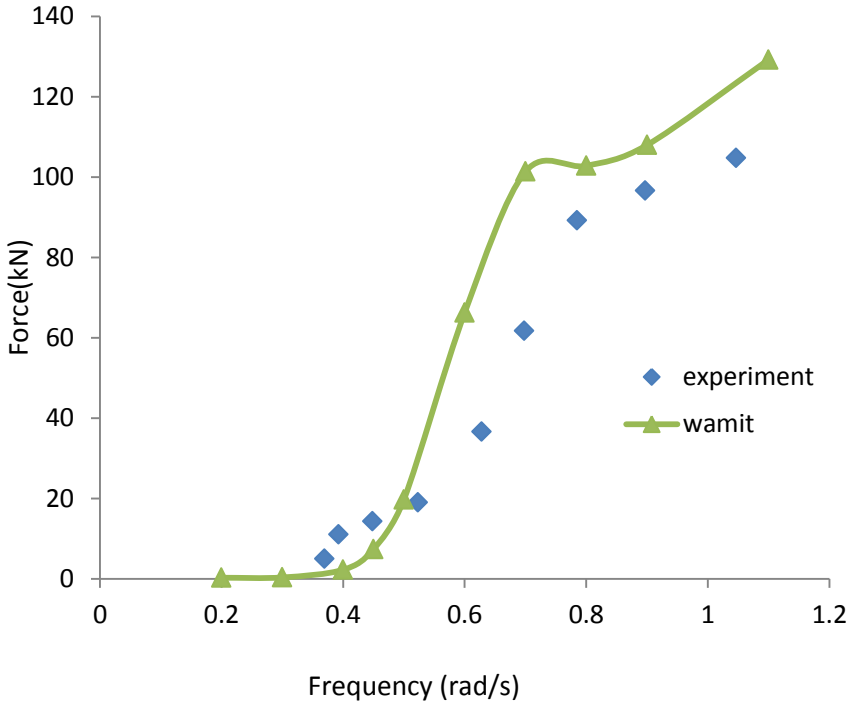

Figure 4.5 Comparison of mean drift force

4.4.3. Calculation of current forces

The current drag loads due to surge and sway relative velocity were calculated in the standard manner:

$$F = \frac{1}{2} C \rho V^2 A \tag{4.16}$$

A current speed of 0.95m/s was chosen at the surface, linearly decreasing to zero on the seabed.

4.4.4. Wave drift damping

Wave drift damping is an important potential flow effect for LF motions (DNV-RP-F205, 2010). In the present study, the effect of wave drift damping is evaluated by modifying the wave drift QTF values. As Newman's Approximation (Newman, 1974) was used in current study, the modified wave drift QTFs were based on Newman's Approximation (i.e the diagonal values of the QTF matrix only). The modified value only applied on surge and sway. The wave drift damping in the case studies were time-dependent, instead of constant value. The modified diagonal QTF Q_{de} is given by (Orcaflex)

$$Q_{de}(\beta,\beta,\tau,\tau) = A_e Q_d(\beta_e,\beta_e,\tau_e,\tau_e) \tag{4.17}$$

4.5. Comparison with available experimental data

In order to check our modelling, motion response results for a mooring system in 318m water depth were compared with available experimental and numerical data (Chen et al., 2001). Four studless chains of length 600m were selected. The main characteristics of mooring line are shown in table 4.2.

Table 4.2(a) Properties of slack mooring lines (chain, catenary, Chen et al., 2001)

Items	Values		
Water depth (m)	318	600	1000
Number of mooring lines	4	4	4
Length of mooring line (m)	600	1200	2000
Mass per unit length (kg/m)	1274	1274	1274
Elastic stiffness (EA, kN)	1.5e6	1.5e6	1.5e6
Pretension (kN)	5100	13000	25000

Table 4.2(b) Properties of taut mooring lines (composite)

Items		Values				
Water depth (m)		1000	1500	2000	2500	3000
Number of mooring lines		4	4	4	4	4
Length of mooring line (m)	Top chain	50	80	80	80	80
	Wire rope	1800	2000	2100	2700	3200
	Ground chain	50	85	85	85	85
Mass per unit length (kg/m)	Top chain	424	424	424	424	424
	Wire rope	75	75	75	75	75
	Ground chain	424	424	424	424	424
Elastic stiffness (EA, kN)	Top chain	1.2e6	1.2e6	1.2e6	1.2e6	1.2e6
	Wire rope	1.7e6	1.7e6	1.7e6	1.7e6	1.7e6
	Ground chain	1.2e6	1.2e6	1.2e6	1.2e6	1.2e6
Pretension (kN)		3100	3500	5000	6800	7700

4.5.1. Irregular sea-state modelling

The incident random wave was simulated using a JONSWAP spectrum with a significant wave height H_s=13.1m and peak period T_p=14s, as selected by Chen et al., (2001). For the selected wave condition we have a wave length λ=305.86m. Thus, the value of H/λ is larger than 1/40 but smaller than 1/20 (The limiting threshold for linearity). So a linear method, the superposition theory was applied for the irregular wave simulation. The expression of JONSWAP spectrum follows the equation below (OrcaFlex)

$$S(f)=\frac{\alpha g^2}{16\pi^4}e^{-\frac{5}{4}[\frac{f}{f_m}]^{-4}}\gamma^{e-\frac{1}{2}\sigma^2[\frac{f}{f_m}-1]^2} \tag{4.18}$$

4.5.2. Comparison of static results

In order to check our modelling, horizontal restoring force and worst loaded line tension results (Figures. 4.6 and 4.7) for a mooring system in 318m water depth were compared with available experimental data (Chen et al., 2001). For the load-offset

graphs and following case studies, the line segment length for chain and wire were around 20m and 100m. They compare well with available experimental data for offset under 15m (Figures 4.6 and 4.7). Current surge responses for all the water depths are less than 15m (Figure 4.15.1), so the comparison of offset larger than 15m is of less importance.

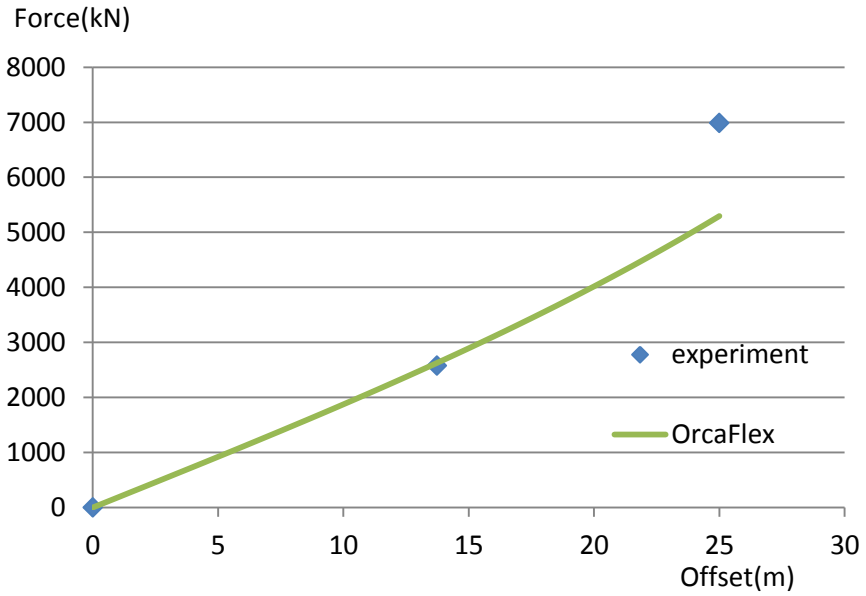

Figure 4.6 Comparison of horizontal restoring force in 318m water depth

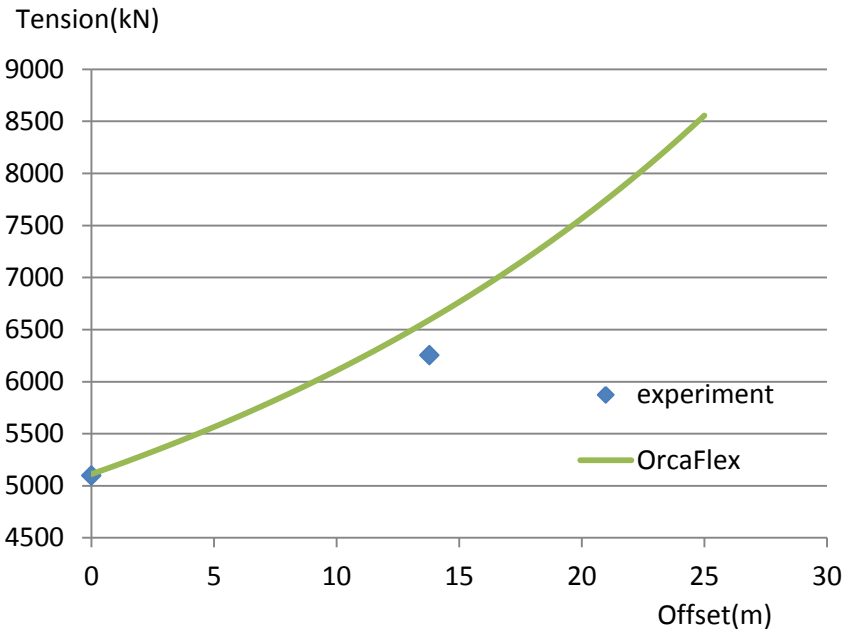

Figure 4.7 Comparison of worst loaded line (line 1) tension in 318m water depth

4.5.3. Comparison of motion response

Fully coupled time domain motion responses of surge, heave and pitch are shown in Table 4.3. From the comparison we can see that mean surge and pitch motion compare well with the experimental data.

Table 4.3 Comparison between experimental data and numerical simulation

		Experiment	Present	Chen
Surge (m)	Mean	4.07	4.03	4.24
	Min	-6.94	-8.13	-10.93
	Max	7.19	16.34	11.51
	Std Dev	2.61	4.19	3.78
Heave (m)	Mean	0.024	-1.40	
	Min	-1.83	-2.52	
	Max	1.75	-0.85	
	Std Dev	0.71	0.13	
Pitch (m)	Mean	0.27	0.25	
	Min	-3.71	-1.20	
	Max	4.25	2.32	
	Std Dev	1.39	0.47	

4.6. Parametric study

Table 4.2(a) and 4.2(b) show the properties of mooring line in different water depths from 318m to 3000m. The three analysis methods mentioned in section 4.3.2 were applied under a wave only condition and a wave plus current condition, respectively. For the parametric studies, the incident random wave had a significant wave height H_s=3.25m and peak period T_p=9.7s, which has an over 20% percentage probability of sea (Lee, et al, 1985). The simulation time was 3 hours. Table 4.4 shows a list of case studies and environmental conditions.

Table 4.4 Case studies against water depth

Case studies	Method of analysis	Environmental condition
Case1	Quasi-static	Wave only condition
Case2	Coupled LF	Wave only condition
Case3	Fully-coupled	Wave only condition
Case4	Quasi-static	Wave + current condition
Case5	Coupled LF	Wave + current condition
Case6	Fully-coupled	Wave + current condition

4.7. Load-offset graph for different water depths

In view of the large number of parameters, a comparison was undertaken using the static load-offset data in Figure 4.8, selecting the static horizontal stiffness according to water depth so that the mean horizontal offsets were similar. The mooring line properties in Table 4.2(b) were generated based on Figure 4.8.

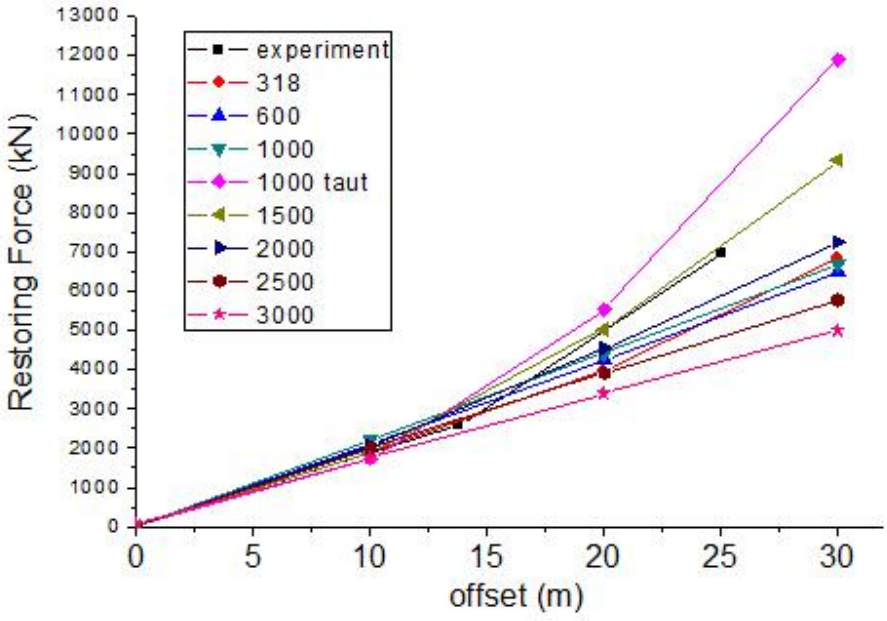

Figure 4.8 Load-offset graph of the Spar

4.8. Simulation results

Figures. 4.10~4.13 show the spectral density of motion response and line tension time history. The spectral density was smoothed to reduce the noise from Fourier Transform (OrcaFlex user's Manual). Statistical value of motion responses and line tension are given in Figures 4.14 and 4.15. For Figures 4.14 and 4.15, the first column in the legend is water depth while the second column represents statistical value or case studies. The maximum heave value in Figures 4.14.2 and 4.15.2 are absolute maximum value. For the fully-coupled method, a time step of 0.1s was applied while a variable time step was used for the coupled LF method.

Surge, pitch and heave natural period from simulation are around 250s, 41s and 28s for all the water depths. Although the static load-offset graph is similar between each water depth (Figure 4.8), when dynamic aspects are taking into consideration, discrepancy can be seen between cases and different water depths (Figures 4.10-Figures 4.15). From cases 1-3 in Figure 4.14.1 we can see that the quasi-static and coupled LF methods overestimate the mean surge motion in comparison with the fully coupled method. Mean value of surge motion from coupled LF method is about 4% larger than fully coupled method, decreasing to around 2% under a wave plus current condition. This difference is almost independent of water depth, except for 3000m-water depth wave only condition (the difference is 15%). Current loading increases the floating body mean and maximum position, but only affects the LF part of surge motion, as can be seen from surge motion spectrum in Figure 4.10. It is further observed that in Figure 4.15.1 maximum value of surge response is under-predicted by coupled LF method, compared with fully coupled method. But unlike mean surge response, the difference between coupled LF and fully coupled method increase with the increasing of water depth. Pitch motion follows a similar trend as surge motion response, especially for the mean value (Figures 4.14.3 and 4.15.3). One reason is the surge and pitch motion are coupled. Mean pitch motion is almost independent of water depth (Figure 4.14.3). But different from surge motion, maximum pitch motion results from coupled LF method are almost two-fold of fully coupled analysis (Figure 4.15.3).

However, it is interesting to observe that in contrast to surge and pitch motion, statistical value of heave motion is independent of analysis method and loading condition (Figures 4.14.2 and 4.15.2). The absolute maximum value of heave motion is 1000m water depth with catenary chain (Figure 4.15.2). One possible reason for this phenomenon is the total weight of chain under 1000m water depth accounts for 10% of the floating body mass. But for 318m water depth, this ratio is less than 0.5%. The phenomena investigated in current case studies may come from the large heave natural period (28s), which is far from the incident wave peak period (9.7s). To this end, a FPSO with a smaller heave natural period (8.33s) was selected for case study. The FPSO is an internal turret-moored vessel with four mooring lines. Main particular of the FPSO and mooring line characteristics are given in Table 4.5 and 4.6. Three water depths, 914m 2000m and 3000m were studied to investigate water depth variation on heave motion. Similar to the Spar case studies, the static load-offset graph was similar for all the water depth, as shown in Figure 4.9. From the heave motion spectrum in Figure 4.16 we can see that the heave motion is complete determined by WF response. Peak value of heave spectrum decreases with the increasing of water depth. Current has an effect on the maximum heave motion, especially for larger water depth. Under wave only condition, heave spectrum of coupled LF analysis and fully coupled analysis are almost identical. But on the contrary, current effect increases the difference between coupled LF and fully coupled method. In 914m water depth, maximum value of heave response predicting by fully coupled method is less than 1% larger than the counterpart of coupled LF method. But this difference increase to 7.5% in 3000m water depth. However, mean heave motion is still less sensitive to water depth, especially for wave-only condition.

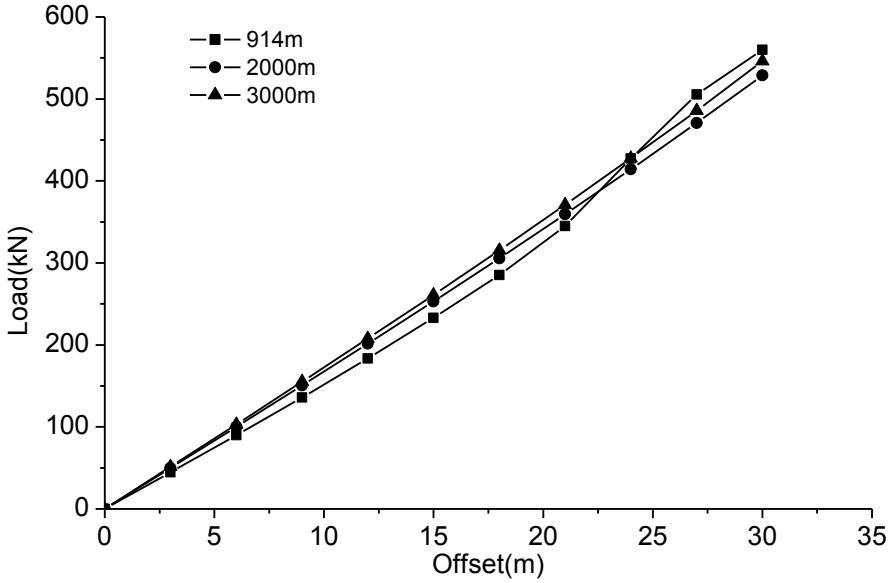

Figure 4.9 Load-offset graph of the FPSO

Table 4.5 Main particular of FPSO (Wichers and Devlin, 2001)

Parameters	Values
Length between perpendiculars Fpp (m)	311
Breadth (m)	47.18
Draft (m)	18.9
Vertical centre of gravity (m)	-5.58
Transverse radius of gyration in air (m)	14.77
Longitudinal radius of gyration in air (m)	77.47
Yaw radius of gyration in air (m)	79.3
Turret behind Fpp (m)	63.55
Turret elevation below tanker base (m)	1.52
Mass (te)	255000

Table 4.6 FPSO mooring line characteristic

Items		Values		
Water depth (m)		914	2000	3000
Number of mooring lines		4	4	4
Length of mooring line (m)	Top chain	45.7	45.7	45.7
	Wire rope	1127.8	1730	2520
	Ground chain	914.4	914.4	914.4
Mass per unit length (kg/m)	Top chain	165	165	165
	Wire rope	41	41	41
	Ground chain	165	165	165
Elastic stiffness (EA, kN)	Top chain	794.484e3	794.484e3	794.484e3
	Wire rope	689.858e3	689.858e3	689.858e3
	Ground chain	794.484e3	794.484e3	794.484e3

For catenary chain and taut line, both mean and maximum mooring line tension increases with the increasing of water depth (Figures 4.14.4 and 4.15.4). Among all the water depths, the maximum line tension comes from 1000m water depth with catenary chain, instead of 3000m water depth. The reason is the mooring system initial tension accounts for a large amount of total maximum line tension. Initial tension of slack chain in 1000m water depth was 25000kN, while for taut mooring under 1000m water depth, the initial tension was 3100kN. For slack mooring line, the difference between coupled LF and fully coupled method on predicting mooring line mean tension is 0.04% in 318m water depth, decreasing to 0.01% in 1000m water depth. But for taut mooring line, the difference increases slightly from 0.08% to 0.09% in 2000m water depth and decreases to 0.07% in 3000m water depth (Figure 4.14.4). For catenary chain, current effect becomes less important on mooring line tension with the increasing of water depth, as can be seen from Figures 4.14.4 and 4.15.4. Mean line tension under a wave plus current loading is 2.02% larger than wave only condition in 318m water depth, decreasing to 0.75% in 1000m water depth. But for taut line, the discrepancy is less than 5% for 1000m water depth, peaking at 2000m water depth (6.06%) and decreases to 5% in 3000m water depth.

Surge motion is determined by LF response, as we can see from Figure 4.10. LF surge response varies with different water depth. But water depth variation does not appreciably impact surge WF response, as shown in Figure 4.10. In the LF range, peak value of surge spectral density predicted by fully coupled method shows a fairly good agreement with the coupled LF method. It also can be seen that WF surge spectrum shows a significant difference between coupled LF and fully coupled method and the difference is less sensitive to water depth. But as surge motion is primarily dominated by LF response, the difference of WF response under different method does not significantly affect the whole motion response.

Pitch motion spectral density follows the same trend as surge motion, but determined by both LF and WF response (Figures 4.10 and 4.12). But unlike surge and pitch motion response, heave motion spectral density seems independent of water depth,

especially for water depth less than 1000m where catenary was applied (Figures 4.11). Current and method of analysis have an effect on heave LF motion response for water depth larger than 1500m, but not significantly varied (Figures 4.11.4-4.11.8).

Figures 4.13 show the spectral density of worst loaded line (line1) for different water depths. For catenary chain (between 300m and 1000m), both LF and WF mooring line responses increase with the increasing of water depth while WF mooring line response becomes increasingly important from 300m to 1000m. But when considering greater water depths up to 3000m, for which a taut mooring line is applied, the LF range mooring line tension spectral density increases with water depth up to 2500m water depth and decreases slightly in 3000m water depth. Current effect has an impact on mooring line LF response, but results of mooring line LF response spectrum does not vary significantly by using coupled LF and fully coupled method. Unlike mooring line LF response, there is a significant difference between WF response predicted by coupled LF and fully coupled method (Figures 4.13). For water depth larger than 1500m, peak value of mooring line WF spectrum predicting by coupled LF method is much smaller than the counterpart predicted by fully coupled method (Figures 4.13.6-4.13.7).

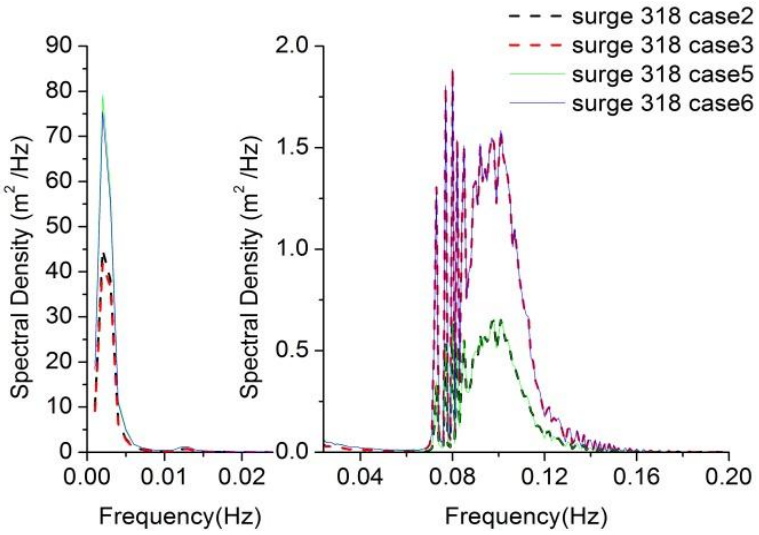

Figure 4.10.1 Surge 318

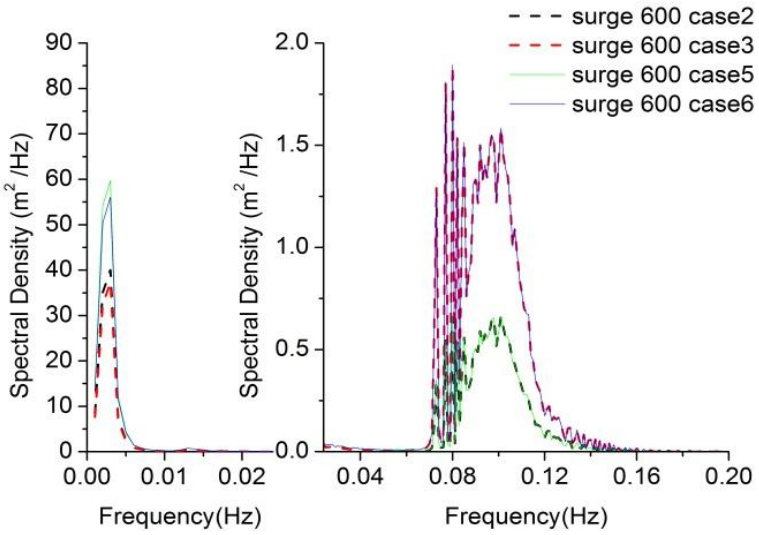

Figure 4.10.2 Surge 600

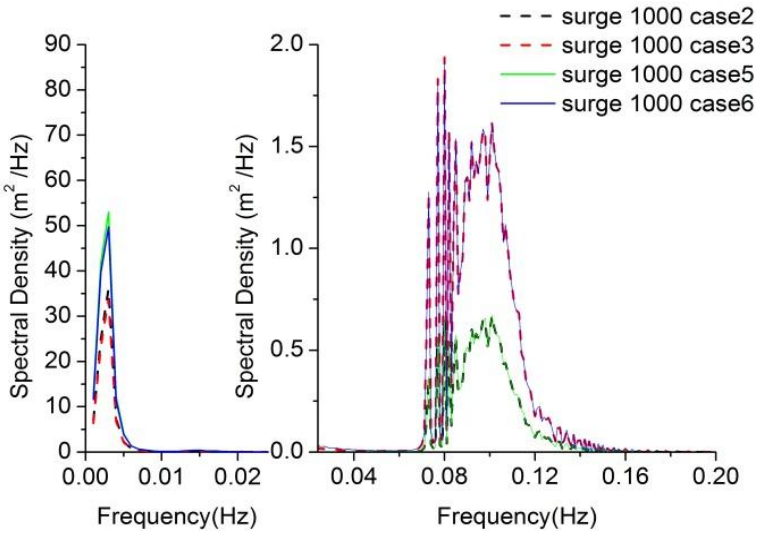

Figure 4.10.3 Surge 1000

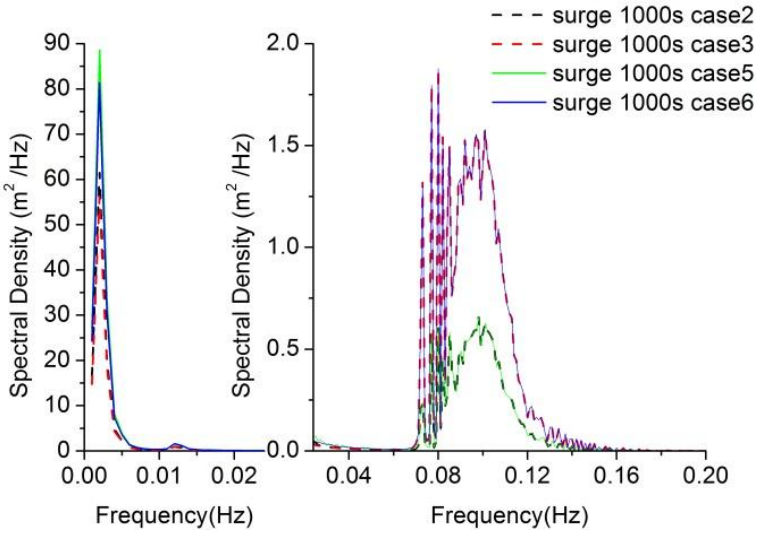

Figure 4.10.4 Surge 1000 semi-taut

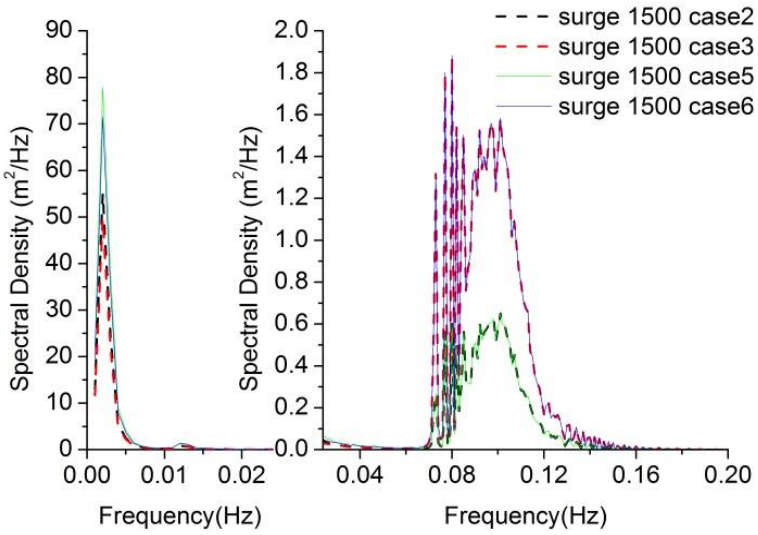

Figure 4.10.5 Surge 1500

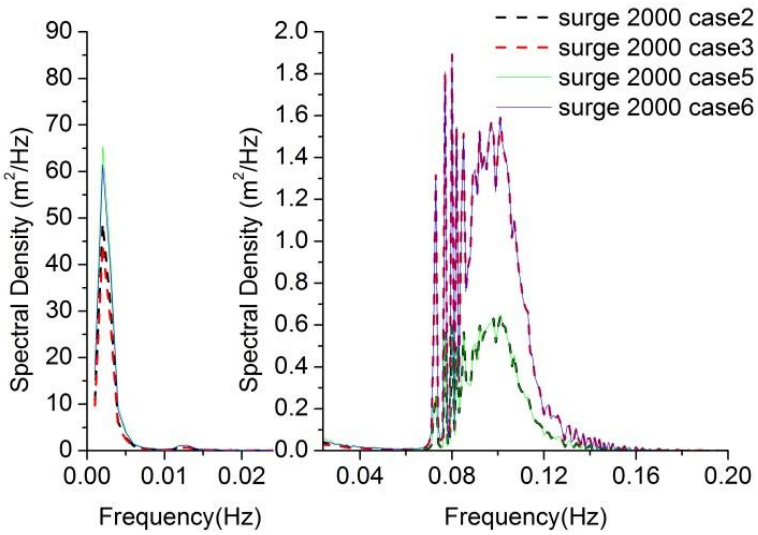

Figure 4.10.6 Surge 2000

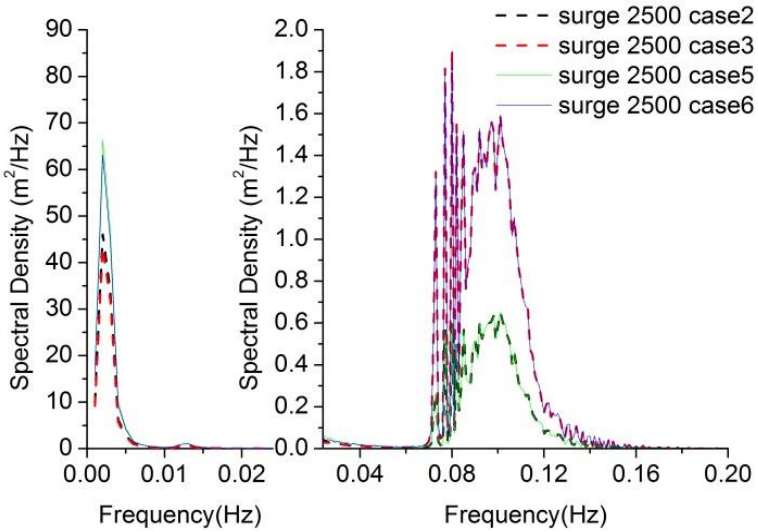

Figure 4.10.7 Surge 2500

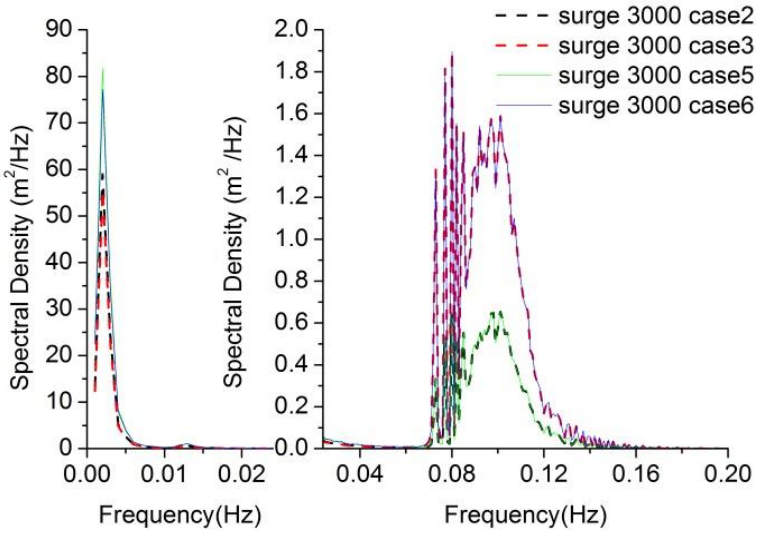

Figure 4.10.8 Surge 3000

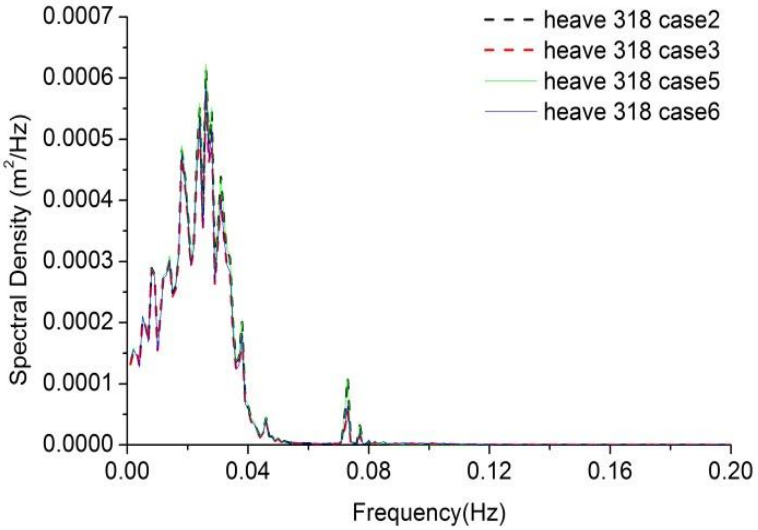

Figure 4.11.1 Heave 318

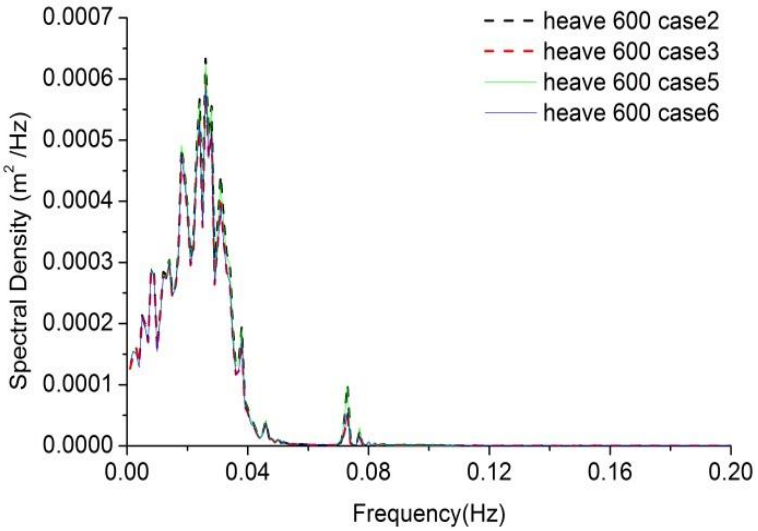

Figure 4.11.2 Heave 600

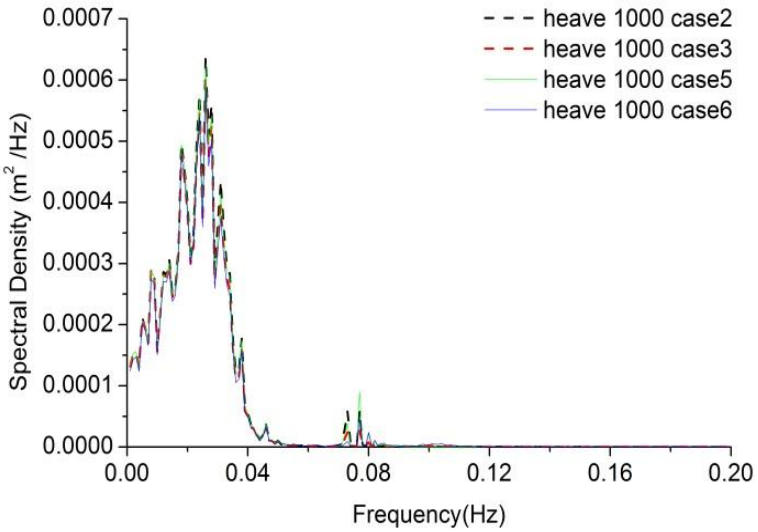

Figure 4.11.3 Heave 1000

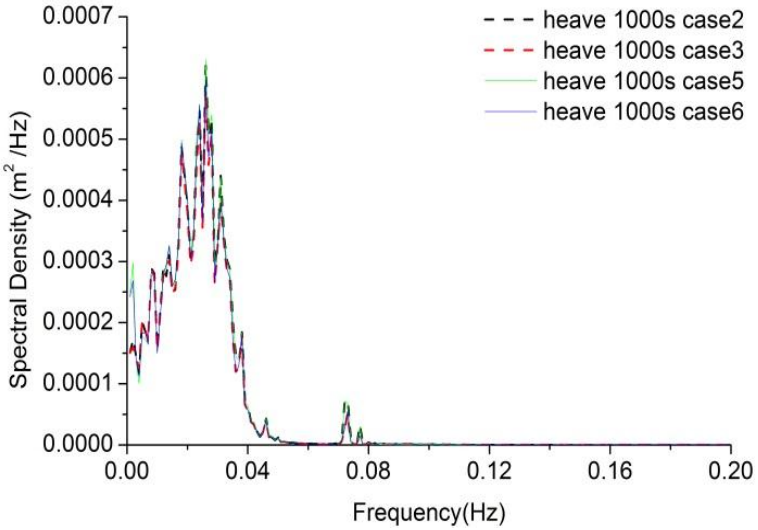

Figure 4.11.4 Heave 1000 semi taut

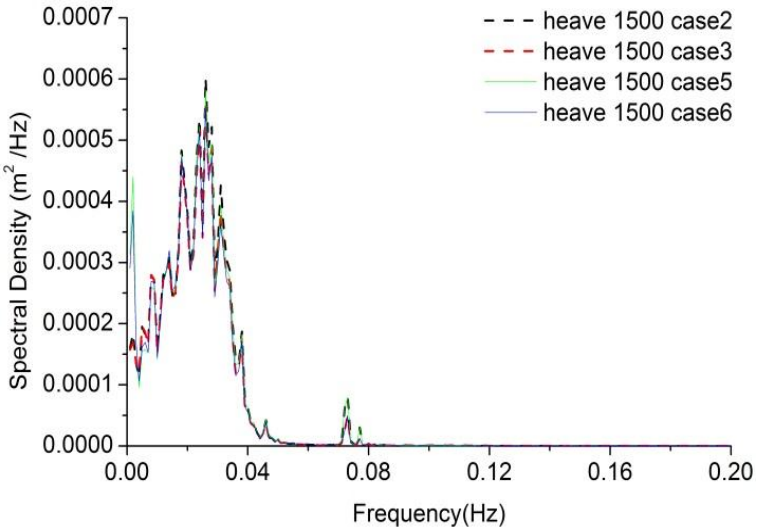

Figure 4.11.5 Heave 1500

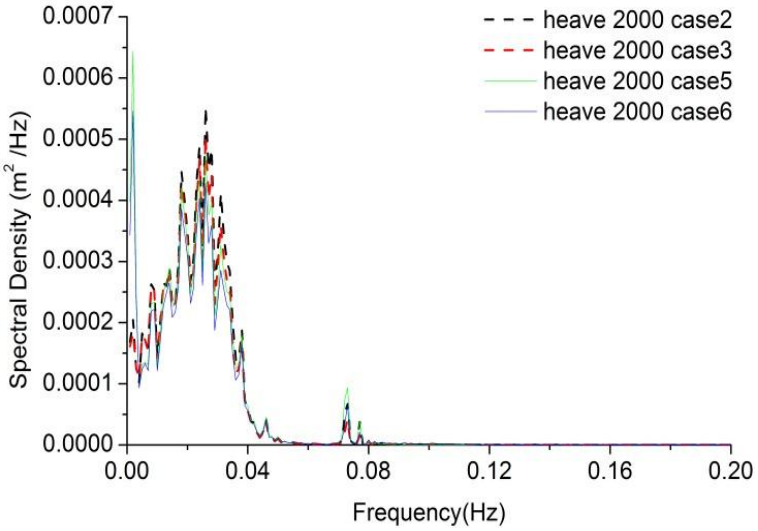

Figure 4.11.6 Heave 2000

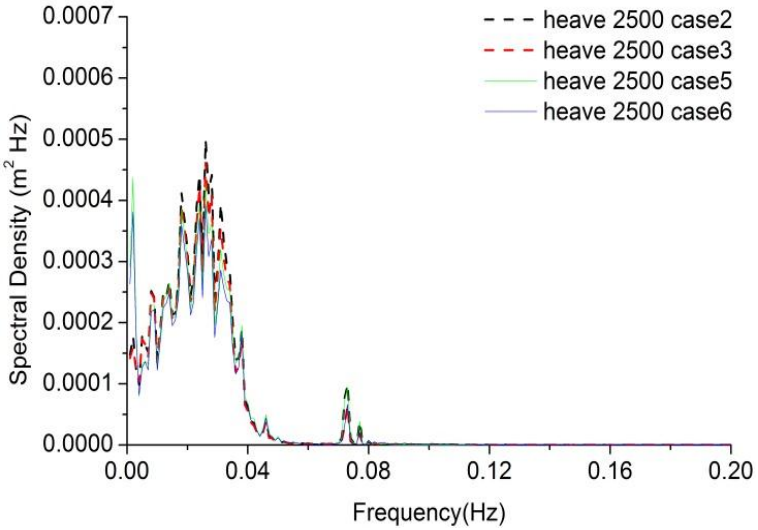

Figure 4.11.7 Heave 2500

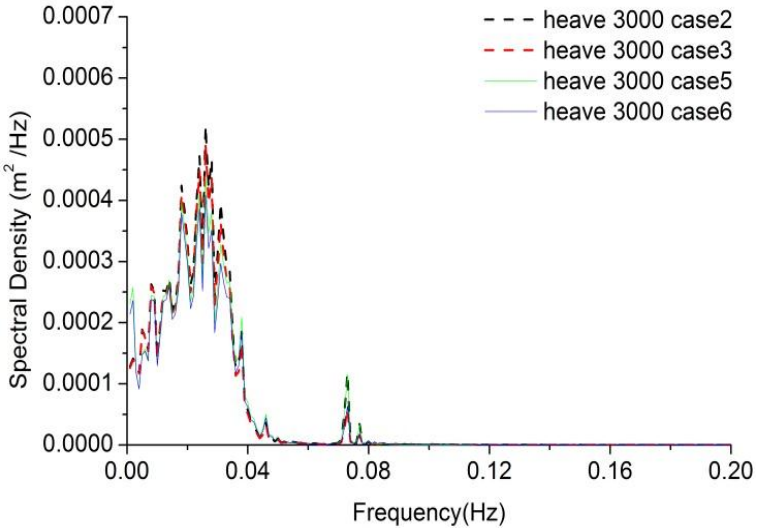

Figure 4.11.8 Heave 3000

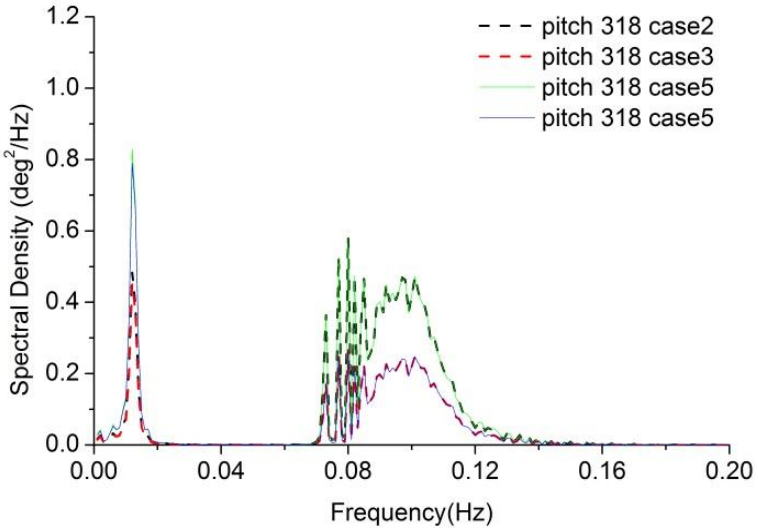

Figure 4.12.1 Pitch 318

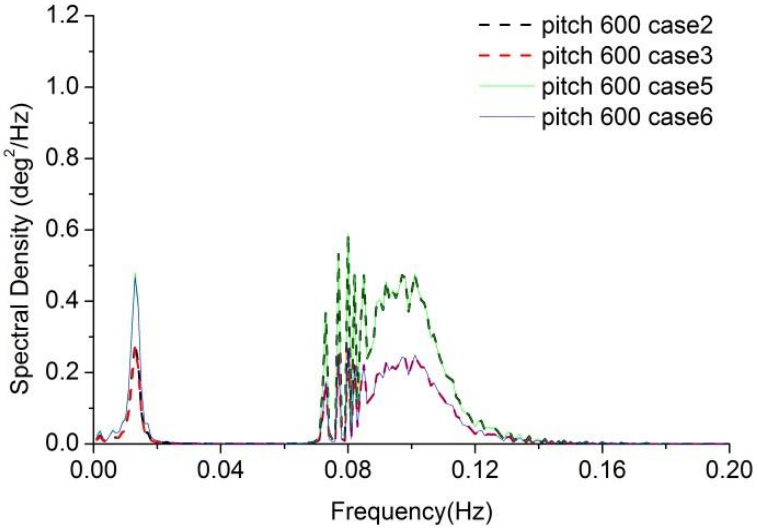

Figure 4.12.2 Pitch 600

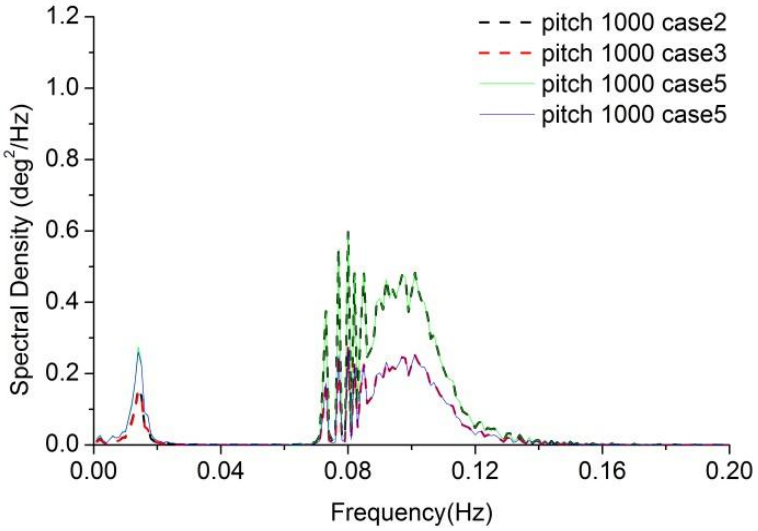

Figure 4.12.3 Pitch 1000

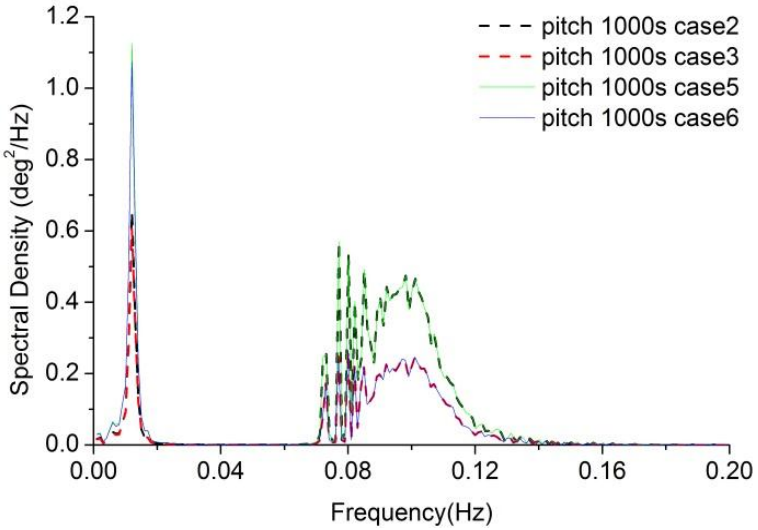

Figure 4.12.4 Pitch 1000 semi taut

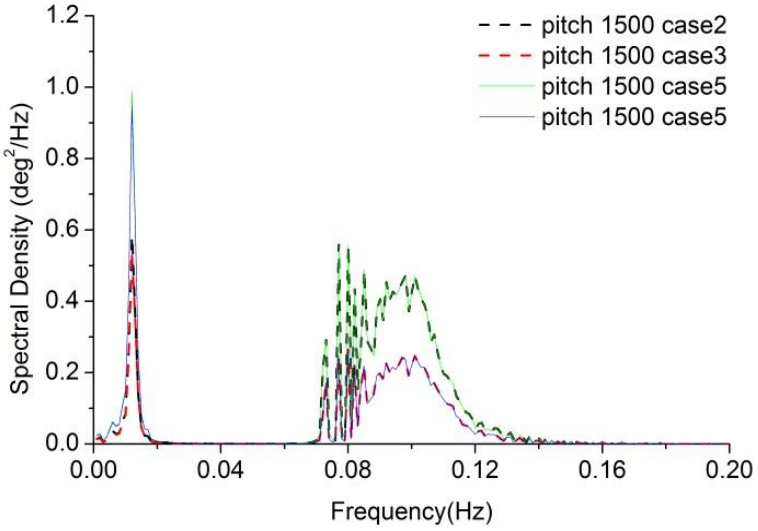

Figure 4.12.5 Pitch 1500

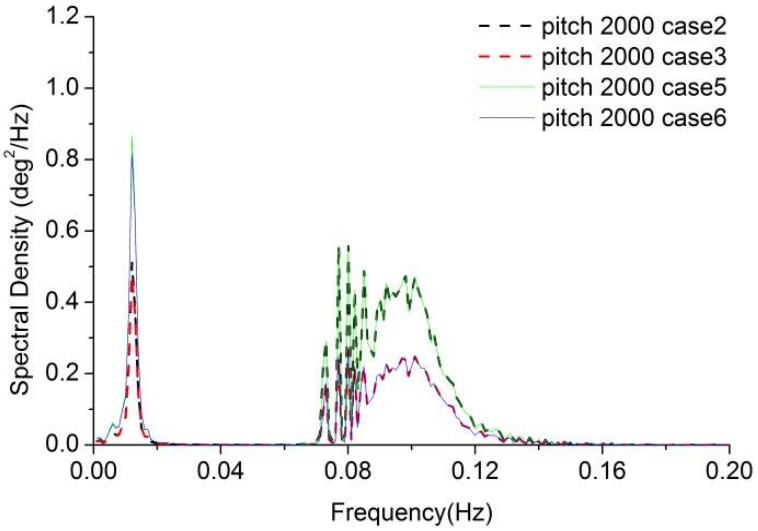

Figure 4.12.6 Pitch 2000

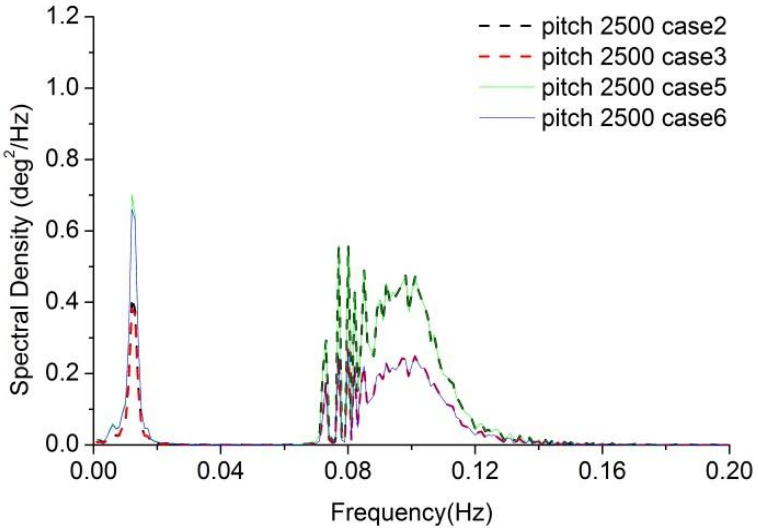

Figure 4.12.7 Pitch 2500

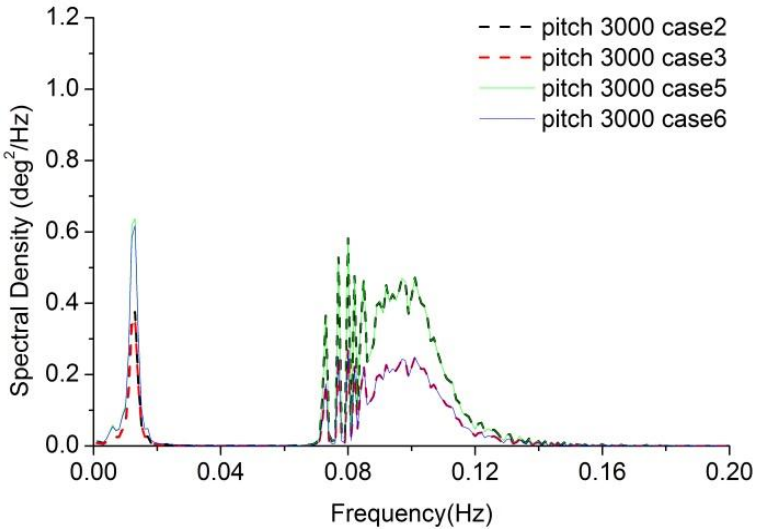

Figure 4.12.8 Pitch 3000

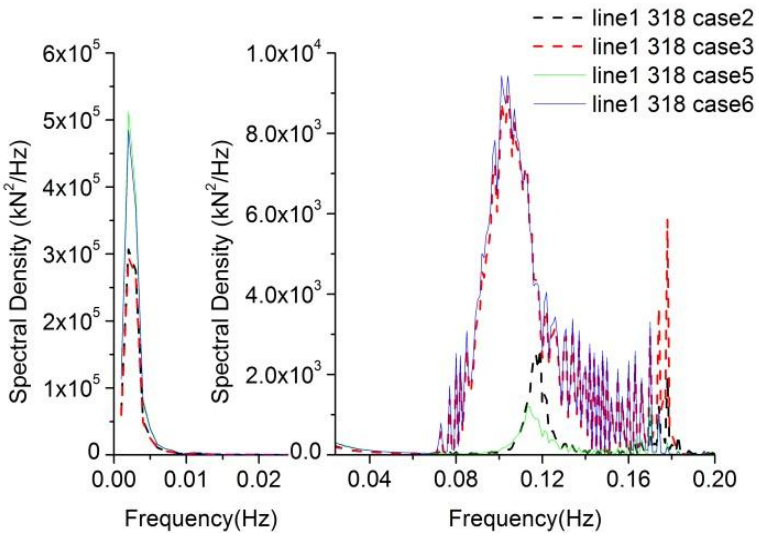

Figure 4.13.1 Line 1 tension 318

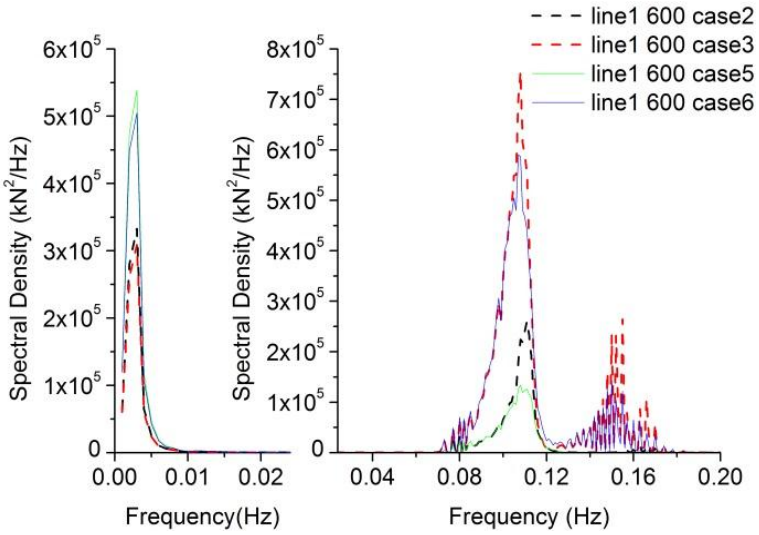

Figure 4.13.2 Line 1 tension 600

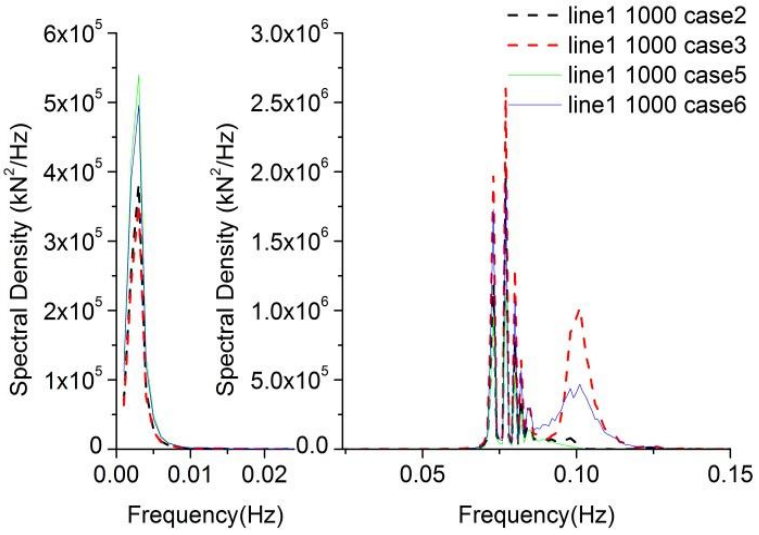

Figure 4.13.3 Line1 tension 1000

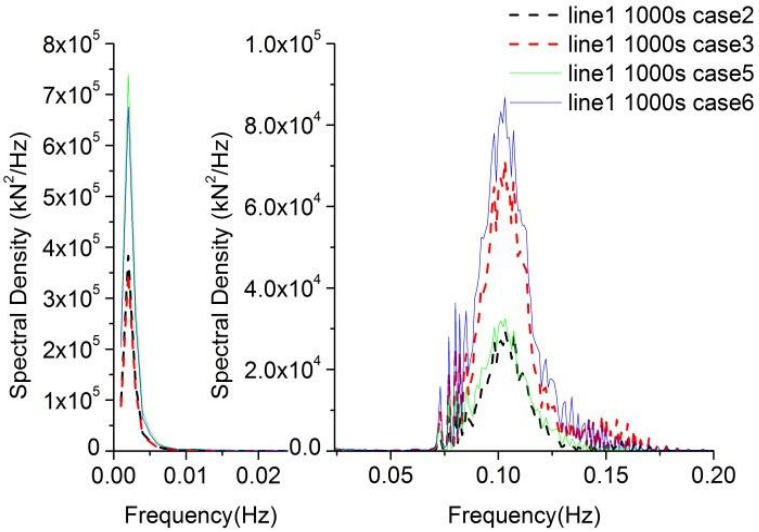

Figure 4.13.4 Line 1 tension 1000 taut

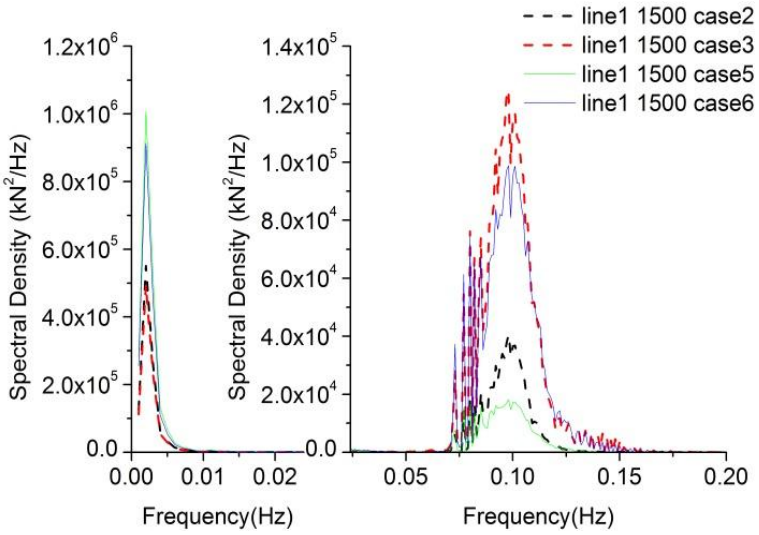

Figure 4.13.5 Line 1 tension 1500

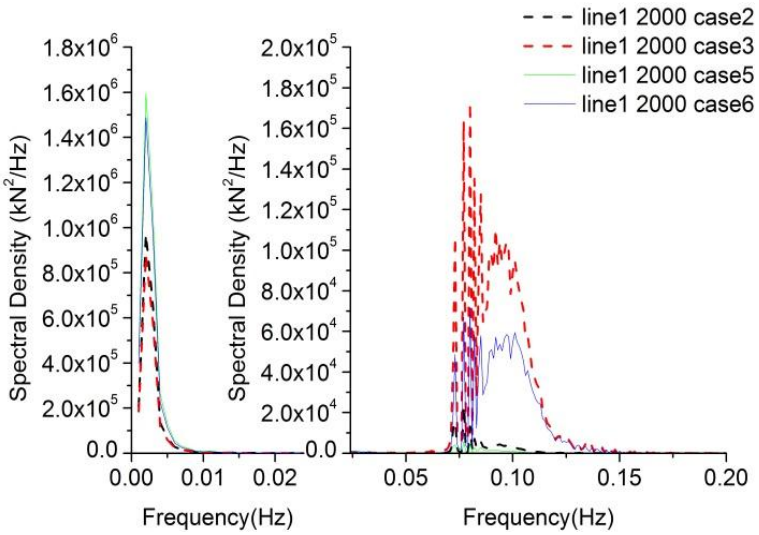

Figure 4.13.6 Line 1 tension 2000

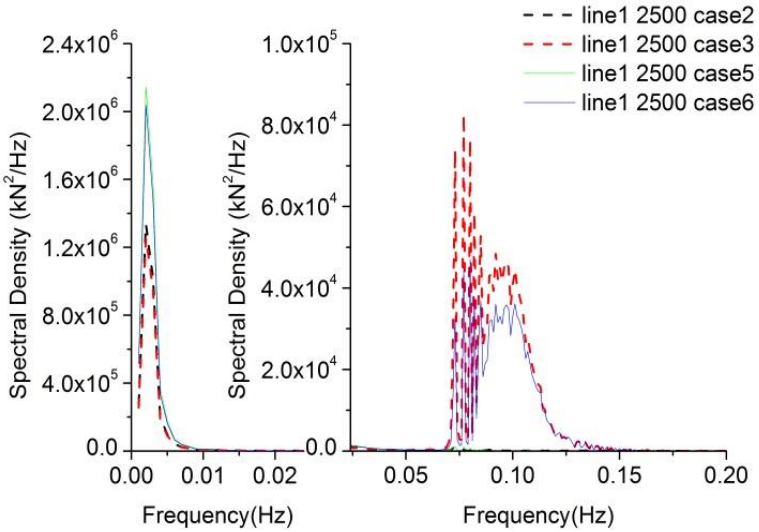

Figure 4.13.7 Line 1 tension 2500

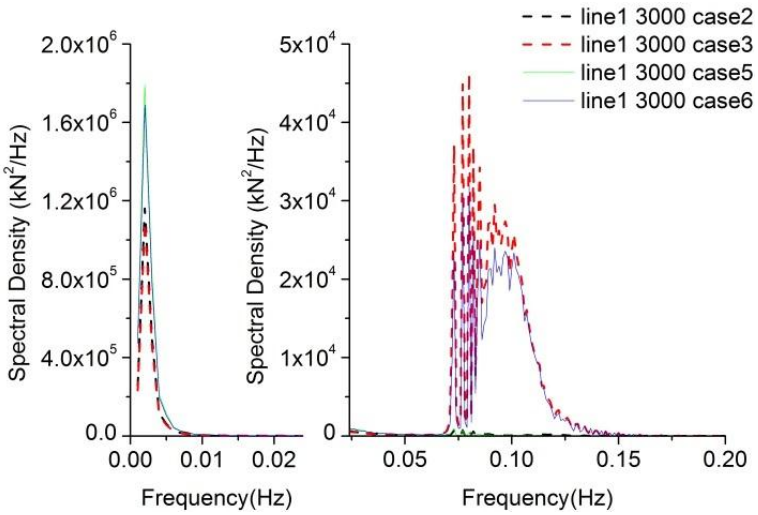

Figure 4.13.8 Line 1 tension 3000

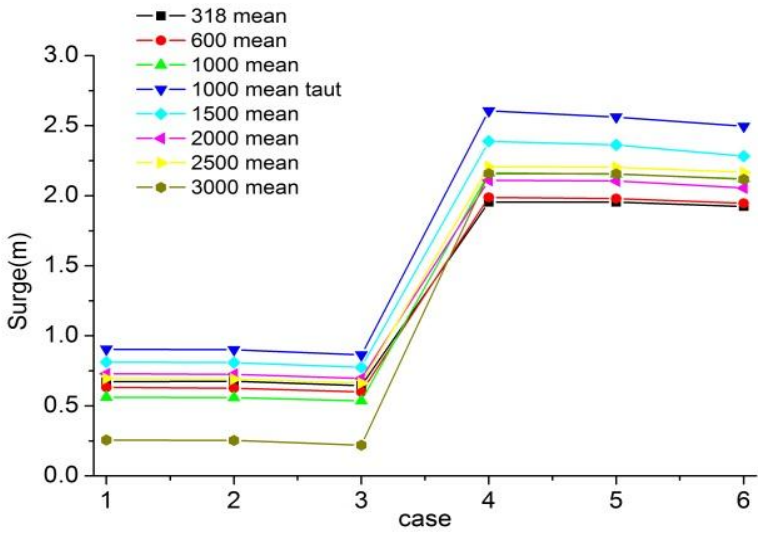

Figure 4.14.1 Surge mean

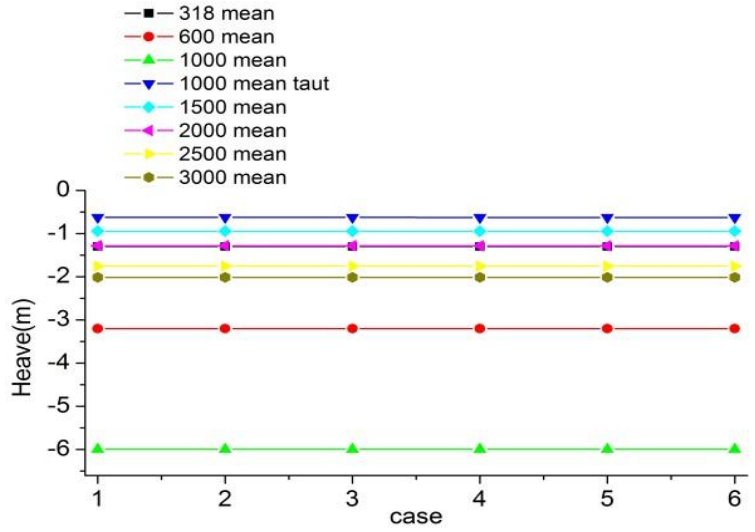

Figure 4.14.2 Heave mean

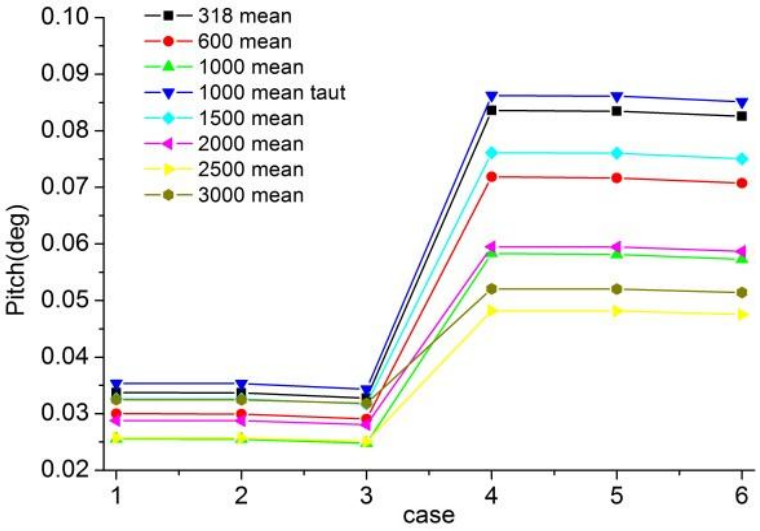

Figure 4.14.3 Pitch mean

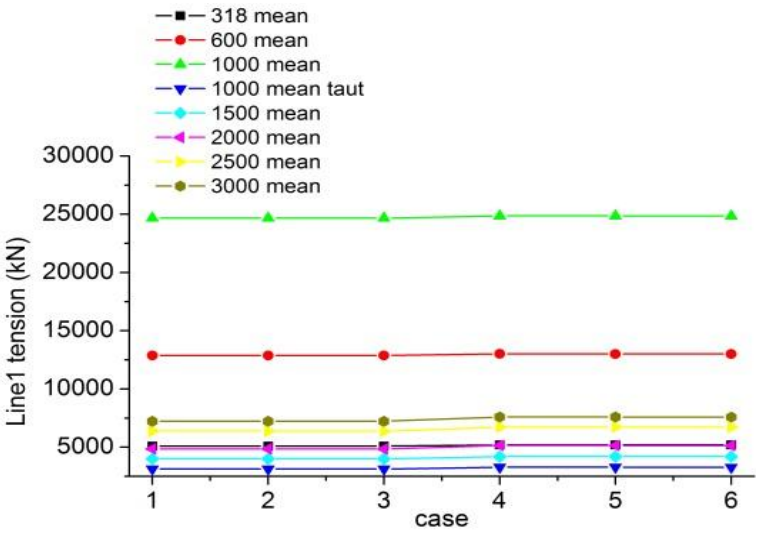

Figure 4.14.4 Line 1 tension mean

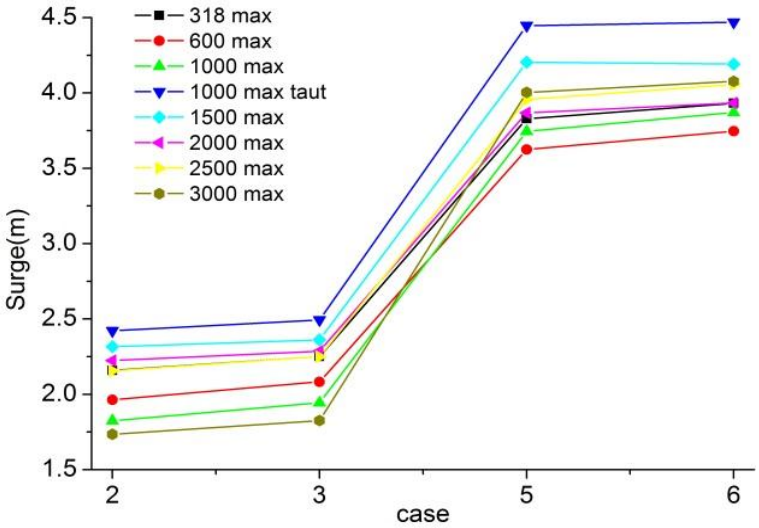

Figure 4.15.1 Surge max

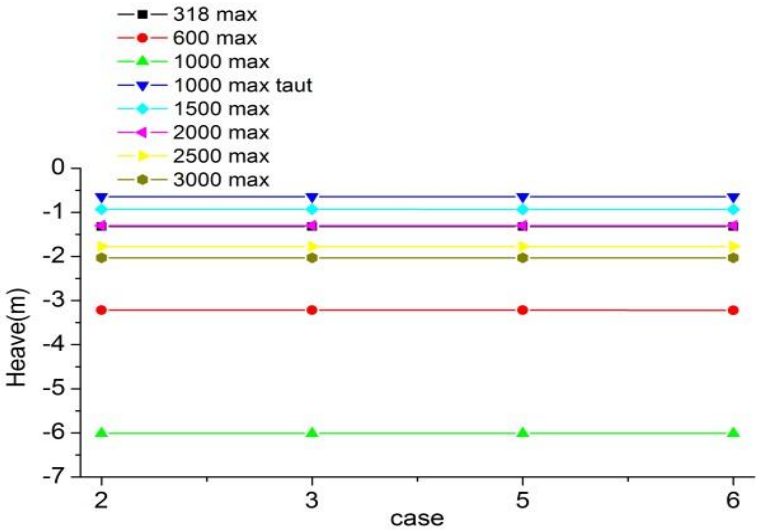

Figure 4.15.2 Heave max

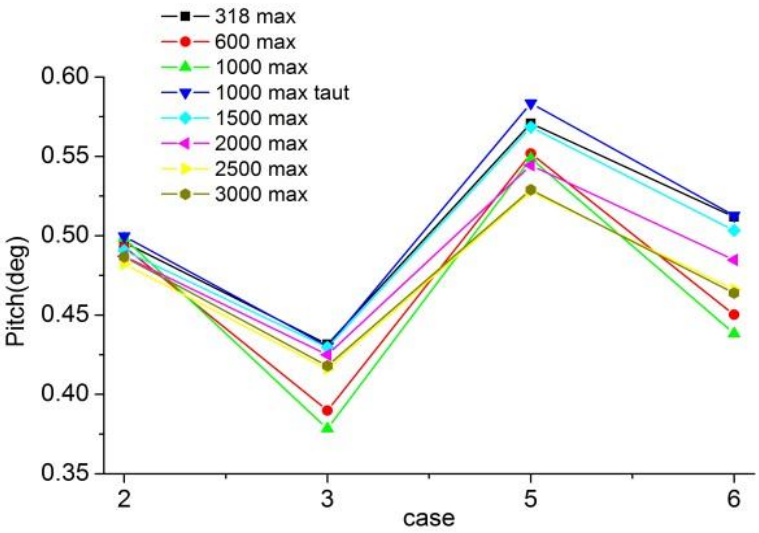

Figure 4.15.3 Pitch max

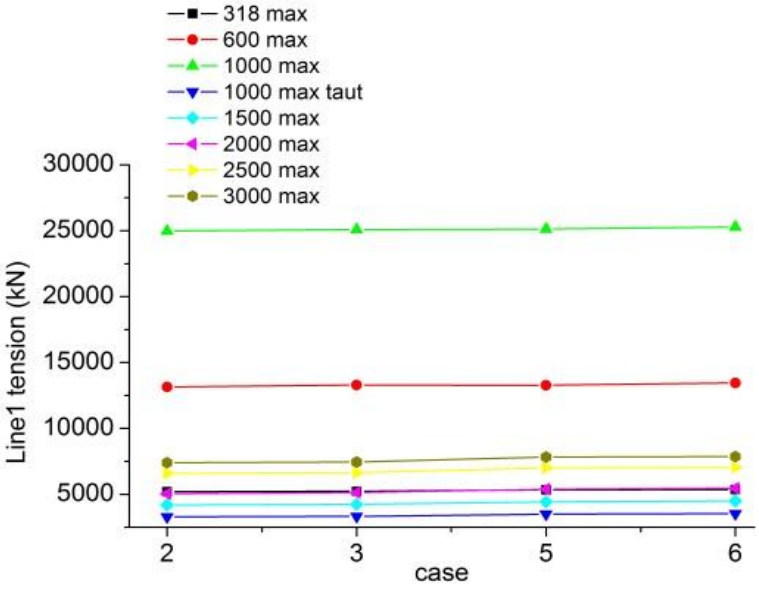

Figure 4.15.4 Line 1 tension max

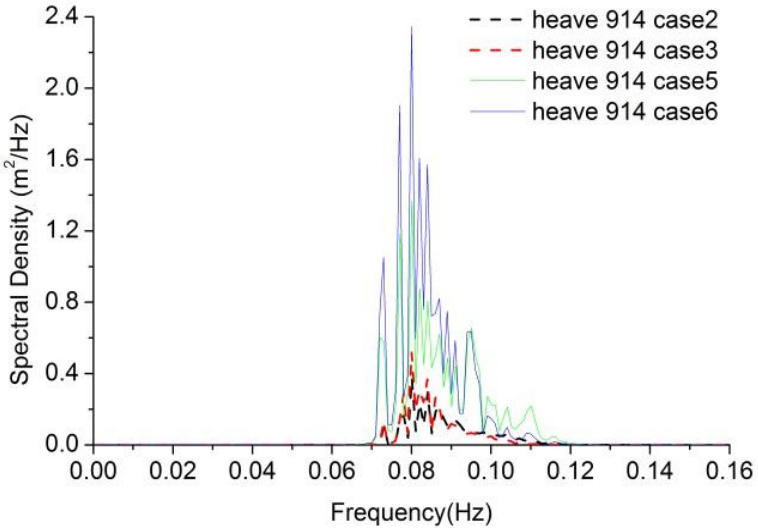

Figure 4.16.1 Heave 914 FPSO

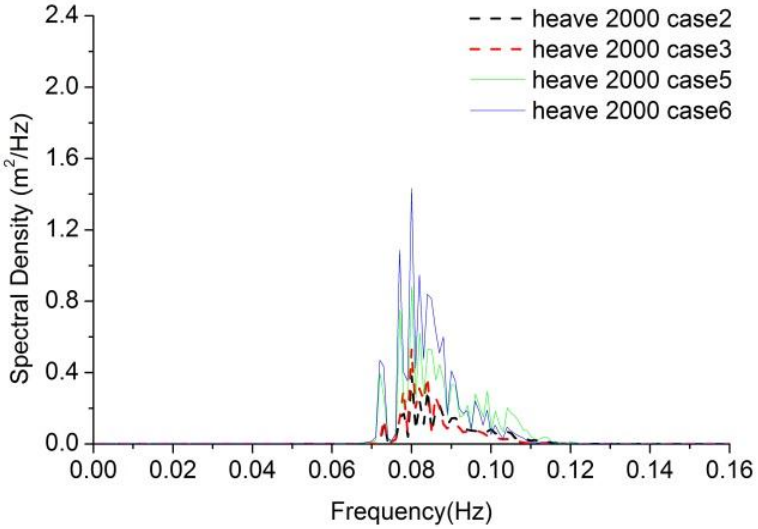

Figure 4.16.2 Heave 2000 FPSO

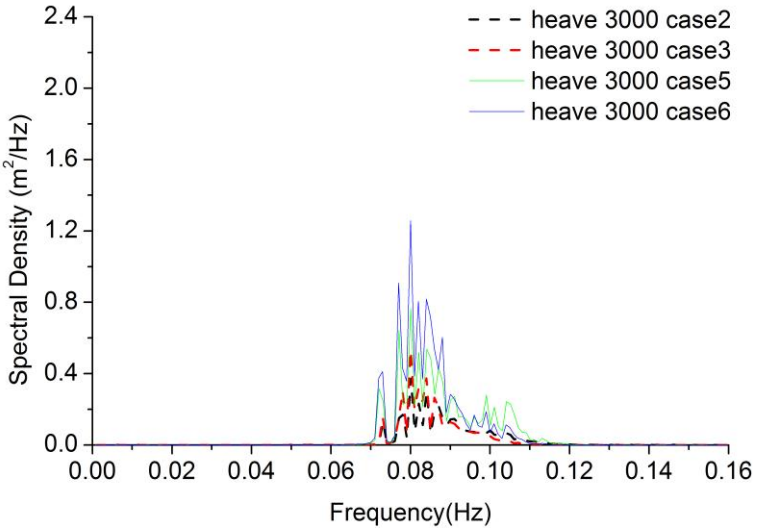

Figure 4.16.3 Heave 3000 FPSO

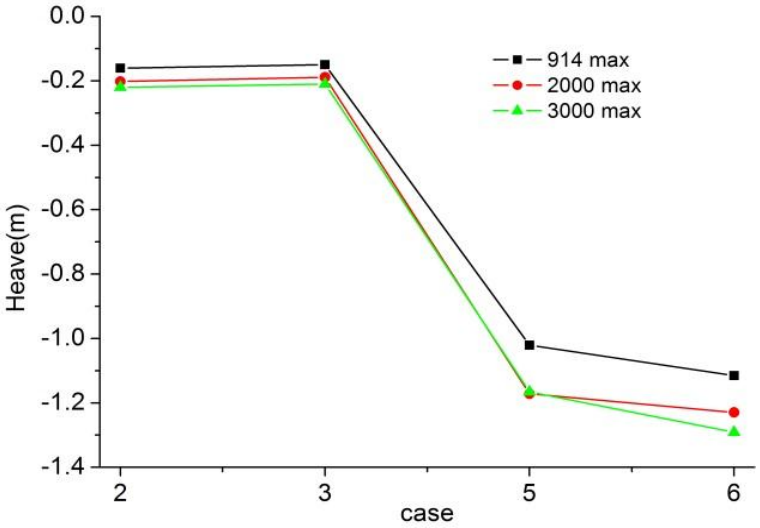

Figure 4.17 Heave max FPSO

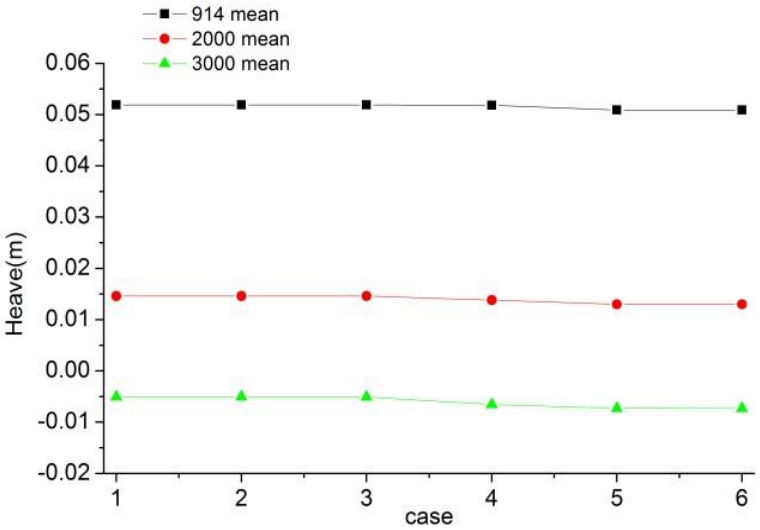

Figure 4.18 Heave mean FPSO

5. Time-domain analysis for a catenary moored Spar-type FOWT

5.1. Introduction

This chapter aims to investigate the effect of water depth on the hydrodynamic performance of a floating structure that is representative of a horizontal floating offshore wind turbine, with special focus on the influence of low frequency wave exciting force and turbine thrust force. The present study has considered a model of a 5MW baseline Spar-type offshore wind turbine, based on a design of the NREL. A fully-coupled analysis has been simulated in the time domain, using Fastlink for both operational and shutdown conditions. Guidance on mooring system analysis is discussed.

Spread moorings are used to restrain the horizontal drift motions of a floating platform, and water depth is well known to be an important parameter in system design (Luo and Baudic, 2003): mooring line length, material and configuration are required to satisfy strict criteria. The inherent coupling effects between a FOWT and its mooring lines also change with water depth. As water depth increases, second–order effects play a key role on the behaviour of the platform. The slowly varying effect becomes increasingly more important, and sometimes the whole motion is dominated by the LF motion. However, due to the highly non-linear characteristics of the wave-structure interaction, the second-order wave forces may induce LF resonant response for non-taut (slack) moorings (Ormberg and Larsen 1998). Roald et al (2013) studied the effect of second-order hydrodynamics using the proprietary software WAMIT and FAST (Jonkman, 2005). Their key result for a spar-type wind turbine showed that the second-order difference-frequency hydrodynamic force was less important than the turbine thrust force. It is important to note that Roald's research considered one water depth only. The mooring line response in FAST (Version 7) uses a quasi-static coupled method and this needs to be extended in order to analyse the interactions between a floating body and its mooring system. The global motion

response of an offshore wind turbine has been well studied by many researchers (e.g. Masciola, et al, 2013), but mainly focused on comparisons between:

1) Morison's equation and diffraction theory(e.g. Karimirad,2013);
2) Coupled and non-coupled or semi-coupled methods(e.g. Karimirad,2013);
3) Linear and nonlinear incident wave theory and their impact on design and performance (e.g. Wehmeyer and Rasmussen, 2015).

For floating structures, water depth is one of the most important parameters affecting design and operation. Hence, in this chapter, the main purpose is to use a fully coupled numerical model to investigate the effect of water depth on the mooring system. By studying both operating and shutdown conditions, the effects of the second-order difference-frequency exciting forces are investigated.

5.2. Description of the wind turbine

The present study selected a baseline offshore wind turbine design of NREL, the 5MW OC-3 Hywind (Jonkman 2010). This is a spar-type FOWT, moored by three symmetrically-oriented catenary mooring lines. The main characteristics of the wind turbine are shown in Table 5.1, while the layout of the wind turbine mooring system and environmental conditions are shown in Figure 5.1. The base (design) water depth is 320m. The submerged section of the spar comprises a circular cylinder of draft 120m and diameter 9.7m. In order to reduce the hydrodynamic loads near free surface, a smaller Spar was incorporated, of length 4m and diameter 6.5m. The two cylinders were connected by a taper of length 8m, along which the diameter increased linearly from 6.5m to 9.7m. Further details are given by Jonkman (2010).

Table 5.1 Structural properties of the wind turbine (Jonkman 2010)

Items	Values
Draft (m)	120
Elevation to Platform Top (Tower Base) above SWL (m)	10
Depth to Top of Taper below SWL (m)	4
Depth to Bottom of Taper below SWL (m)	12
Platform Diameter above Taper (m)	6.5
Platform Diameter below Taper (m)	9.4
Platform Mass, including ballast (Kg)	7.46E6
CM Location below SWL along Platform Centreline (m)	89.91
Platform Roll Inertia about CM (kg*m^2)	4229.2E6
Platform Pitch Inertia about CM (kg*m^2)	4229.2E6
Platform Yaw Inertia about Platform Centreline (kg*m^2)	164.2E6

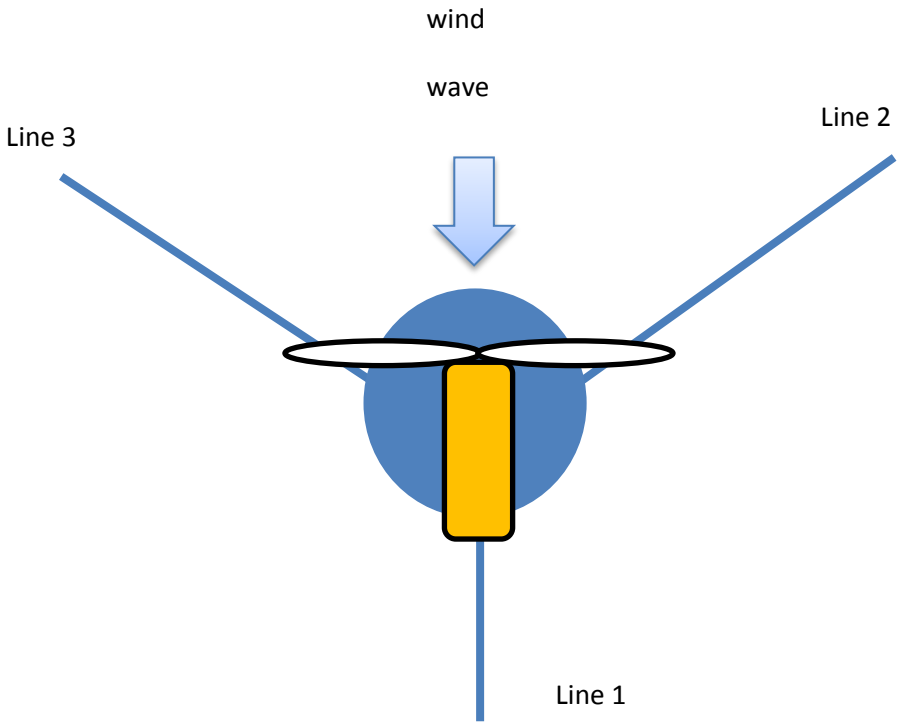

Figure 5.1 Plan view of the FOWT mooring configuration

5.3. Methodology

5.3.1. Aerodynamic modelling

As a detailed modelling of turbine thrust force is beyond the aim of the present study, the turbine thrust force was calculated using FAST (Version 7), a time-domain tool used in the design of both land-based and offshore wind turbines; it is able to incorporate aerodynamics (based on blade element momentum theory), hydrodynamics, control and electronic system dynamics and mooring line dynamics. However, to calculate the turbine thrust, we have used only the aerodynamic part of FAST. The thrust force calculated in FAST includes the turbine gravity and drag force, as well as the aerodynamic force on the blade. However, the term *thrust force* in this thesis refers to the aerodynamic loading, be it on a static or a rotating turbine. The aerodynamic loading can be evaluated either by a static turbine or a rotating turbine. In this thesis, effects from both static and rotating turbine are considered and compared.

5.3.2. Hydrodynamic modelling

Wave forces were calculated using potential flow theory and WAMIT. By solving the linear BVP, the added mass, radiation damping and wave exciting forces were calculated in the frequency domain, before running a time-domain analysis. The second–order excitation forces only include the mean drift force, which can be evaluated from the first-order BVP. In view of the long simulation time required for calculating the full QTFs, the slowly varying forces (the difference part of second–order force) were determined by Newman's approximation (Newman, 1974), which has proven to be an accurate and effective approximation of the difference part of full QTFs in deep water. As shown in the case studies of Roald et al (2013) the higher-order excitation has little effect on the spar motion; thus the sum-frequency QTFs were not included by us.

5.3.3 Mooring system modelling

Mooring system global performance was simulated by using Fastlink, a combination of FAST (Version 7) and OrcaFlex. Based on the impulse response function theory (Cummins, 1962), the wave exciting force, added mass and radiation damping were converted into time-domain exciting force, infinite added mass matrix and retardation function, respectively. By using the fully coupled time-domain simulation method, the effect of mooring line damping and the interaction between mooring line and floating body are accounted for automatically. A lumped mass model was used for the dynamic response of the mooring line. As the above wave-structure interaction modelling are based on potential flow theory, the viscous drag resulting from the relative motion between mooring line and water was evaluated as per the viscous part of Morison′s equation (Masciola et al, 2013).

5.4. Load-offset graph

Three water depths: 320m, 600m and 900m were selected for case study (Table 5.2). To reduce the number of unknowns, the mooring line tensions were determined by the static load offsets, as shown in Figure 5.2. (The asymmetry is due to the 3-line configuration shown in Figure5.1). A constant time-step of 0.01s was applied for dynamic analysis and the mooring chain segment length in OrcaFlex was 20m for all three water depths.

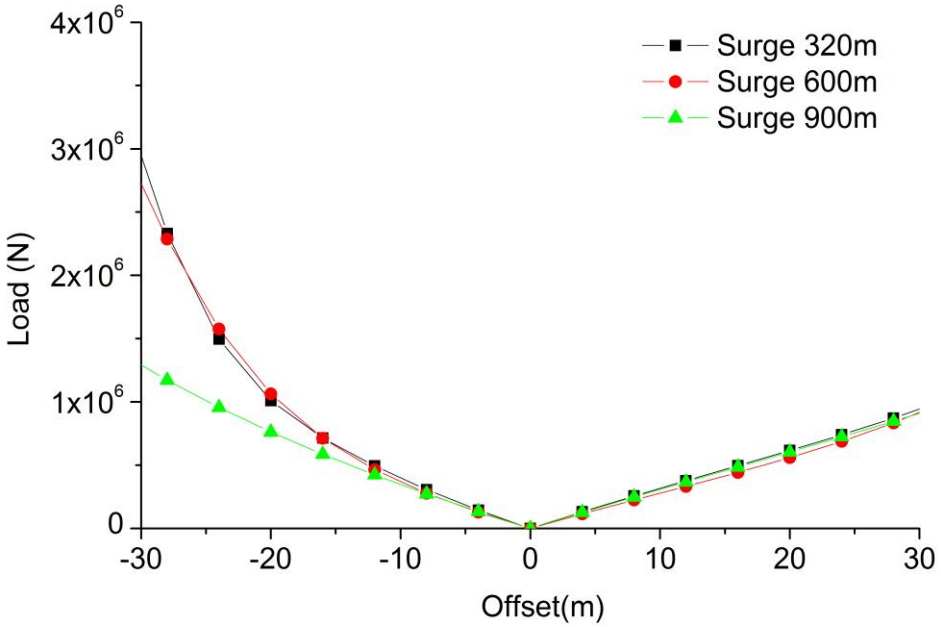

Figure 5.2(a) Surge load-offset graph

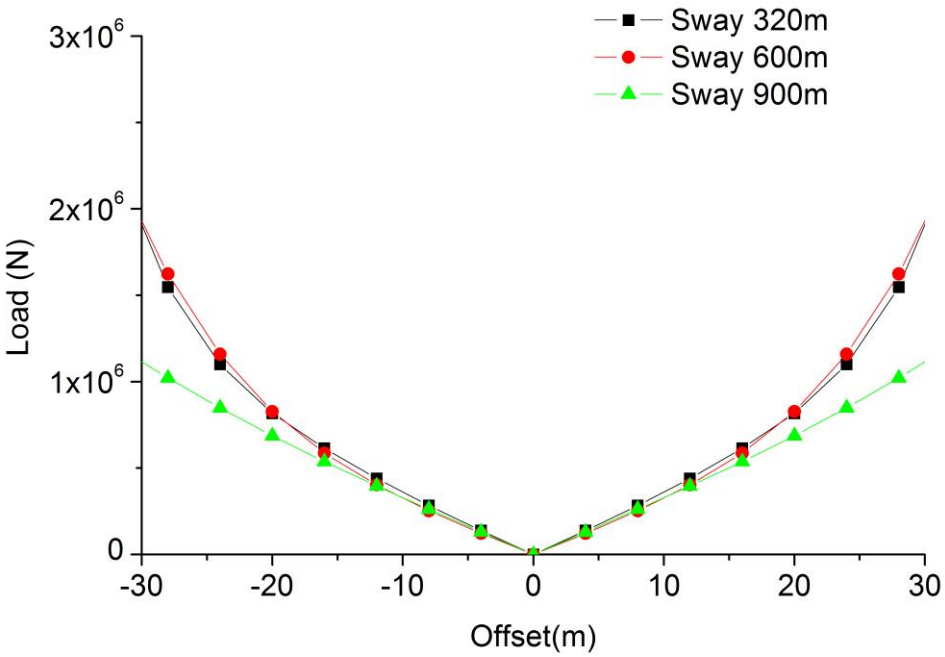

Figure 5.2(b) Sway load-offset graph

Table 5.2 Mooring system properties for different water depth

Items	Values		
Water Depth (m)	320	600	900
Number of Mooring Lines	3	3	3
Angle between adjacent lines (degree)	120	120	120
Depth to Fairleads below SWL (m)	70	70	70
Radius to Fairleads from Platform Centreline (m)	5.2	5.2	5.2
Mooring Line length (m)	902.2	1100	2180
Mooring Chain diameter (m)	0.09	0.09	0.09
Mooring chain mass (Kg/m)	77.70	77.70	77.70
Mooring chain elastic stiffness (EA) (N)	384.2E6	384.2E6	384.2E6

5.5. Validation of the floating body hydrodynamic data

As the main aim is to offer guidance on mooring system design for a FOWT, it is important and beneficial to check the validity of the present approach against published results. In terms of the mean drift force, it is also important to check the results from the first-order analysis of WAMIT, as we were unable to obtain sufficient third-party validation data. Figure 5.4 shows the spectrum of motion response and mooring line tension (Line1). The data in the figure was based on the mesh generation shown in Figure 5.3. A total 3060 meshes were generated on a quarter of the Spar. For validation purposes, the environmental conditions H_s=2.5m, T_p=9.8s, wind speed=8m/s were used, as shown in Table 5.3. The turbine status in Table 5.3 and the condition of operating and shutdown refer to the calculation of aerodynamic loading, e.g. calculated (on a static or a rotating turbine) or disabled. Results in Figure 5.4 were computed for a static turbine. The random wave for this validation and the following case studies were generated based on the JONSWAP spectrum. The very good agreement of the comparison offers a good preparation for the following case studies. The mean drift force was calculated based on the pressure integration method.

Table 5.3 List of environmental conditions for validation and case studies

(Karimirad, 2013)

Wind speed (m/s)	H_s(m)	T_p(sec)	Turbine status
8	2.5	9.8	Static turbine
8	2.5	9.8	Rotating turbine
8	2.5	9.8	Shutdown

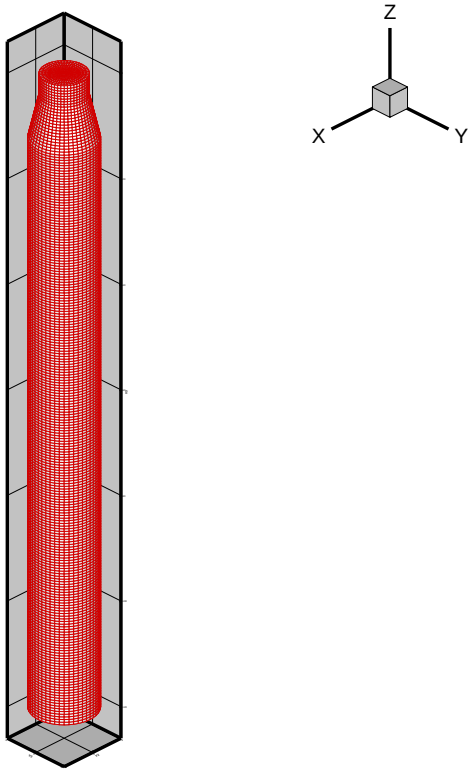

Figure 5.3 Computational mesh for the Spar

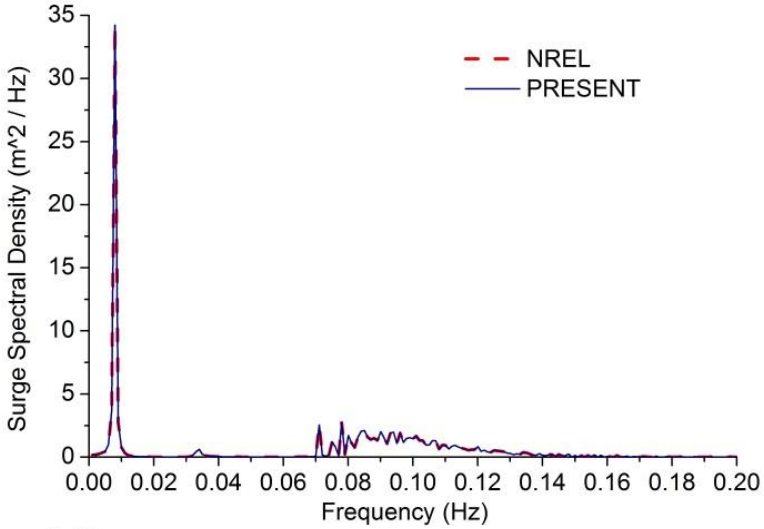
NREL
PRESENT
Surge Spectral Density (m^2 / Hz)
Frequency (Hz)
0
5
10
15
20
25
30
35
0.00
0.02
0.04
0.06
0.08
0.10
0.12
0.14
0.16
0.18
0.20

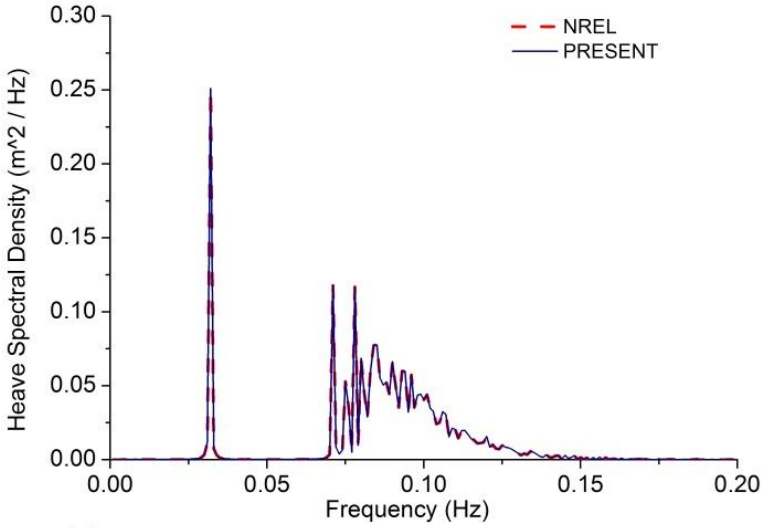
NREL
PRESENT
Heave Spectral Density (m^2 / Hz)
Frequency (Hz)
0.00
0.05
0.10
0.15
0.20
0.25
0.30
0.00
0.05
0.10
0.15
0.20

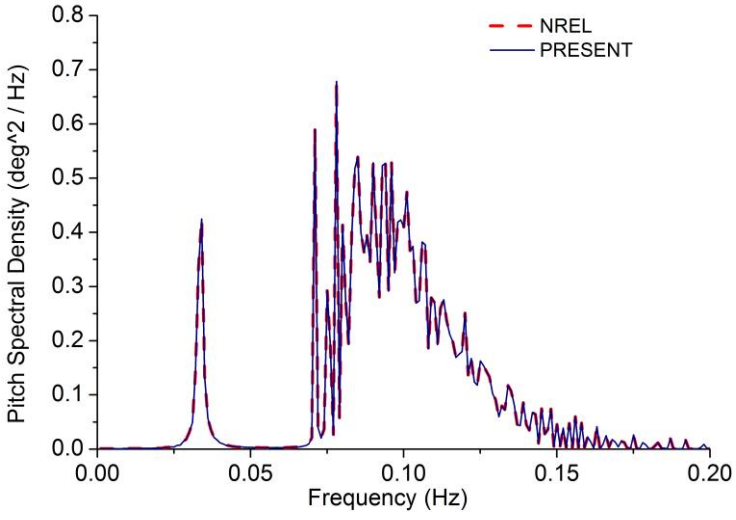
NREL
PRESENT
Pitch Spectral Density (deg^2 / Hz)
Frequency (Hz)
0.0
0.1
0.2
0.3
0.4
0.5
0.6
0.7
0.8
0.00
0.05
0.10
0.15
0.20

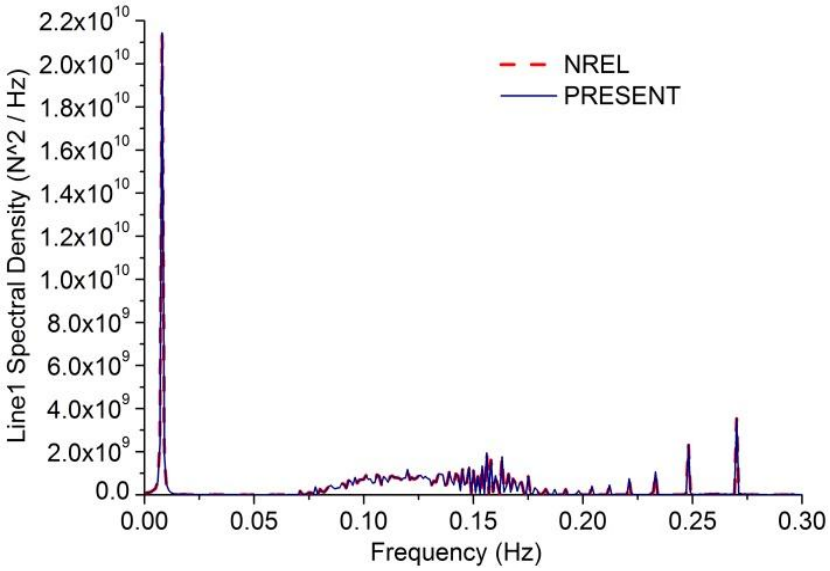

Figure 5.4 Comparison of spectral density results

5.6. Parametric study results

The selected sea state for the case studies corresponds approximately to limiting conditions between operational and shutdown scenarios. Three water depths are considered: 320m, 600m and 900m; see Tables 5.3 and 5.4. The total simulation time was 4600s. The operating turbine refers to the evaluation of the aerodynamic loading. The initial transit behaviour (1000s) was deleted for the present spectral analysis. Table 5.5 shows the natural frequency of the FOWT.

Table 5.4 List of case studies of the FOWT

1	320m,op no drift, static rotor	7	600m,op no drift, static rotor	13	900m,op no drift, static rotor
2	320m,op no drift, dynamic rotor	8	600m,op no drift, dynamic rotor	14	900m,op no drift, dynamic rotor
3	320m,op with drift, static rotor	9	600m,op with drift, static rotor	15	600m,op with drift, static rotor
4	320m,op with drift, dynamic rotor	10	600m,op with drift, dynamic rotor	16	900m,op with drift, dynamic rotor
5	320m,sd no drift	11	600m,sd no drift	17	900m,sd no drift
6	320m,sd with drift	12	600m,sd with drift	18	900m,sd with drift

Table 5.5 Natural frequencies of the FOWT (Karimirad, 2013)

Motion	Natural frequency (Hz)
Surge/Sway	0.008
Pitch/roll	0.035
Heave	0.032
Yaw	0.134

Figures 5.5~5.8 show the motion response and line tension. Figures 5.9 and 5.10 illustrate statistical comparisons: mean and maximum results, plus standard deviations. Operating and shutdown conditions were simulated with and without second-order drift forces. Each spectral density was smoothed via a Fourier Transform to reduce noise (OrcaFlex). For heave, the FOWT was placed at the vertical static mean position before running the time-domain simulations.

From the motion response spectra in Figures 5.5~5.7 we can see that the WF motion response is almost independent of water depth and has no difference between case studies, in contrast to the LF motion. The turbine thrust force has no effect on the WF parts of the motion. However, in the spectrum of the mooring line tension (Figure 5.8), the LF response plays an important role when the water depth is 320m. The WF mooring line response increases with water depth and for 900m the mooring line tension response is completely determined by the WF response. For a catenary chain, the dynamic response becomes more important as water depth increases, which is in accordance with the results of a JIP Spar moored by four equal chains (Chen et al, 2001).

- **Surge motion**

It can be seen from Figure 5.5 that the LF surge motion is affected by both drift force and turbine thrust. The effect of the drift force is less important for larger water depths (>~900m) as the surge spectral density is dominated by the WF response. There is another peak of the surge spectrum near 0.035Hz. This is due to surge and pitch coupling: the natural frequency of pitch is 0.035Hz. However, this coupling is less important when the turbine is operating (both static and rotating turbine). The thrust

force increases both mean and maximum values of surge, as is seen in Figure 5.9.1. The mean surge position is approximately zero under shutdown and static turbine conditions, but increases to 13m when the turbine is rotating, in 320m. However, the effect of the turbine only affects the mean position of the Spar. The difference between the mean and maximum values of surge is almost unchanged.

- **Heave motion**

In contrast to its effect on surge, the drift force significantly influences the LF part of heave motion, especially for relatively shallower water depth (320m, Figure 5.6.1). However, it is interesting to see that the turbine thrust force has little effect on the heave motion, especially for large water depth. Under static turbine condition, heave spectrum shows no difference compared with shutdown condition (e.g. the green line and the pink line in Figure 5.6.1). The dynamic thrust force has an effect on the LF motion on heave under 320m water depth. But when water depth increases (e.g. 900n), there is no difference between rotating or static turbine. So, in the design process, a non-coupled analysis, treating the substructure and the upper structure separately, can be used for the heave motion, under water depth larger than 900m. Furthermore, Figure 5.9.2 shows the statistical results of heave motion. The dynamic thrust force increases the absolute mean and maximum value of heave motion, but this effect is less important for 900m water depth, which is in accordance with the heave spectrum.

- **Pitch motion**

Drift affects the pitch motion only under the shutdown condition (Figures 5.7). The pitch spectral densities are dominated by WF response except for a shutdown plus drift force condition. Similar to surge response, treating the aerodynamic loading as an applied load fails to predict the mean and maximum pitch position, but the difference between mean value and maximum value is independent of water depth and different case studies (Figure 5.9.3). Unlike surge and heave motion, the standard deviation of pitch motion is less sensitive to water depths and case studies, as can be

seen from Figure 5.10.1.

- **Yaw motion**

Because of the mooring line layout and the direction of environmental loading (Figure 5.1), the theoretical yaw motion response is zero degree. There is a noticeable difference of yaw motion between a rotating turbine and shut down condition and a less significant difference between a static turbine and shutdown condition (Figures 5.8, 5.10.4 and 5.11.3). However, the maximum difference of yaw motion is within 1 degree, even for a rotating turbine.

- **Worst loaded line tension (line2)**

Drift has an effect on mooring line LF response for 320m water depth (Figure 5.8.1), but becomes less important as depth increases, as the mooring line tension response is completely determined by the WF response. The effect of a rotating turbine has a significant effect on mooring line WF response and this becomes increasingly important for large water depth (>~900m), where the mooring line response is dominated by the WF response. From Figure 5.9.4 we can see that both maximum and mean values of mooring line tension increase with water depth. The dynamic thrust force increases the mean value of mooring line tension, but the results for the mooring line tension show no difference between a static turbine and shut down condition. As for the motion responses, the dynamic thrust force only increases the mean value of mooring tension, while the difference between mean and maximum values remain constant. The wave drift force, in contrast to the dynamic thrust force, has no effect on the standard deviation of mooring line tension, as can be seen from Figure 5.10.2.

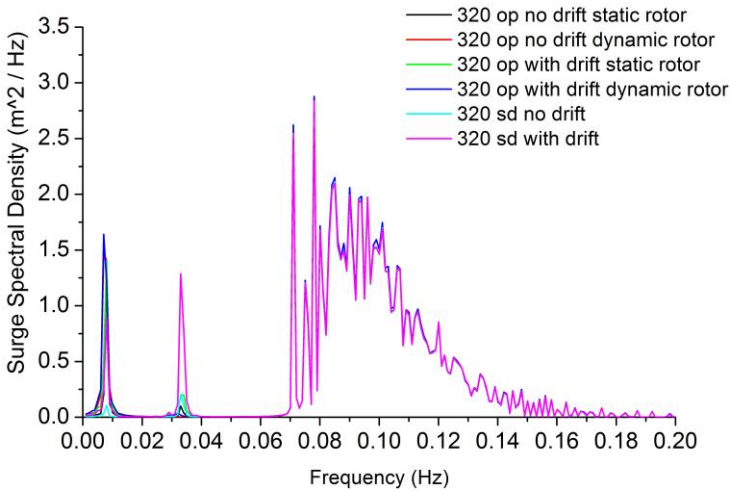

Figure 5.5.1 Surge 320m Hs2.5 Tp9.8

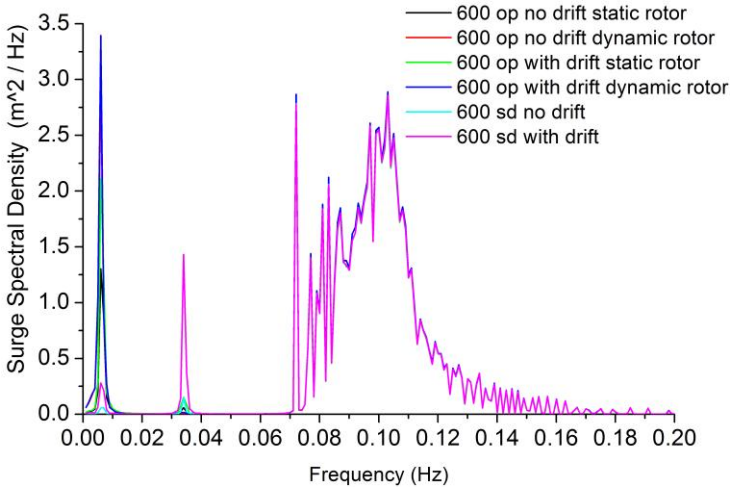

Figure 5.5.2 Surge 600m Hs2.5 Tp9.8

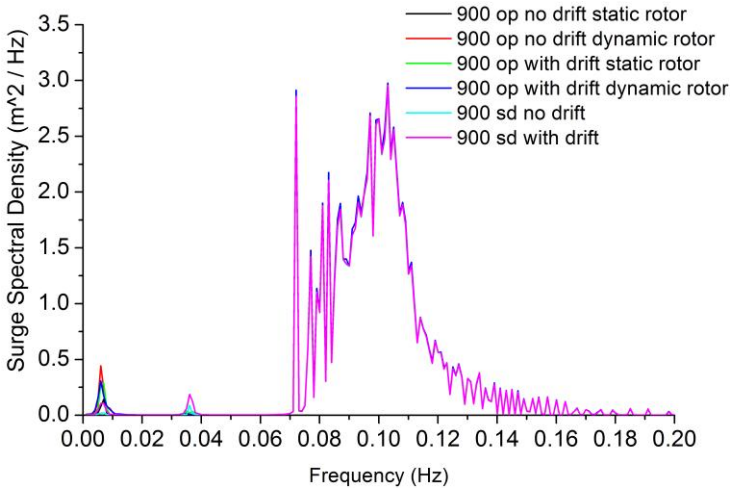

Figure 5.5.3 Surge 900m Hs2.5 Tp9.8

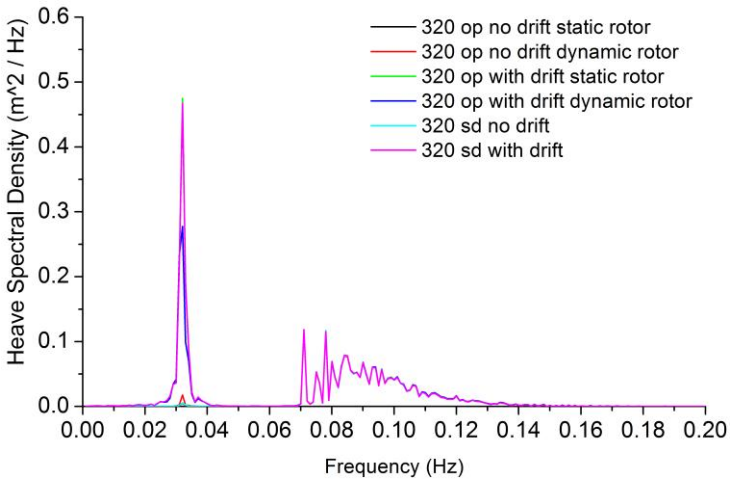

Figure 5.6.1 Heave 320m Hs2.5 Tp9.8

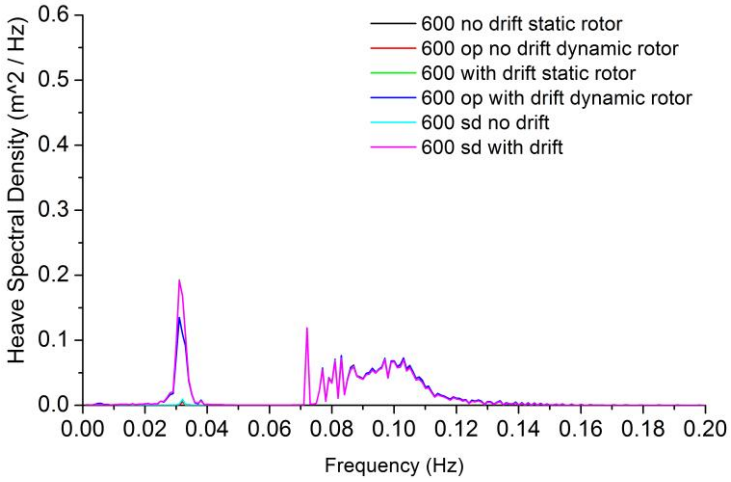

Figure 5.6.2 Heave 600m Hs2.5 Tp9.8

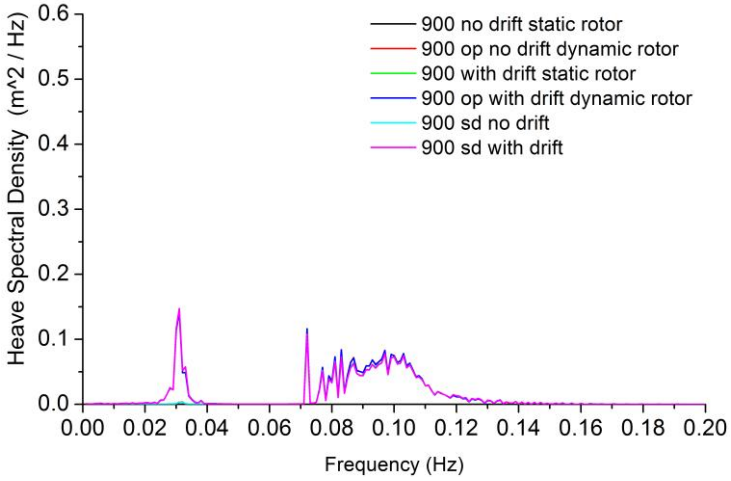

Figure 5.6.3 Heave 900m Hs2.5 Tp9.8

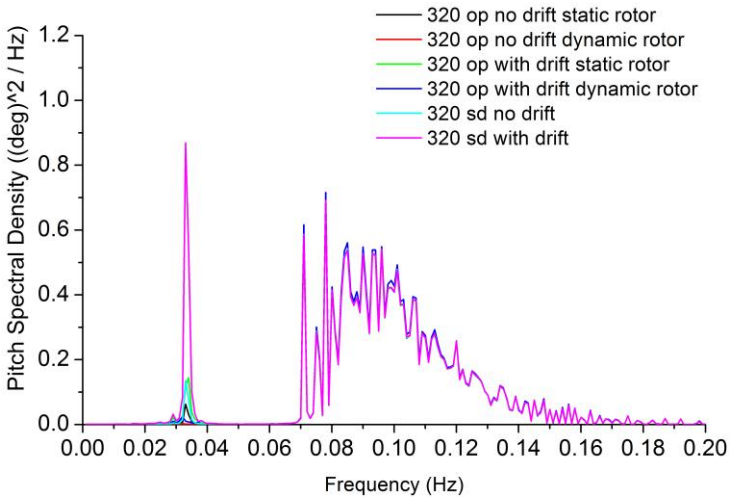

Figure 5.7.1 Pitch 320m Hs2.5 Tp9.8

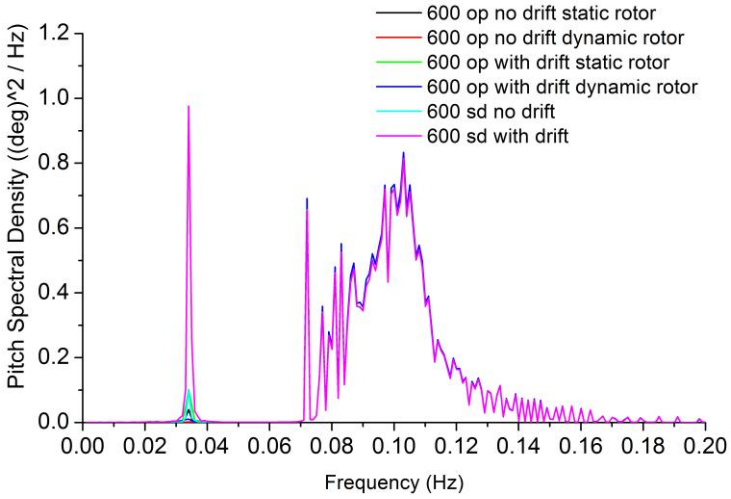

Figure 5.7.2 Pitch 600m Hs2.5 Tp9.8

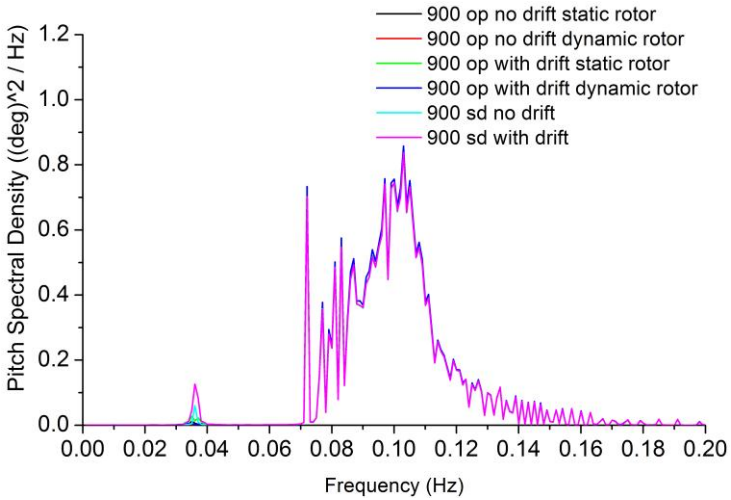

Figure 5.7.3 Pitch 900m Hs2.5 Tp9.8

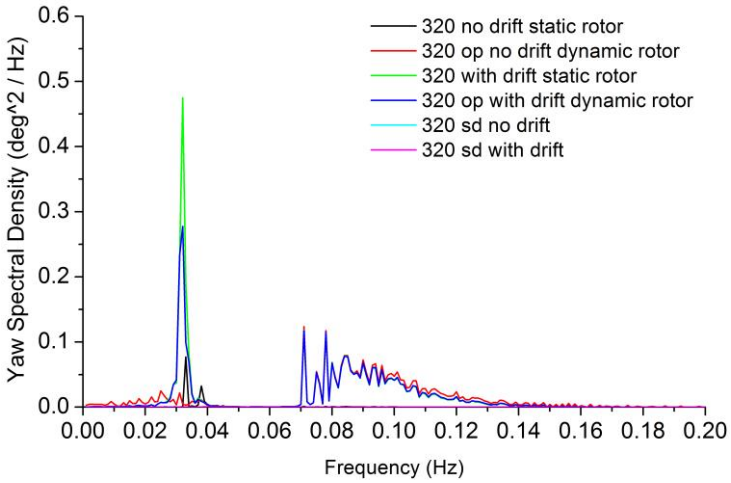

Figure 5.8.1 Yaw 320m Hs2.5 Tp9.8

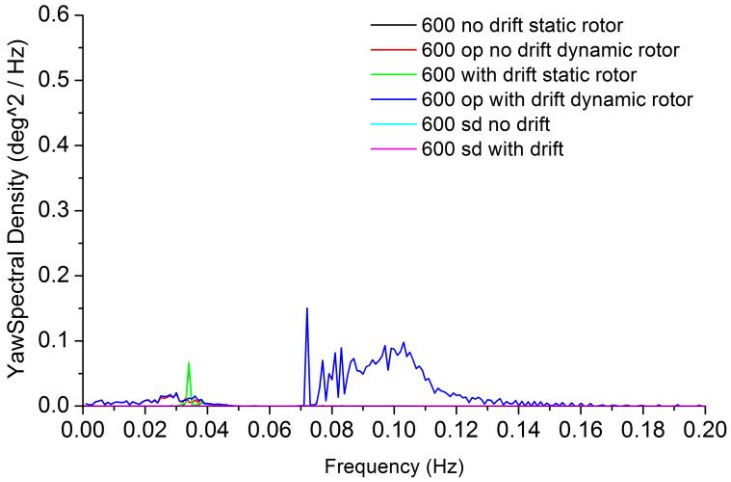

Figure 5.8.2 Yaw 600m Hs2.5 Tp9.8

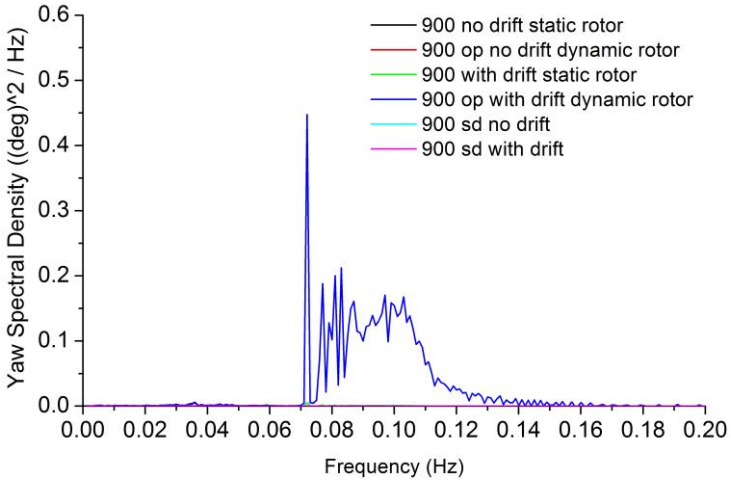

Figure 5.8.3 Yaw 900m Hs2.5 Tp9.8

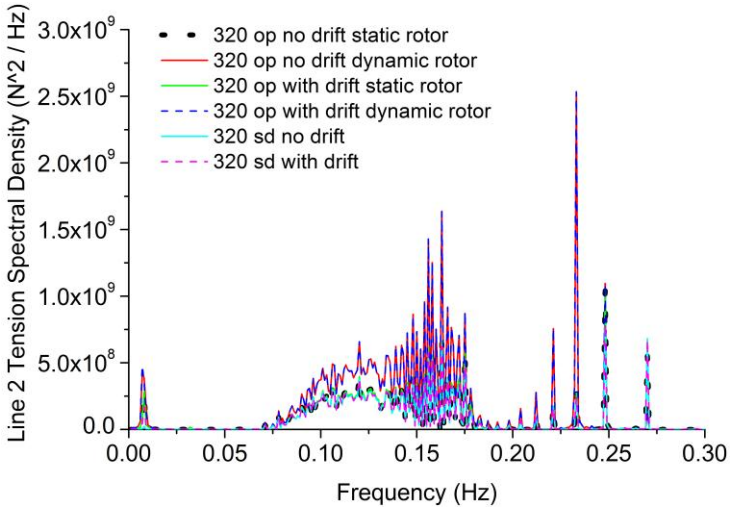

Figure 5.9.1 Line2 Tension 320m Hs2.5 Tp9.8

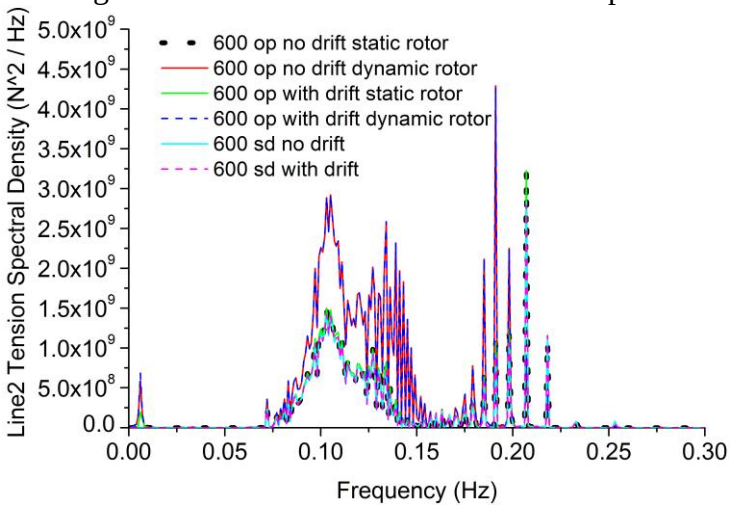

Figure 5.9.2 Line2 Tension 600m Hs2.5 Tp9.8

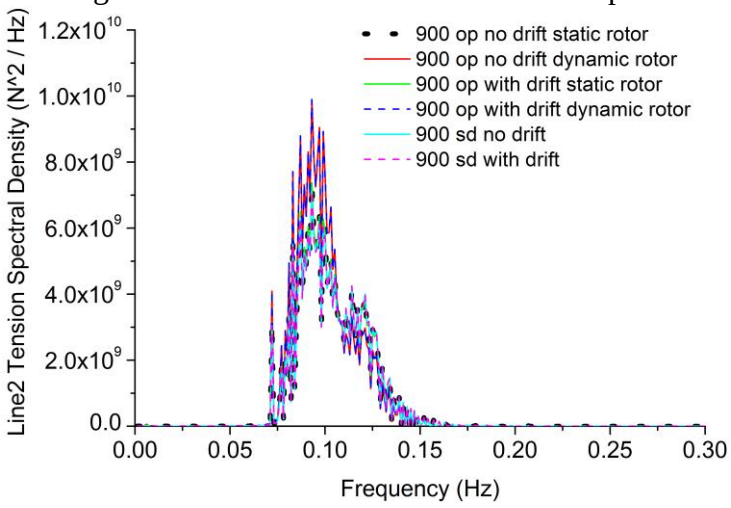

Figure 5.9.3 Line2 Tension 900m Hs2.5 Tp9.8

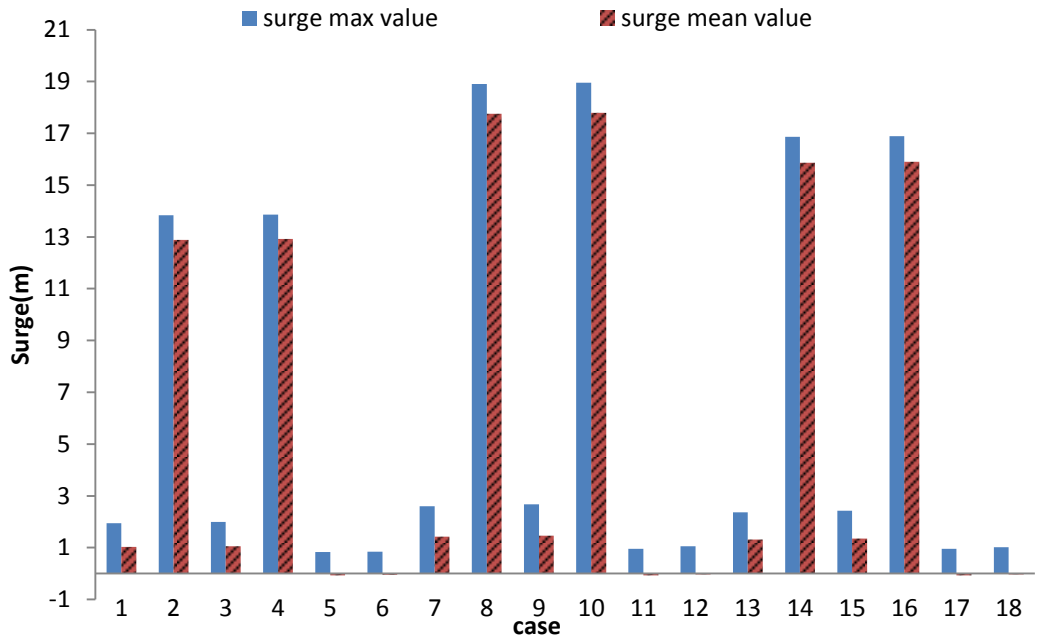

Figure 5.10.1 Surge motion statistics Hs2.5 Tp9.8

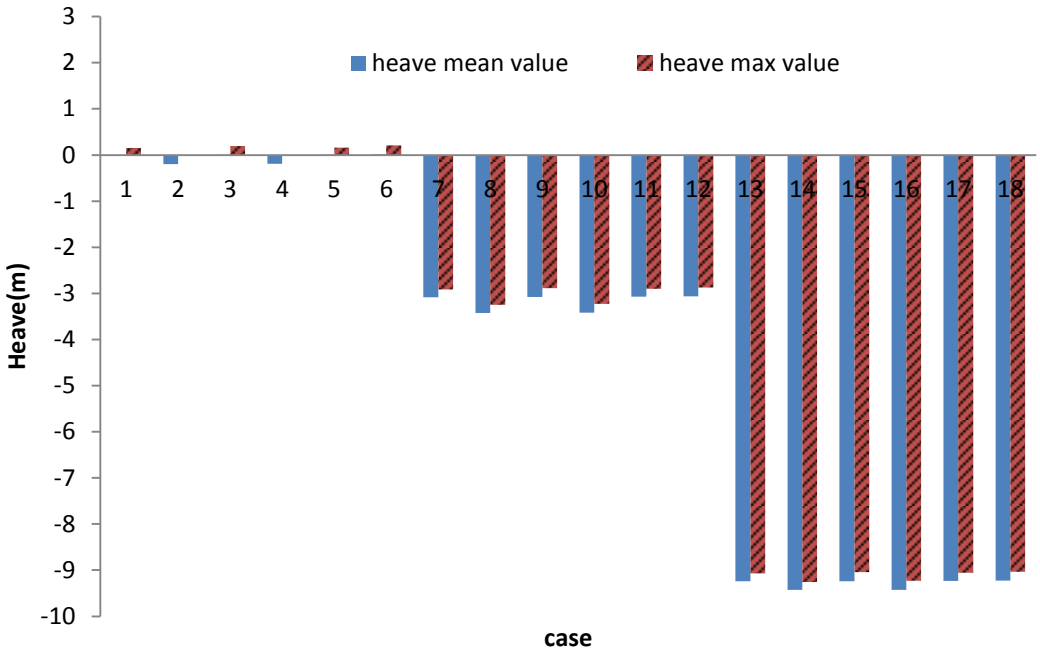

Figure 5.10.2 Heave motion statistics Hs2.5 Tp9.8

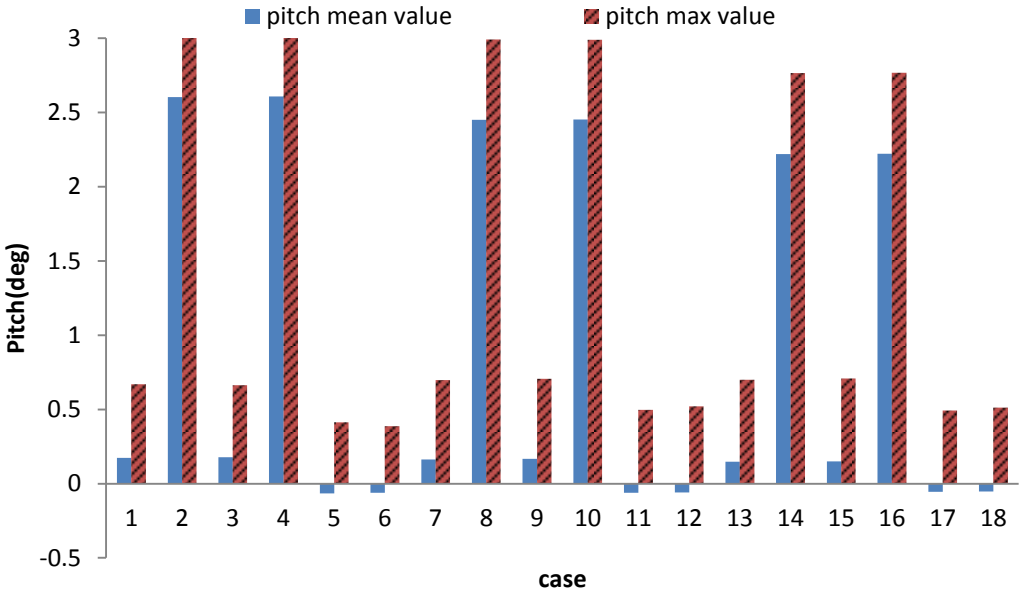

Figure 5.10.3 Pitch motion statistics Hs2.5 Tp9.8

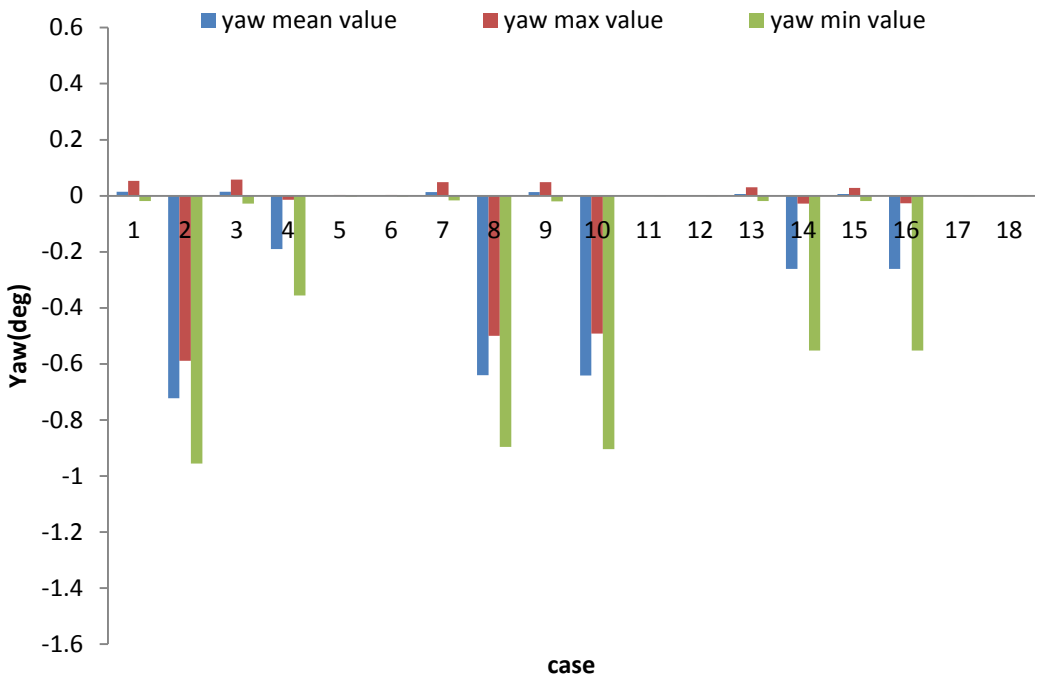

Figure 5.10.4 Yaw motion statistics Hs2.5 Tp9.8

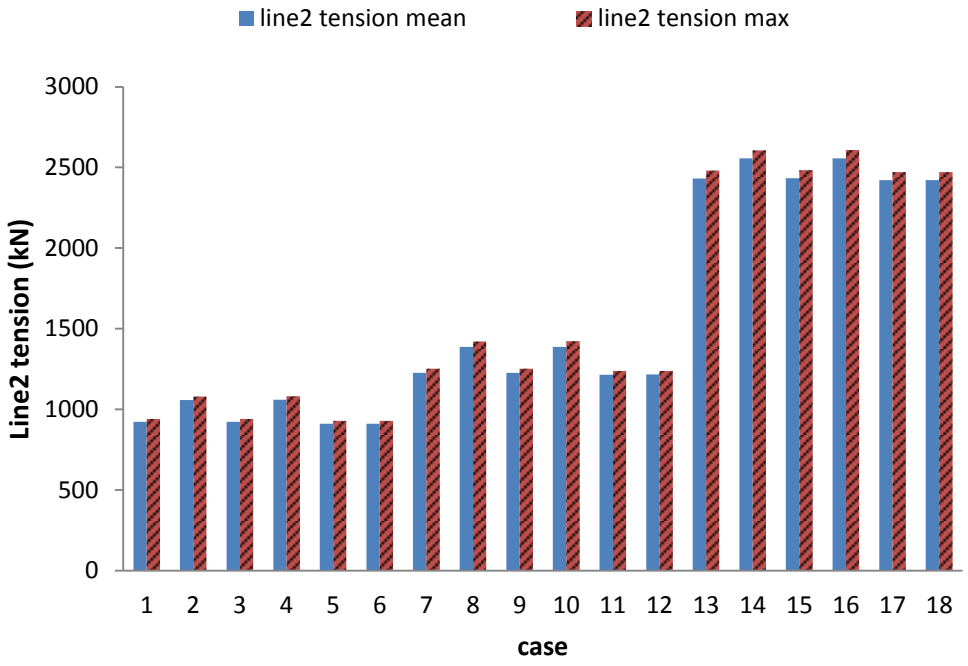

Figure 5.10.5 Line2 tension statistics Hs2.5 Tp9.8

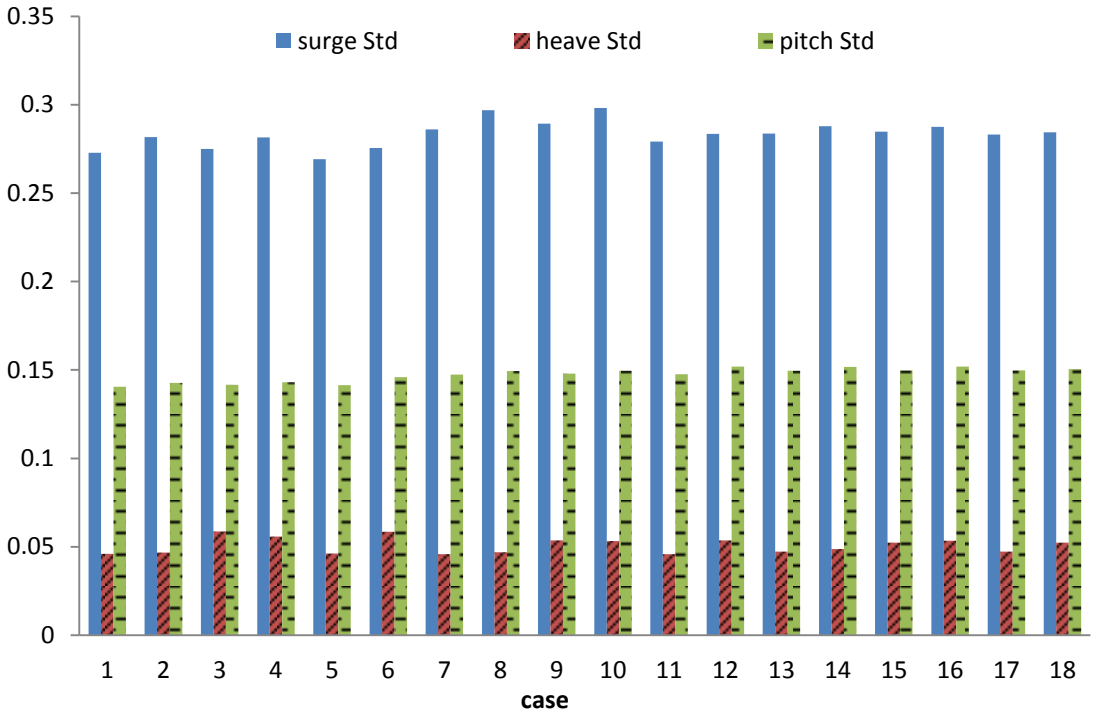

Figure 5.11.1 Standard deviation of motion responses(surge, heave and pitch) Hs2.5 Tp9.8

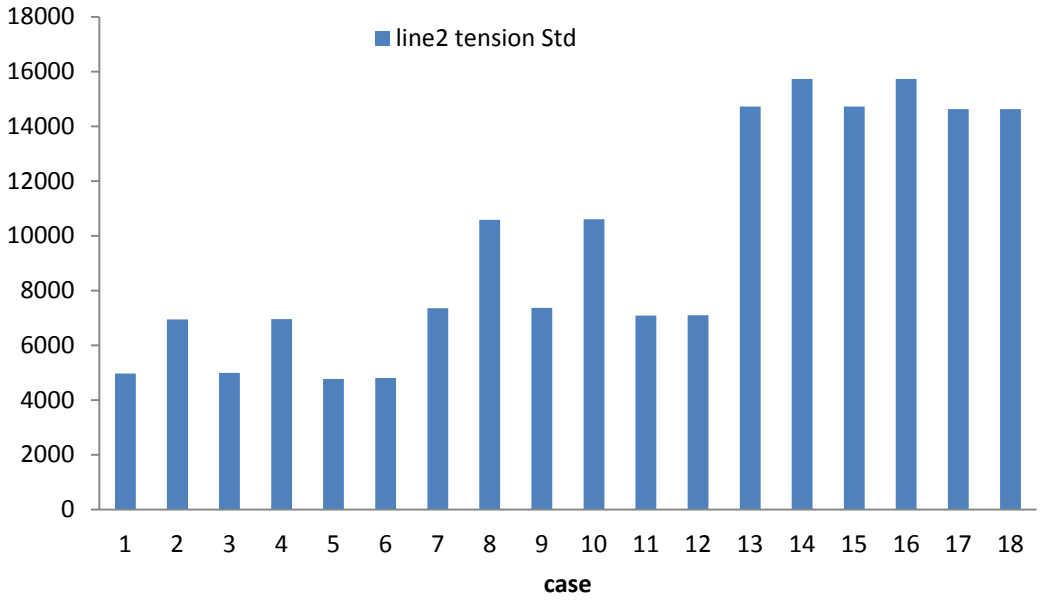

Figure 5.11.2 Standard deviation of line2 tension Hs2.5 Tp9.8

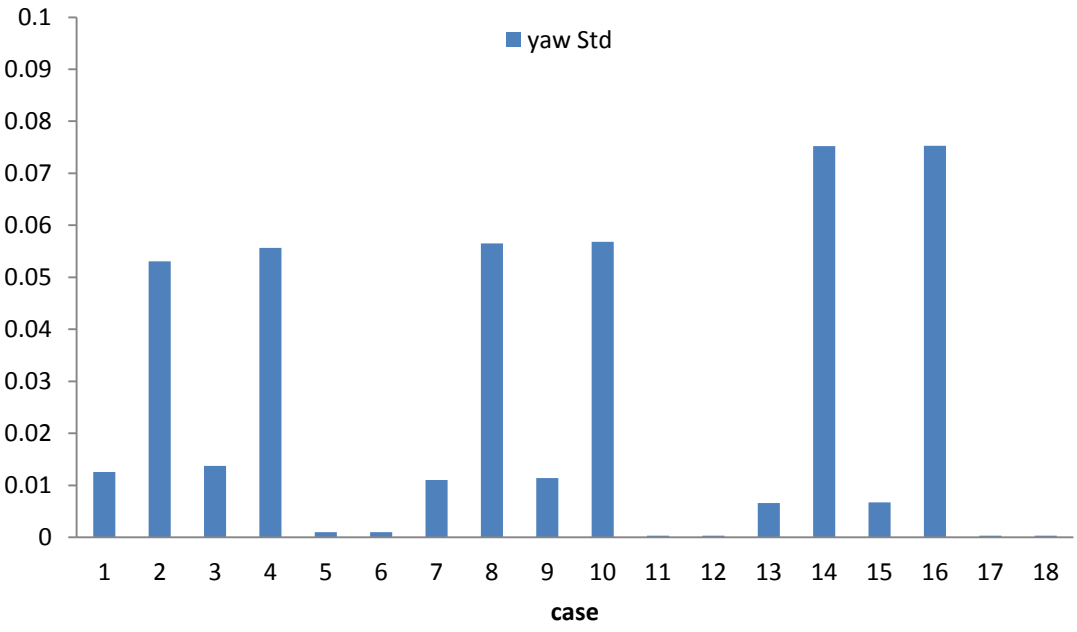

Figure 5.11.3 Standard deviation of Yaw motion Hs2.5 Tp9.8

6. Dynamic analysis of elastic lines

6.1. Introduction

In this chapter, balancing between the efficiency and accuracy, the elastic rod theory has been applied for the simulation of mooring line. First the formulations of the elastic rod theory are presented, followed by the numerical method and validation. The traditional rod theory has been extended to allow for large stretch by applying an enhanced stiffness method. By using an approximation of the nonlinear tension-elongation relationship with Taylor series expansion (Ćatipović et al., 2011), the mathematical and numerical formulation of large extensible mooring line are developed.

The developed elastic line modelling has been applied on the simulation of a taut moored FOWT with three mooring lines. The maximum mooring line tension along arc length was compared, under wave only condition. A fully coupled method has been applied for the analysis of the motion response and mooring line tension of the wind turbine in waves. Comparisons between different orders of Taylor series expansion show the accuracy of the elongation condition. This chapter also studied a taut-moored FOWT with one mooring line broken. Comparisons of motion responses and line tension were made between intact and damaged condition. Another application of the developed method is the comparison between current method and the linear spring method for a taut-moored FOWT, under both operating and shutdown condition.

6.2. Formulation of the elastic rod theory

6.2.1. Equation of motion for polyester mooring line

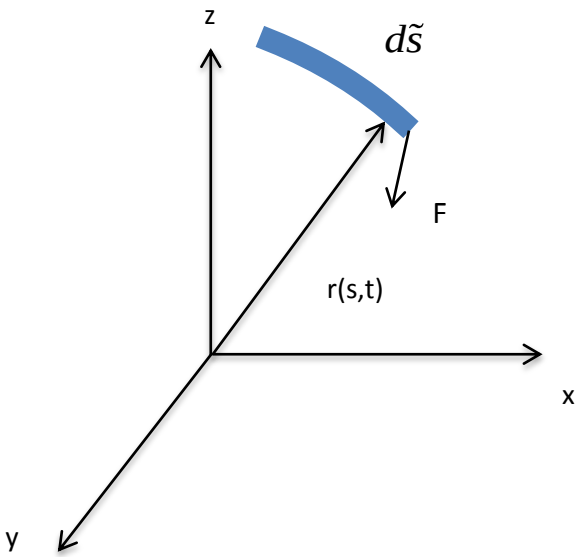

Figure 6.1 Coordinate of Rod

The following equation of motion for an elastic rod and the elongation condition follow Garrett (1982) and Ćatipović et al. (2011). The centreline of each rod is described by a space-time curve $r(s,t)$. So the unit tangent to the space curve is r'. The principle normal and bi-normal are directed along r'' and $r'\times r''$, respectively. Considering a stretchable rod element shown in Figure 6.1, the un-stretched and stretched lengths are s and $\tilde{s}$. The force and moment equilibrium equations can be written as

$$F' + q = \rho\ddot{r} \tag{6.1}$$

$$M' + r' \times F + m = 0 \tag{6.2}$$

In equations (6.1), (6.2) and the following derivations, we have $F' = \frac{dF}{d\tilde{s}}$ and $M' = \frac{dM}{d\tilde{s}}$. F and q are the resultant force and distribute load, respectively. M and m are resultant moment and applied moment per unit length. The dot with respect to r denotes time derivation.

For an elastic rod with equal bending stiffness, the resultant moment M satisfy the following equation (Garrett, 1982)

$$M = Br' \times Hr'' \tag{6.3}$$

where B and H are bending stiffness and torque.

Substituting (6.3) into (6.2), we have

$$r' \times [(Br'')' + F] + H'r' + Hr'' + m = 0 \tag{6.4}$$

Assuming both the torque H and the applied moment per unit length m to be zero, (6.4) becomes

$$r' \times [(Br'')' + F] = 0 \tag{6.5}$$

Re-arranging (6.5) we have

$$F = -(Br'')' + \lambda r' \tag{6.6}$$

where

$$\lambda = F \cdot r' + (Br'')' \cdot r' = T - B\kappa^2 \tag{6.7}$$

where κ is the curvature of the rod and T the effective tension.
The scalar product $\lambda(s,t)$ is a Lagrange multiplier, for which the physical meaning is the effective tension of the mooring line/riser. For mooring lines, bending stiffness can be ignored, so we have

$$\lambda = F \cdot r' = T \tag{6.8}$$

Combining (6.6) and (6.8) with (6.1) we have the equation of motion for an elastic line

$$\frac{d}{d\tilde{s}}(\lambda \frac{dr}{d\tilde{s}}) + q_E = \rho \ddot{r} \tag{6.9}$$

Plus, the elastic line must satisfy the following equation

$$\frac{dr}{d\tilde{s}} \frac{dr}{d\tilde{s}} = 1 \tag{6.10}$$

The standard definition of the elongation ε can be written as

$$\varepsilon = \frac{d\tilde{s} - ds}{ds} \tag{6.11}$$

so we have the following relationship

$$d\tilde{s} = (1+\varepsilon)ds \tag{6.12}$$

Substituting (6.12) into (6.9) and (6.10), we have the following rod equation of motion (Ćatipović,et al, 2011)

$$\frac{d}{ds}\left(\frac{T_E}{1+\varepsilon}\frac{dr}{ds}\right) + (1+\varepsilon)q_E = (1+\varepsilon)\rho\ddot{r} \tag{6.13}$$

$$\frac{1}{(1+\varepsilon)^2}\frac{dr}{ds}\frac{dr}{ds} = 1 \tag{6.14}$$

where q_E is the load acting on the rod, including its submerged weight, the hydrostatic force and the hydrodynamic loading. Morison's equation (1950) was used to calculate the hydrodynamic loads on the mooring line:

$$q_n = C_M \rho A_e \ddot{r}_n + C_I \rho A_e \dot{V}_n + \frac{1}{2} C_D \rho \left|V_n - \dot{r}_n\right| (V_n - \dot{r}_n) \tag{6.15}$$

where *n* denotes the normal component.

The rod velocity and acceleration normal are given by

$$\dot{r}_n = \dot{r} - (\dot{r} \cdot r') \cdot r' \tag{6.16}$$

$$\ddot{r}_n = \ddot{r} - (\ddot{r} \cdot r') \cdot r' \tag{6.17}$$

Following Ćatipović et al, assuming equal principal stiffness, the relationship between the effective tension T_E and elongation can be written as

$$\varepsilon = \frac{T_E}{AE} \tag{6.18}$$

where *AE* is the axial stiffness.

In the static problem, the weight and diameter of the mooring line are related to the elongation ε .The cross-sectional area and weight after elongation can be written as $A/(1+\varepsilon)$ and $m/(1+\varepsilon)$, respectively (Ćatipović, et,al 2011), where *A* and *m* are the cross-section area and weight of the mooring line without stretch. Applying the above

relationship to the motion equation, we see that the term $(1+\varepsilon)$ cancels out when multiplied by the applied force q_E . For the hydrodynamic force calculated by Morison's equation, the weight and cross-sectional area for one element are assumed constant.

Equations (6.13) and (6.14) show the rod motion equation and elongation condition, respectively. They are non-linear. In the following section, we will describe a numerical procedure for solving this non-linear equation and the required order of approximation for the elongation condition.

6.2.2. Numerical Implementation

6.2.2.1. Static Problem

For the static problem, the space-time curve r is independent of time. Consequently the inertial term in equation (6.13) is deleted. We therefore have

$$\frac{d}{ds}\left(\frac{T_E}{1+e}\frac{dr}{ds}\right)+q=0 \tag{6.19}$$

Using the Taylor series expansion, the elongation relationship can be written as:

$$\frac{1}{(1+e)^2}=1-2e+3e^2+o(e^3) \tag{6.20}$$

However, it is not clear, *a priori*, whether the third-order term should be included explicitly. In the present paper, the order of expansion and subsequent results will be discussed.

In the FEM, the variables r_i and T_E may be approximated (Garrett, 1982) as

$$r_i(s,t)=\sum_{k=1}^{4}A_k(s)U_{ik}(t) \tag{6.21}$$

$$T_E(s,t)=\sum_{m=1}^{3}P_m(s)\lambda_m(t) \tag{6.22}$$

where A_k and P_m are shape functions. The definition of the shape functions is as follows (Garrett, 1982)

$$\begin{aligned} A_1 &= 1-3\xi^2+2\xi^3 \\ A_2 &= \xi-2\xi^2+\xi^3 \\ A_3 &= 3\xi^2-2\xi^3 \\ A_4 &= \xi^2-2\xi^3 \end{aligned} \tag{6.23}$$

$$\begin{aligned} P_1 &= 1-3\xi\ +2\xi^2 \\ P_2 &= 4\xi\ (1-\xi) \\ P_3 &= \xi\ (2\xi-1) \end{aligned} \tag{6.24}$$

U_{ik} and l_m are unknown variables. The subscript *i* of U_{ik} denotes the dimension of the element. For the 3-dimensional problem, *i*=3. For *k*=1 and 3, U_{ik} represents the space position of the rod at two ends while for *k*=2 and 4 U_{ik} denotes the space derivative at both ends. λ is the Lagrange multiplier. The physical meaning of λ is mooring line tension at both end and middle of the rod.

The variable U_{ik} and λ are defined as:

$$\begin{aligned} U_{i1} &= r_i(0,t), U_{i2} = Lr_i'(0,t) \\ U_{i3} &= r_i(L,t), U_{i4} = Lr_i'(L,t) \end{aligned} \tag{6.25}$$

$$\lambda_1 = \lambda\ (0,t), \lambda_2 = \lambda\ (\frac{L}{2},t), \lambda_3 = \lambda\ (L,t) \tag{6.26}$$

Using Galerkin's method (Bathe, 1996) and integrating the motion equation from 0 to *L* over the length of the element, the final form of motion equation for static problem in notation form can be written as

$$\hat{K}_{nijlk}\lambda_n U_{jk} - F_{il} = 0 \tag{6.27}$$

where

$$\hat{K}_{nijlk} = K^0_{nijlk} + \lambda_m K^1_{nmijlk} + \lambda_m\lambda_p K^2_{nmpijlk} \tag{6.28}$$

$$K^0_{nijlk} = \int_0^L P_n A_l' A_k' \delta_{ij} ds \tag{6.29}$$

$$K^1_{nmijlk} = -\int_0^L \frac{1}{EA} P_n P_m A_l' A_k' \delta_{ij} ds \tag{6.30}$$

$$K^2_{nmqijlk} = \int_0^L \frac{1}{(EA)^2} P_n P_m P_q A_l' A_k' \delta_{ij} ds \tag{6.31}$$

where δ is Kronecker Delta function and the standard double-suffix summation condition has been used.

The elongation condition, incorporating Taylor series expansion to second order, can be written as

$$\hat{B}_{mil}U_{ki}U_{kl} - C_m = 0 \tag{6.32}$$

where

$$\hat{B}_{mil} = B^0_{mil} + \lambda_n B^1_{nmil} + \lambda_n\lambda_p B^2_{npmil} \tag{6.33}$$

$$B^0_{mil} = \int_0^L P_m A'_i A'_l ds \tag{6.34}$$

$$B^1_{nmil} = -\int_0^L \frac{2}{EA} P_m P_n A'_i A'_l ds \tag{6.35}$$

$$B^2_{mnqil} = \int_0^L \frac{3}{(EA)^2} P_m P_n P_q A'_i A'_l ds \tag{6.36}$$

$$C_m = \int_0^L P_m ds \tag{6.37}$$

Recalling the motion equation (6.27) and the elongation condition (6.32), Newton-Raphson iteration was applied to the static problem (Ran, 2000). Omitting higher order components, we have

$$R^{(n+1)}_{il} = R^{(n)}_{il} + \frac{\partial R_{il}}{\partial U_{jk}}(\Delta U_{jk}) + \frac{\partial R_{il}}{\partial \lambda_n}(\Delta\lambda_n) = 0 \tag{6.38}$$

$$G^{(n+1)}_{m} = G^{(n)}_{m} + \frac{\partial G_{m}}{\partial U_{jk}}(\Delta U_{jk}) + \frac{\partial G_{m}}{\partial \lambda_n}(\Delta\lambda_n) = 0 \tag{6.39}$$

Re-arranging (6.38) and (6.39), we have

$$\begin{bmatrix} K^{11(n)}_{ijlk} & K^{12(n)}_{iln} \\ K^{21(n)}_{mjk} & K^{22(n)}_{mn} \end{bmatrix} \begin{Bmatrix} \Delta U_{jk} \\ \Delta\lambda_n \end{Bmatrix} = -\begin{Bmatrix} R^{(n)}_{il} \\ G^{(n)}_{m} \end{Bmatrix} \tag{6.40}$$

where

$$K^{11(n)}_{ijlk} = \hat{K}^{(n)}_{nijlk}\lambda^{(n)}_n \tag{6.41}$$

$$K^{12(n)}_{iln} = K^0_{nijlk} + 2\lambda_m K^1_{nmijlk} + 3\lambda_m\lambda_p K^2_{nmpijlk} U^{(n)}_{jk} \tag{6.42}$$

$$K^{21(n)}_{mjk} = K^{12(n)}_{iln} \tag{6.43}$$

$$K^{22(n)}_{mn} = (B^1_{mnkl} + 2\lambda_p B^2_{pmnkl}) U^{(n)}_{jl} U^{(n)}_{jk} \tag{6.44}$$

$$R_{il}^{(n)} = \hat{K}_{nijlk}^{(n)} U_{jk}^{(n)} - F_{il} \tag{6.45}$$

$$G_{m}^{(n)} = \hat{B}_{mil} U_{ki} U_{kl} - C_{m} \tag{6.46}$$

In the program, the above equation of the Newton-Raphson method can be written in matrix form

$$K^{(n)}(\Delta y) = F^{(n)} \tag{6.47}$$

where K and F are the same as the stiffness matrix and forcing vector in equation (6.40). Δy includes ΔU_{jk} and $\Delta \lambda_n$. In the static problem, n represents the step of iteration. Figure 6.2 shows a flowchart of static analysis.

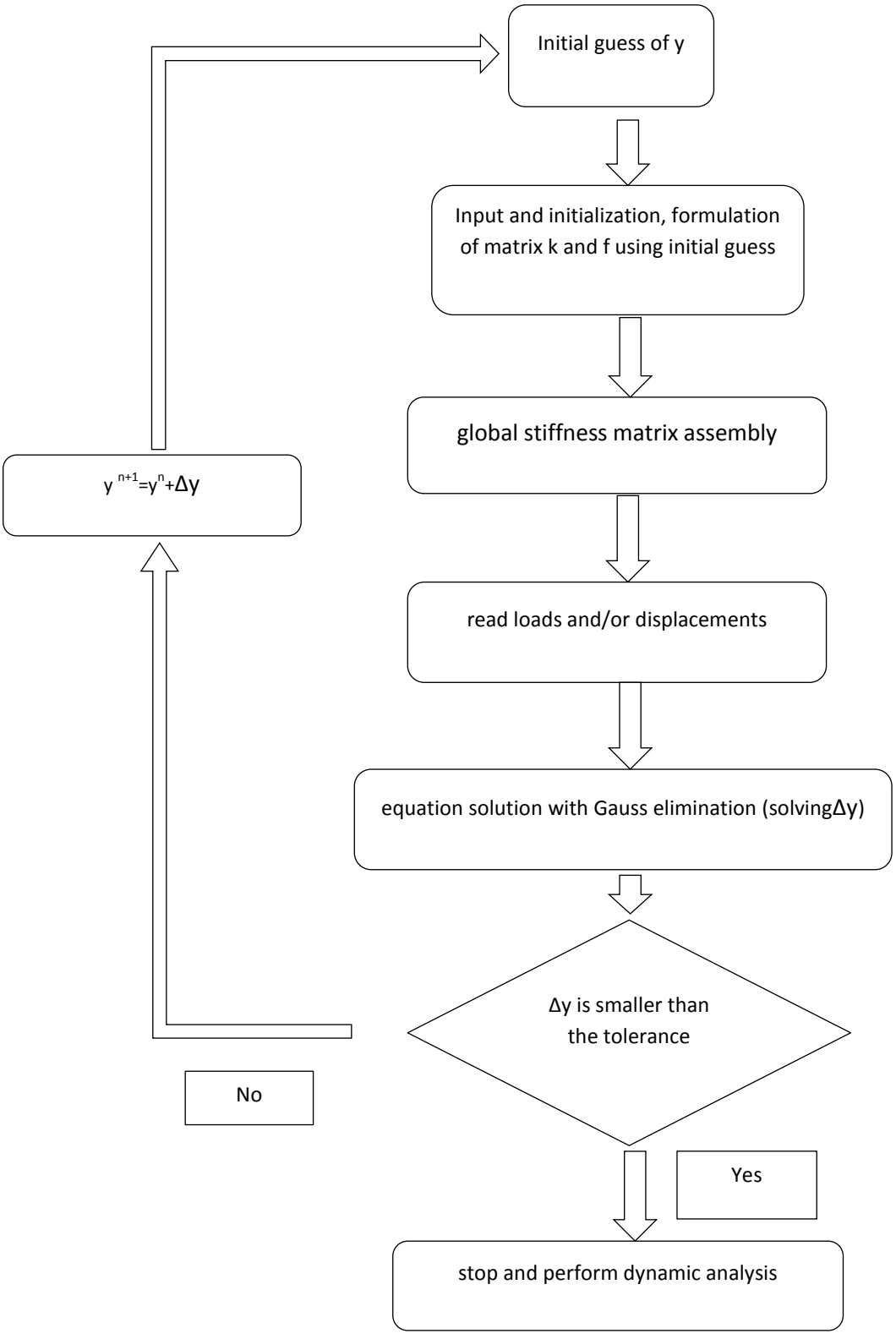

Figure 6.2 Flow chart of mooring line static analysis based on the elastic rod theory

6.2.2.2. Dynamic Problem

The inertial term in the motion equation cannot be neglected in the dynamic problem. For the dynamic problem, the elongation condition can be approximated by

$$\frac{1}{1+\varepsilon} = 1-\varepsilon+\varepsilon^2+o(\varepsilon^3) \tag{6.48}$$

The definition of r_i and T_E are the same as in the static case. Integrating over the element generates the discretized form of the equation of motion. Incorporating the elongation condition, we have

$$(\hat{M}_{ijlk})U_{jk} = -\lambda_n \hat{K}_{nijlk} U_{jk} + F_{il} \tag{6.49}$$

$$G_m = \hat{B}_{mil} U_{ki} U_{kl} - B_m - C_{mt}\lambda_t = 0 \tag{6.50}$$

where

$$\hat{M}_{ijlk} = M_{ijlk} + M^a_{ijlk} \tag{6.51}$$

To solve the second-order differential equation of motion, Ran (2000) introduced a new variable V:

$$\hat{M}_{ijlk}\dot{V}_{jk} = -\lambda_n \hat{K}_{nijlk} U_{jk} + F_{il} \tag{6.52}$$

$$\dot{U}_{jk} = V_{jk} \tag{6.53}$$

To solve these two equations, we need to integrate from *t(n)* to *t(n+1)*. Ran assumed a constant value $\hat{M}^{(n+0.5)}_{ijlk}$ during this time interval, leading to the equation:

$$\begin{aligned} &\hat{M}^{(n+0.5)}_{ijlk} V^{(n+1)}_{jk} - \hat{M}^{(n+0.5)}_{ijlk} V^{(n)}_{jk} = \\ &\int_{t(n)}^{t(n+1)} (-\lambda_n \hat{K}_{nijlk} U_{jk} + F_{il})dt \end{aligned} \tag{6.54}$$

Using the first-order Adam-Moulton method, equation (6.53) can be written as (Ran, 2000)

$$U^{(n+1)}_{jk} = U^{(n)}_{jk} + \frac{\Delta t}{2}[V^{(n+1)}_{jk} + V^{(n)}_{jk}] \tag{6.55}$$

Substituting (6.55) into (6.54) and re-arranging (6.55), we have

$$\frac{4}{\Delta t^2}\hat{M}_{ijlk}(\Delta U_{jk}) = \frac{4}{\Delta t}\hat{M}_{ijlk}(V_{jk}^{(n)}) + \frac{2}{\Delta t}\int_{t(n)}^{t(n+1)}(-\lambda_n \hat{K}_{nijlk}U_{jk} + F_{il})dt \tag{6.56}$$

$$V_{jk}^{(n+1)} = \frac{2}{\Delta t}(\Delta U_{jk}) - V_{jk}^{(n)} \tag{6.57}$$

Applying the first-order Adam-Moulton method on the right hand side of (6.54), we have

$$\begin{aligned}&\int_{t(n)}^{t(n+1)} \lambda_n \hat{K}_{nijlk}U_{jk}dt \\ &= \frac{\Delta t}{2}[\lambda_n^{(n+1)}\hat{K}_{nijlk}U_{jk}^{(n+1)} + \lambda_n^{(n)}\hat{K}_{nijlk}U_{jk}^{(n)}] \\ &\approx \frac{\Delta t}{2}[\lambda_n^{(n+0.5)}\hat{K}_{nijlk}U_{jk}^{(n+1)} + \lambda_n^{(n+0.5)}\hat{K}_{nijlk}U_{jk}^{(n)}]\end{aligned} \tag{6.58}$$

$$\int_{t(n)}^{t(n+1)} F_{il}dt = \frac{\Delta t}{2}(3F_{il}^{(n)} - 3F_{il}^{(n-1)}) \tag{6.59}$$

$$= \Delta t F_{il}^{(0)} \text{ for step one}$$

Substituting (6.59) and (6.58) into (6.56), we have

$$\begin{aligned}&[\frac{4}{\Delta t^2}\hat{M}_{ijlk}^{(n+0.5)} + \lambda_n^{(n-0.5)}K_{nijlk}]\Delta U_{jk} + 2K_{nijlk}U_{jk}\Delta\lambda_n = \\ &\frac{4}{\Delta t^2}\hat{M}_{ijlk}^{(n+0.5)}V_{jk}^{(n)} + (3F_{il}^{(n)} - F_{il}^{(n-1)}) - 2\lambda_n^{(n-0.5)}\hat{K}_{nijlk}U_{jk}^{(n)}\end{aligned} \tag{6.60}$$

The elongation condition is also approximated by Taylor series expansion (Ran, 2000)

$$\begin{aligned}&0 = 2G_m^{(n+1)} \approx 2G_m^{(n)} + 2\frac{\partial G_m^{(n)}}{\partial U_{jk}}\Delta U_{jk} + 2\frac{\partial G_m^{(n)}}{\partial \lambda_n}\Delta\lambda_n \\ &= 2G_m^{(n)} + 2\hat{K}_{mijlk}U_{il}(\Delta U_{jk}) + D_{mn}^{t(n)}(\Delta\lambda_n)\end{aligned} \tag{6.61}$$

$$\begin{bmatrix} K_{ijlk}^{'11(n)} & K_{iln}^{'12(n)} \\ K_{mjk}^{'21(n)} & K_{mn}^{'22(n)} \end{bmatrix} \begin{Bmatrix} \Delta U_{jk} \\ \Delta\lambda_n \end{Bmatrix} = -\begin{Bmatrix} R_{il}^{'(n)} \\ G_m^{'(n)} \end{Bmatrix} \tag{6.62}$$

where

$$K_{ijlk}^{'11(n)} = \frac{2}{\Delta t^2}\hat{M}_{ijlk}^{(n+0.5)} + \lambda_n^{(n-0.5)}\hat{K}_{nijlk} \tag{6.63}$$

$$K_{iln}^{'12(n)} = 2\hat{K}_{nijlk}U_{jk} \tag{6.64}$$

$$K_{mjk}^{'21(n)} = 2\hat{K}_{mijlk}U_{il} \tag{6.65}$$

$$K_{mn}^{'22(n)} = 2(K_{mn}^{22(n)} + C_{mn}) \tag{6.66}$$

$$\begin{aligned} R_{il}^{'(n)} &= \frac{2}{\Delta t}\hat{M}_{ijlk}^{(n+0.5)}V_{jk}^{(n)} \\ &-2\lambda_n^{(n-0.5)}\hat{K}_{nijlk}U_{jk}^{(n)} + 3F_{il}^{(n)} - F_{il}^{(n-1)} \end{aligned} \tag{6.67}$$

$$G_m^{'(n)} = 2(G_m^{(n)} - C_m) \tag{6.68}$$

at time step n

$$K^{(n)}(\Delta y) = F^{(n)} \tag{6.69}$$

The above numerical procedure was incorporated in the FEAMooring module of FAST. The original FAST program was modified and extended to allow for large elongations, and therefore suitable for polyester lines. An advantage of the present method is that the element stiffness matrix remains symmetric.

6.3. Validation of the enhanced model

6.3.1. Comparison of element length

Since the numerical equations for static and dynamic problems were successfully derived in last section, the main aim of this section is to check the validity of current method. For the polyester line, we will compare current results with available commercial software - OrcaFlex. In OrcaFlex, a lumped-mass and spring model is applied for the simulation of slender bodies. The mooring line layout and environmental loading direction are the same as Figure 6.9 and Table 6.1. For current and the following studies, the taut line drag and added mass coefficients are 1.0 and

1.0, respectively. Figures 6.3 - 6.6 compare the mooring line top end tension and the anchor point tension for different number of element lengths, respectively. For validation purpose, the taut mooring line length was 500m (EA=72.555kN, diameter=0.258m and mass=53kg/m) and the mooring radius was 418m. The time step for validation and the following case studies was 0.0125s. Both calm water and regular wave condition are compared. The initial transit motion in calm water of Figure 6.3 and 6.4 is probably because of the exchange of parameter between the aerodynamic and hydrodynamic analysis. The transit motion is also due to the initial guess of the line tension, as shown in Figure 6.2. From the comparisons in Figures 6.3 and 6.4 we can see that the results converge faster for larger number of elements in calm water. For Figures 6.5 and 6.6 in seastate 6 maximum line tension (after 500s) at top end shows almost no difference between 5 and 10 elements while the difference between 2 and 5 elements is about 2% (around 5% for anchor point).

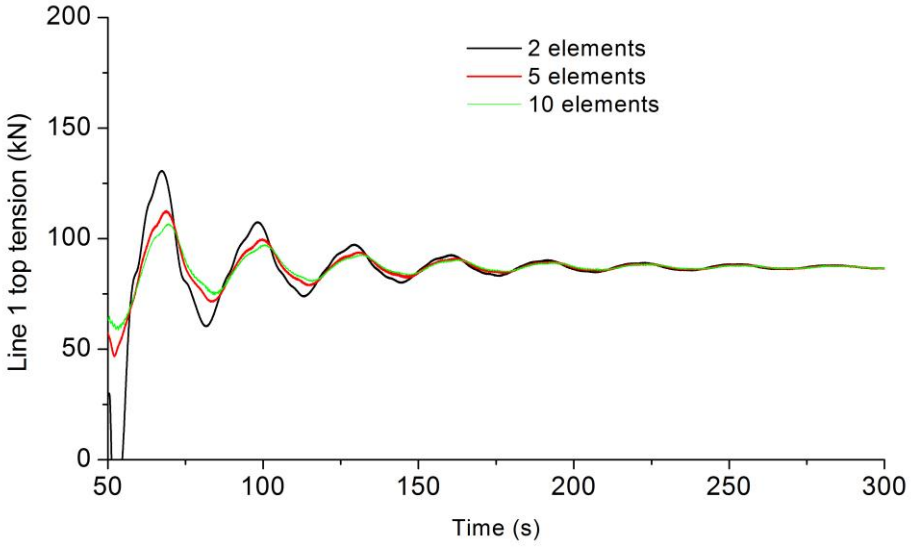

Figure 6.3 Comparison of line 1 top tension with different number of elements in calm water

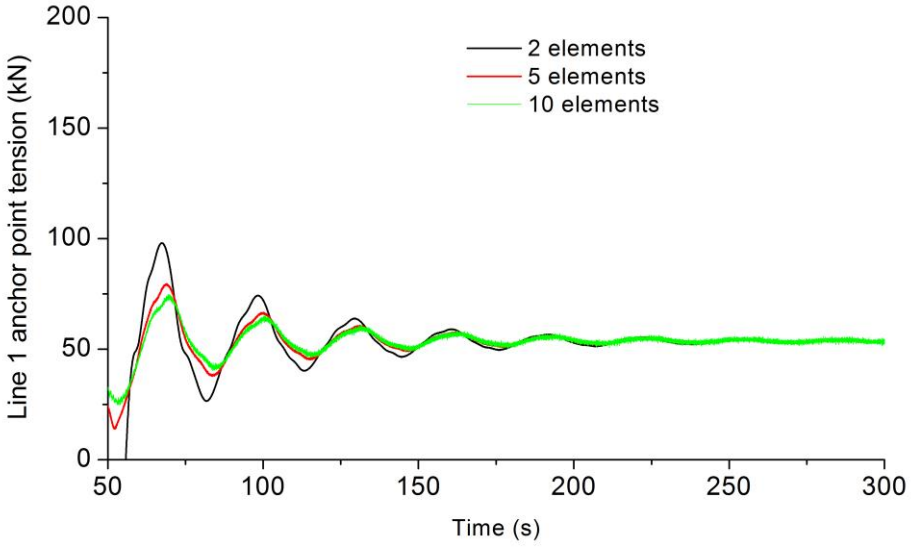

Figure 6.4 Comparison of line 1 anchor point tension with different number of elements in calm water

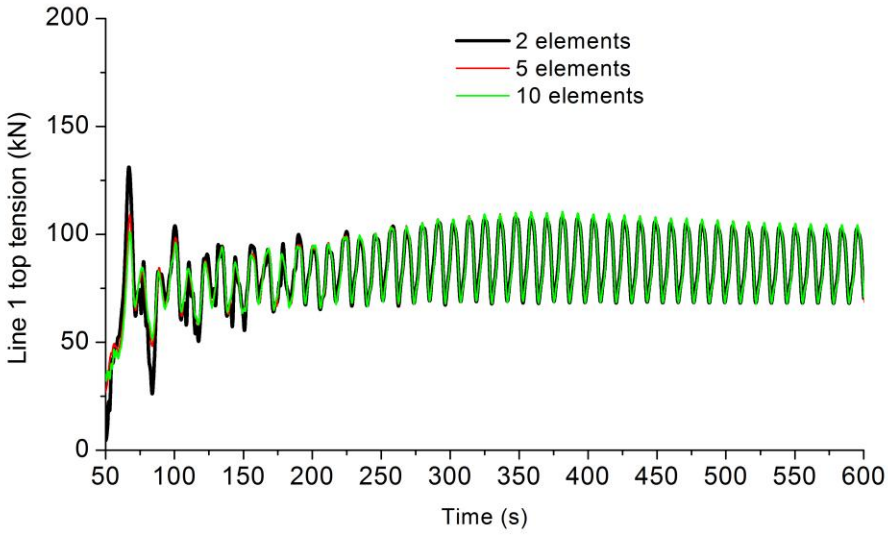

Figure 6.5 Comparison of line 1 top tension with different number of elements in sea state 6

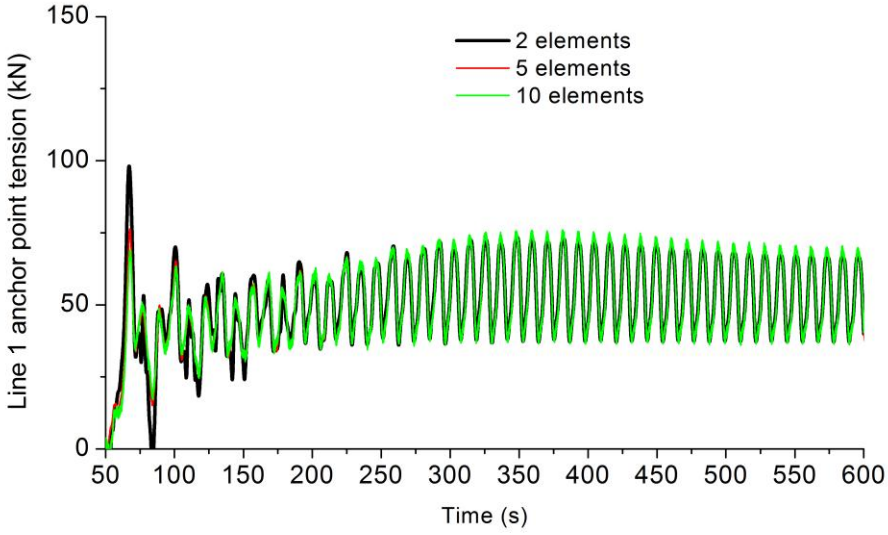

Figure 6.6 Comparison of line 1 anchor point tension with different number of elements in sea state 6

6.3.2. Comparison with Orcaflex

Figures 6.7(a) and 6.7(b) show the dynamic response of line tension in seastate 6 (H=5.5m, T=11.3s). The red line shows the results of Fastlink (FAST+OrcaFlex). In Fastlink, OrcaFlex solves the dynamic response of mooring line in the time domain and passes the mooring line tension to FAST for the coupled response of the mooring system. From this comparison we can see that the Taylor expansion to second order shows little difference compared with the results from third order. They both show very good agreement with the lumped mass and spring method. However, when assuming small elongation (equivalent to an expansion to first order, using the governing equation and elongation condition of the rod by Pauling & Webster,1986) the blue and green lines in Figure 6.7 show poor results for a polyester line.

The present method is also acceptable for modelling a slack mooring line (catenary chain, Tables 5.1 and 5.2) in 320m. Figure 6.8 compares the line tension results under seastate 6 for a catenary chain. Results from the approximation to third order generate the same results as OrcaFlex and the small elongation assumption. From a comparison of Figures 6.7(a), 6.7(b) and 6.8 we can see that the present method can be used for modelling both traditional materials as well as polyester lines. The reduced stiffness and extended stiffness in the graphs denote Taylor series expansion to first and third order, respectively. For the extended stiffness condition, the stiffness term and elongation are:

$$\hat{K}_{nijlk} = K^0_{nijlk} + \lambda_m K^1_{nmijlk} + \lambda_m\lambda_p K^2_{nmpijlk} + \lambda_q\lambda_m\lambda_p K^3_{nmpqijlk} \tag{6.70}$$

$$\hat{B}_{mil} = B^0_{mil} + \lambda_n B^1_{nmil} + \lambda_n\lambda_p B^2_{npmil} + \lambda_n\lambda_p\lambda_q B^3_{npqmil} \tag{6.71}$$

$$K^3_{nmtpqijlk} = -\int_0^L \frac{1}{(EA)^3} P_n P_m P_q P_t A_i' A_k' \delta_{ij} ds \tag{6.72}$$

For static problem,

$$B^3_{nmqtil} = -\int_0^L \frac{4}{(EA)^3} P_n P_m P_q P_t A_i' A_l' ds \tag{6.73}$$

while for dynamic problem,

$$B^3_{npqmil} = -\int_0^L \frac{1}{(EA)^3} P_n P_m P_q P_t A_i' A_l' ds \tag{6.74}$$

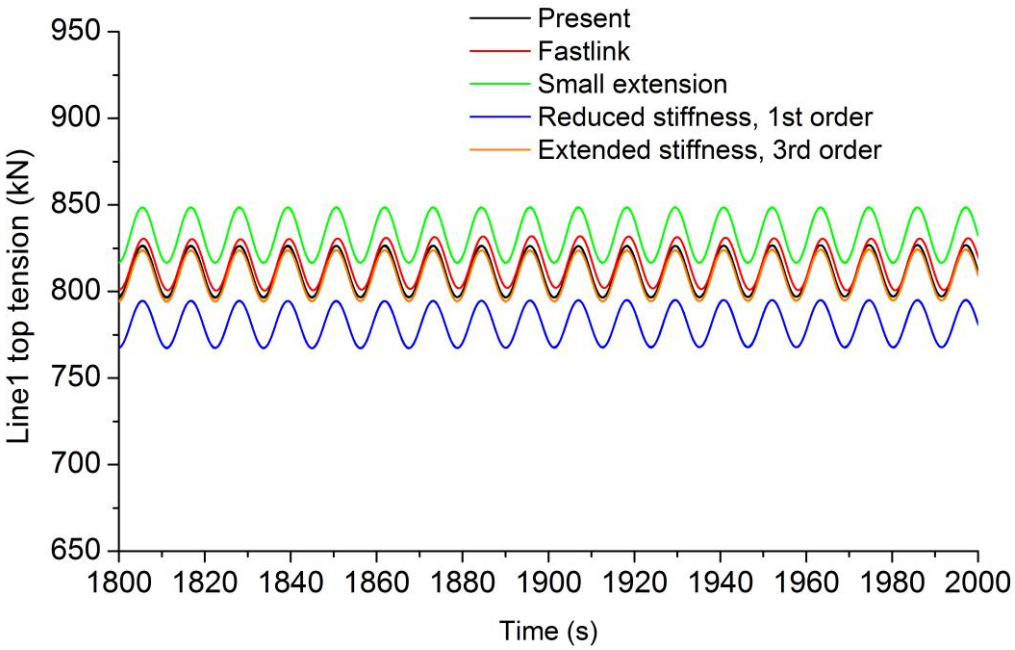

Figure 6.7(a) Comparison with Orcaflex and small extensible rod results in sea state 6 (Line1)

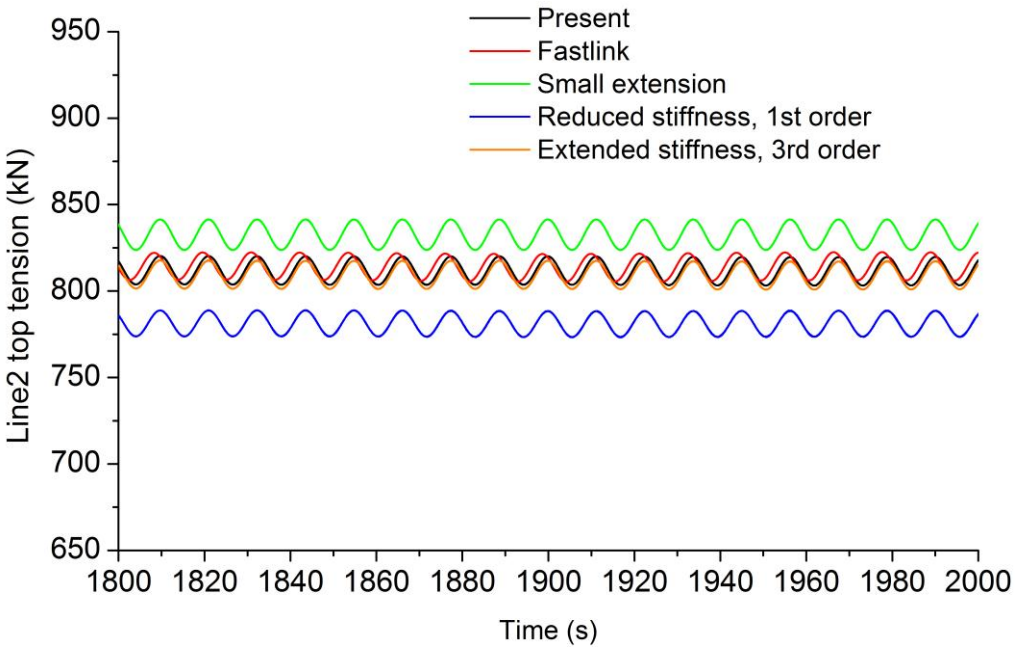

Figure 6.7(b) Comparison with Orcaflex and small extensible rod results in sea state 6 (Line2)

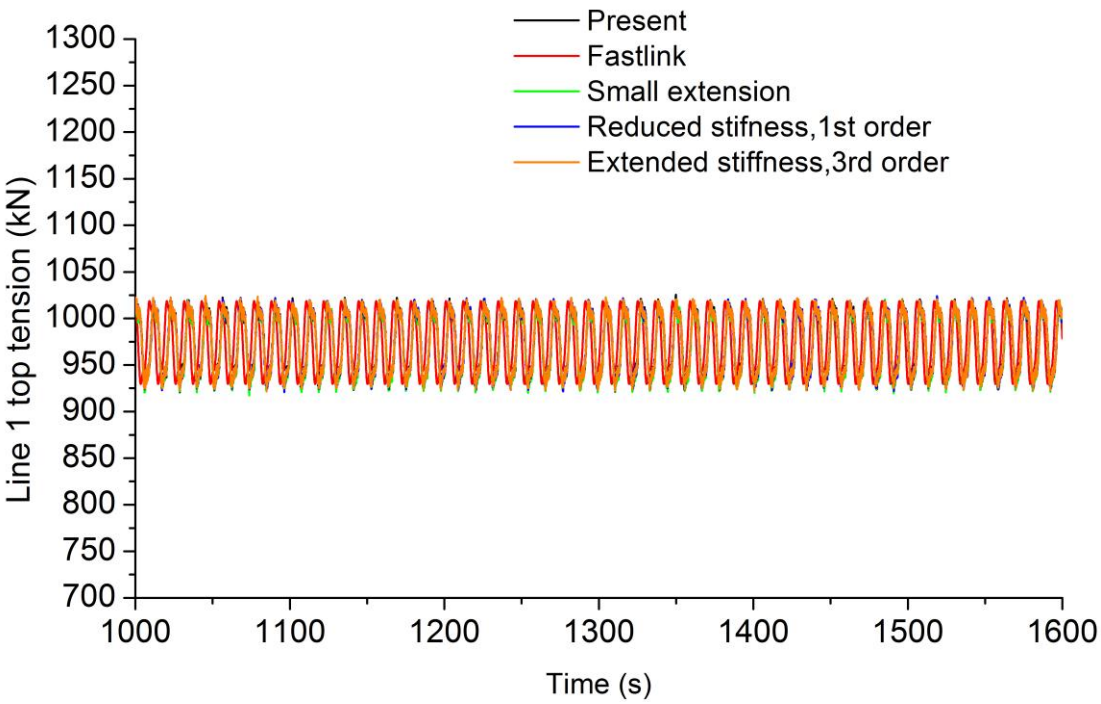

Figure 6.8 Comparison of line tension for a catenary chain under sea state 6

6.4. Time-domain simulation of a floating wind turbine

6.4.1. Properties of the mooring system and methods applied

The same Spar-type floating wind turbine modelling was applied in this chapter for the case studies as the last chapter. The parameters of the floating body and the upper structure are the same, except for the mooring system. In this chapter, we will investigate and discuss the dynamic response of a taut moored FOWT. The properties of the taut mooring line are shown in Table 6.1. For the sake of simplicity, the *Radius to Fairleads from Platform Centreline* was 4.7m, instead of 5.2 m. For the simulation in this chapter, the yaw response is controlled by adding additional yaw spring stiffness in the hydrostatic restoring force matrix (FAST).

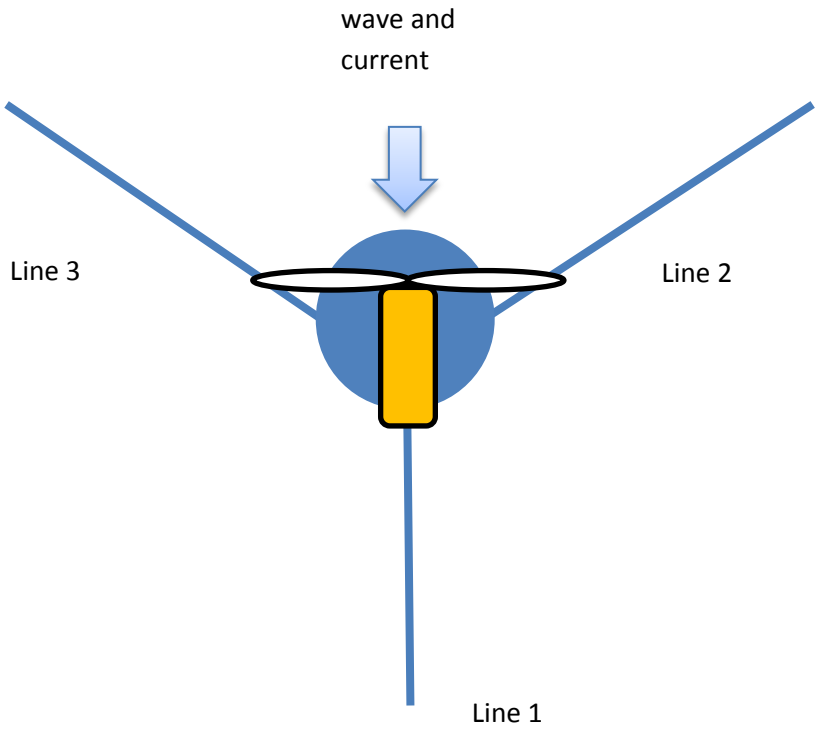

Figure 6.9 Plan view of the mooring system and environmental condition

Table 6.1 Mooring system properties (OrcaFlex)

Items	Values
Mooring line pattern	taut
Water Depth (m)	320
Number of Mooring Lines	3
Angle between adjacent lines (degree)	120
Depth to Fairleads below SWL (m)	70
Radius to Fairleads from Platform Centreline (m)	4.7
Unstretched Mooring Line length (m)	450
Mooring Line diameter (m)	0.086
Mooring system radius (m)	418
Mooring Line mass (Kg/m)	7.978
Mooring Line elastic stiffness (EA) (N)	10.9E6

The hydrodynamic coefficients and wave exciting forces for the OC-3 Spar-type wind turbine were pre-calculated by WAMIT and stored in FAST, only first-order wave forces were included in current study. Cummins's impulse response function method was applied for current time-domain study. The added mass and frequency dependent

radiation damping were transformed into time domain by using Fourier transform. The floating body equation of motion is determined by

$$[M + M^a(\infty)]\ddot{X} + KX + \int_{-\infty}^{t} R(t-\tau)\dot{X}(t)d\tau = F_e \tag{6.75}$$

The external force F_e includes the wave exciting force current force, wind force and mooring force. The memory effect can be evaluated by a convolution. The HydroDyn model of FAST is mainly responsible for calculating the retardation function and motion response of the platform. The retardation function can be evaluated by

$$R(t) = \frac{2}{\pi}\int_{-\infty}^{t} b(\omega)\cos(\omega t)d\omega \tag{6.76}$$

The coupling between the floating body and mooring line applied a loosed coupling method, as introduced by Jonkman (2013). At each time step, the results from different modules were exchanged, but solving their equations separately.

6.4.2. Comparison of line tension with different approximations

6.4.2.1. Wave plus current condition

The last section examined the convergence of the elongation condition under regular wave conditions. It is beneficial to study the line tension results with different ε. Figure 6.10 shows the most loaded line tension time history under wave only and a wave plus current condition, respectively. The near-surface current velocity at still water level in Figure 6.10 and 6.11 are 1m/s and 5m/s, respectively. Detailed modelling of current profile is shown in the HydroDyn manual. From wave only to wave plus current condition, the mean elongation of Line2 changes from 7.4% to 8.7%. However, the difference of mean and maximum line tension predicted by the two orders of approximation shows almost no difference. Figure 6.11 compared the approximation under a larger current velocity. From the comparison we can see that the mean elongation of Line2 changes from 7.4% to about 10%, the difference between the two approximations for mean and maximum line tension changes from about 0.3% to 0.4%.

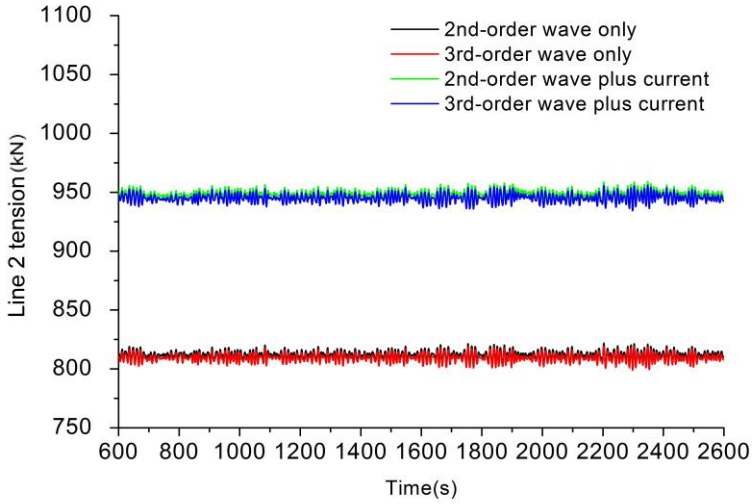

Figure 6.10 Comparison of time history under wave only condition (irregular, seastate6,current velocity 1m/s) and wave plus current condition

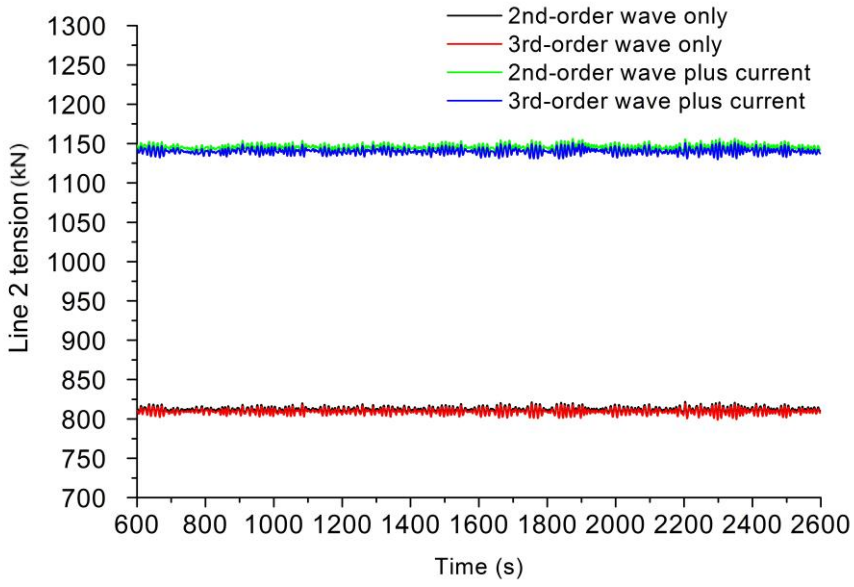

Figure 6.11 Comparison of time history under wave only condition (irregular, seastate6,current velocity 5m/s) and wave plus current condition

6.4.2.2. Wave only condition, reduced line length

In order to further check the different elongation approximation, a reduced line length (420m) was applied for case study. The environmental condition was wave only with the same wave height and frequency as previous section (sea state 6, random wave). From the comparison we can see that the elongation of the mooring line is about 15%, but the difference of mean and maximum line tension predicted by the two methods are both around 1.3% (Figure 6.12). So, from the two case studies we can see that the approximation to second order is sufficient.

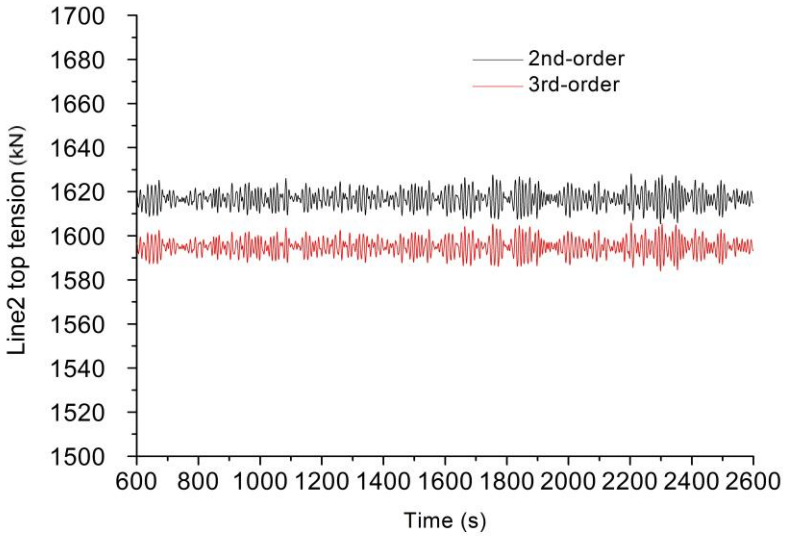

Figure 6.12 Comparison of mooring line fairlead tension for reduced line length

6.4.3. Maximum line tension along the line

Figures 6.13(a) and (b) show the maximum line tension with different arc length. The sea state was the same - seastate6, wave only condition. For each single mooring line, the maximum mooring line tension all appears on the fairlead while the minimum line tension is at the anchor point. One reason for these phenomena is the small horizontal motion responses, especially for the surge motion, see Figures 6.14-6.16. The geometric nonlinearity is small and the WF mooring line response is less significant for current case study. Under seastate 6, the turbine is shutdown. The drift motion

response in surge is less significant under the wave loading. Maximum surge and pitch motion responses are less than 2 m and 2 degree, respectively.

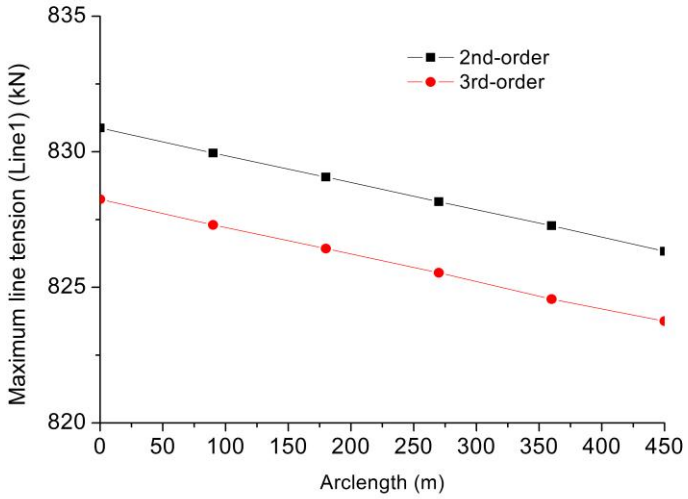

Figure 6.13(a) Comparison of mooring line maximum tension along arc length (Line1)

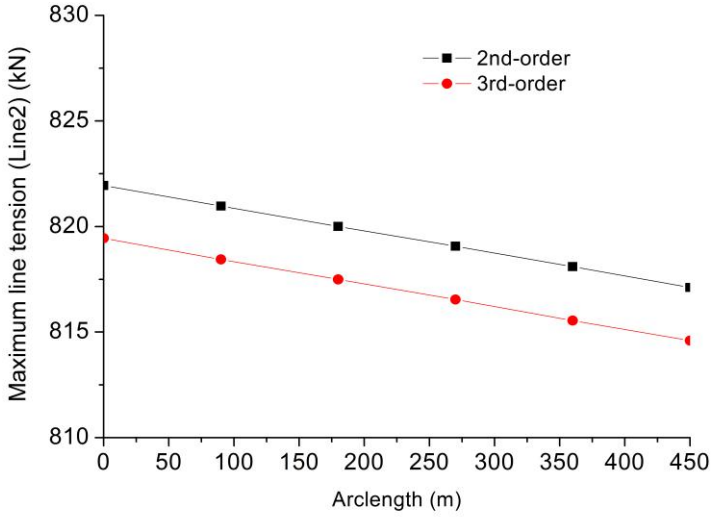

Figure 6.13(b) Comparison of mooring line maximum tension along arc length (Line2)

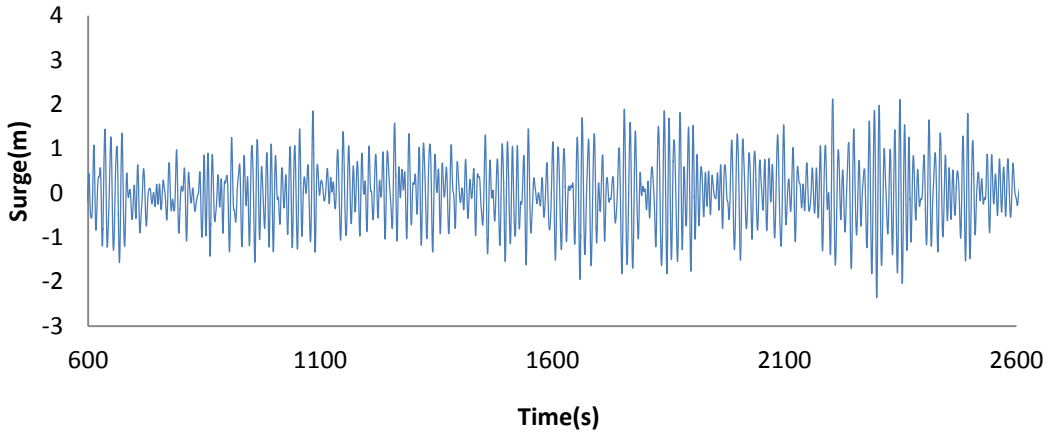

Figure 6.14 Platform surge motion in seastate6

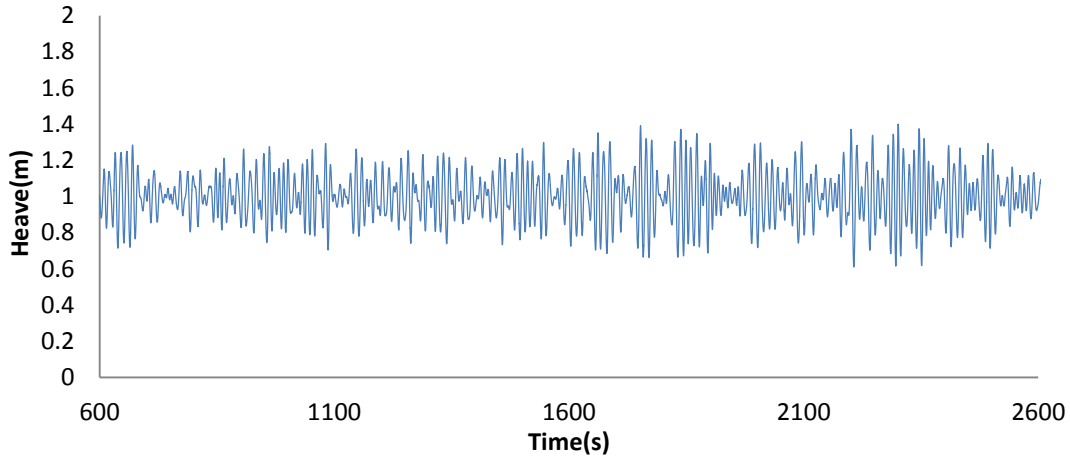

Figure 6.15 Platform heave motion in seastate6

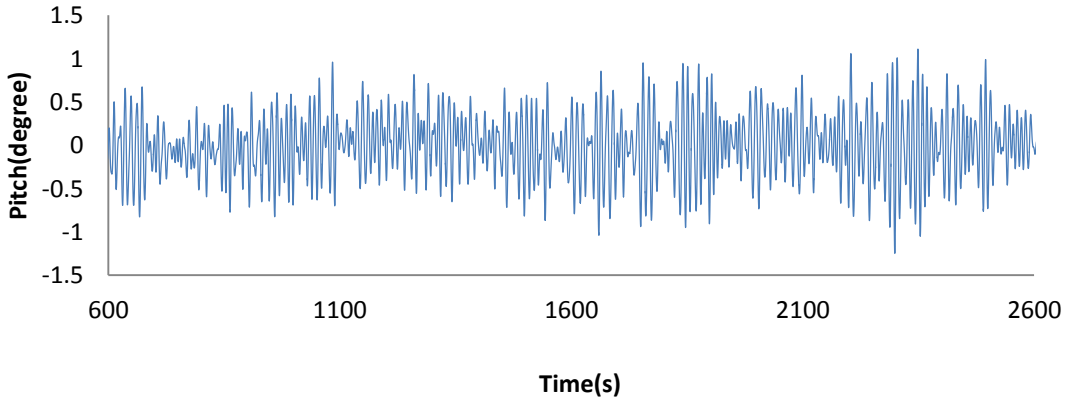

Figure 6.16 Platform pitch motion in seastate6

6.5. Application I : Non-symmetrical mooring line layout

6.5.1. Description of the mooring system layout

In this section, we will study a non-symmetrical mooring system, which can be applied for the analysis of mooring line broken condition. Figure 6.17 shows the plan view of mooring system with one line broken (line4). The properties of the FOWT are the same as Chapter 5. The mooring line properties are the same as Table 6.1 The mooring line layout and environmental conditions are shown in Figure 6.17.

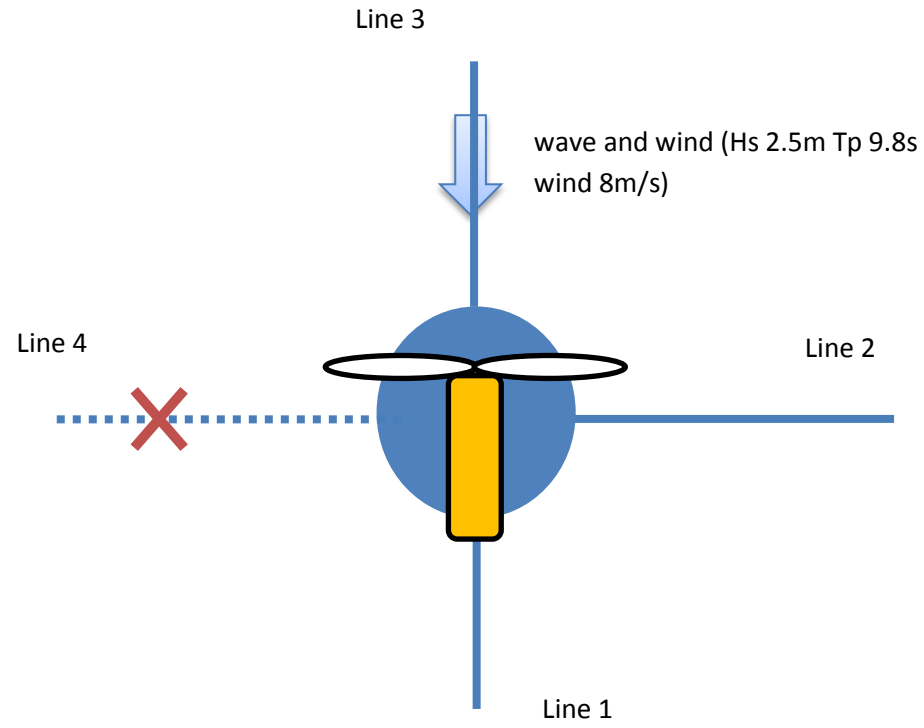

Figure 6.17 Plan view of the non-symmetrical mooring system and environmental condition

6.5.2. Results of motion response and line tension

Figures 6.18-6.22 show the simulation results of motion response and mooring line tension, on a dynamic turbine in wind and irregular waves. The incident wave time series was generated by JONSWAP Spectrum. Due to a combination of wave and wind loading, the platform moved from initial position to a new equilibrant position. In the first 400 seconds, there was a transit phenomenon but this transit disappeared

with the increasing of simulation time. The relative large heave motion response is probably because of the non-symmetrical mooring line layout. The mooring lines are pre-tensioned, but for the non-symmetrical mooring line layout, one of the mooring line's initial tension became zero (the damaged one). Because of the non-symmetrical mooring line layout of the damaged condition, platform sway motion moves from zero to about 30m. Mean surge motion response of damaged conditions about 5% larger than the intact condition. Similar difference was noticed for mean mooring line top tension (Line3, 6%). However, it is interesting to notice that the damaged mooring line almost has no effect on pitch response, which is mainly because of the direction of environmental condition (Parallel to line1 and line3).

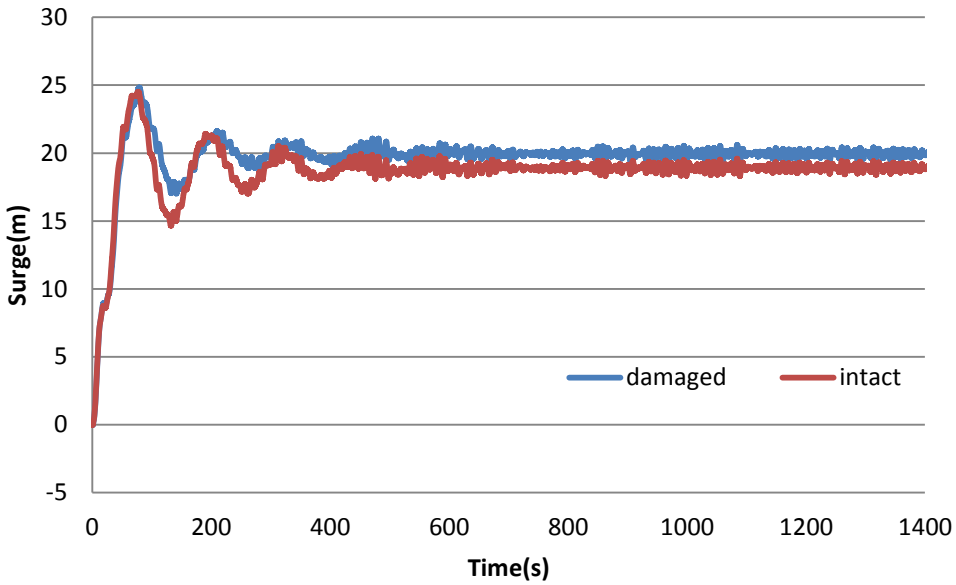

Figure 6.18 Surge response, wave plus wind condition

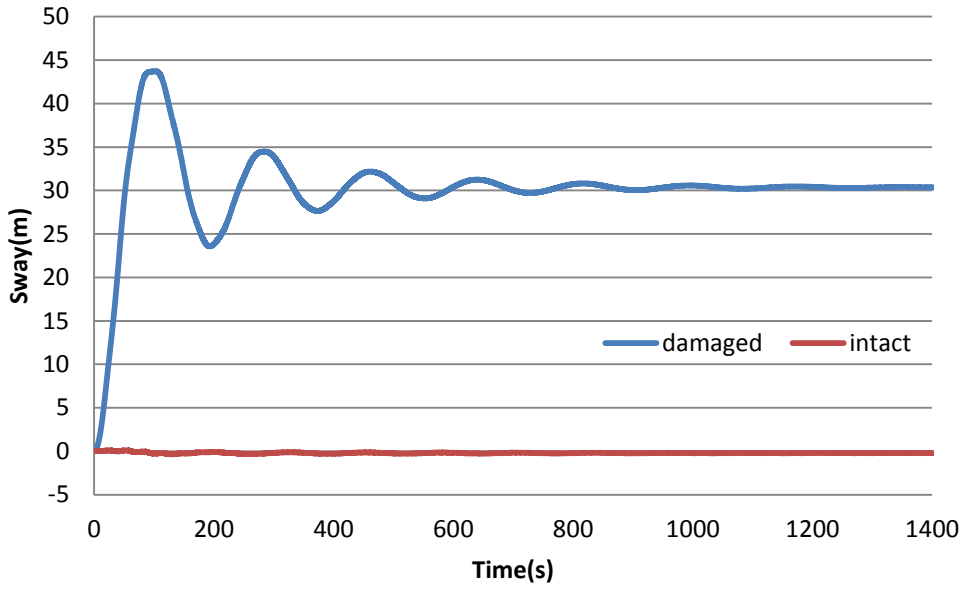

Figure 6.19 Sway response, wave plus wind condition

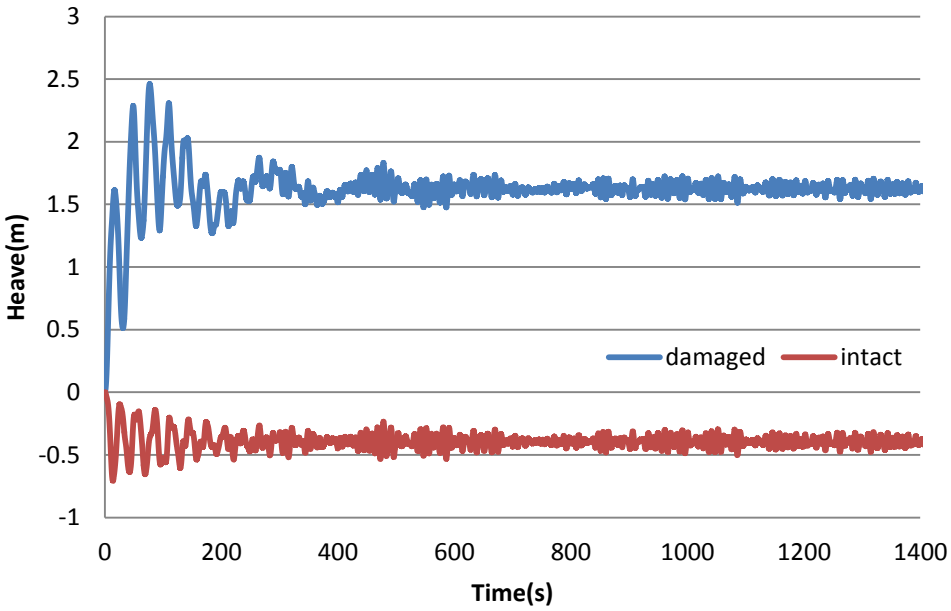

Figure 6.20 heave response, wave plus wind condition

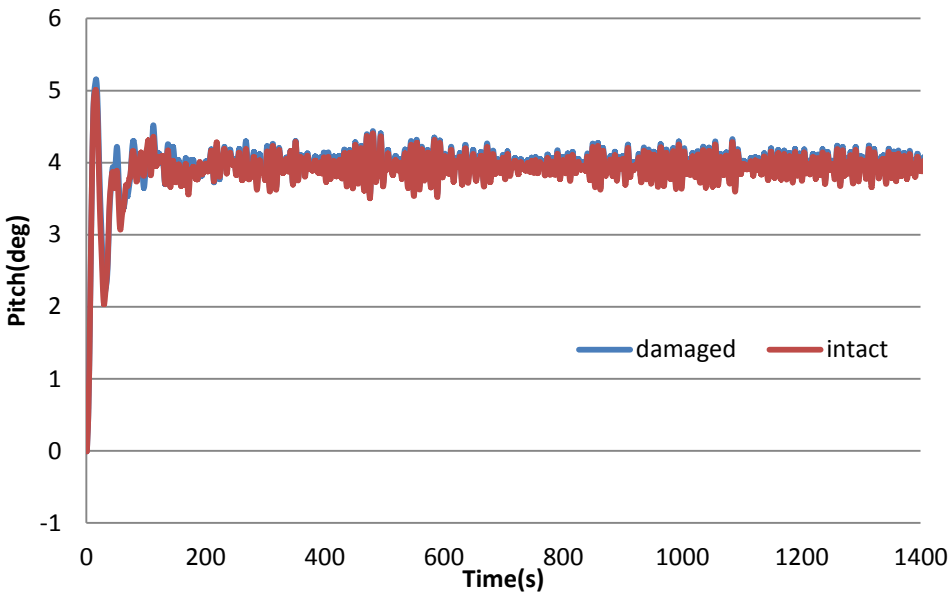

Figure 6.21 pitch response, wave plus wind condition

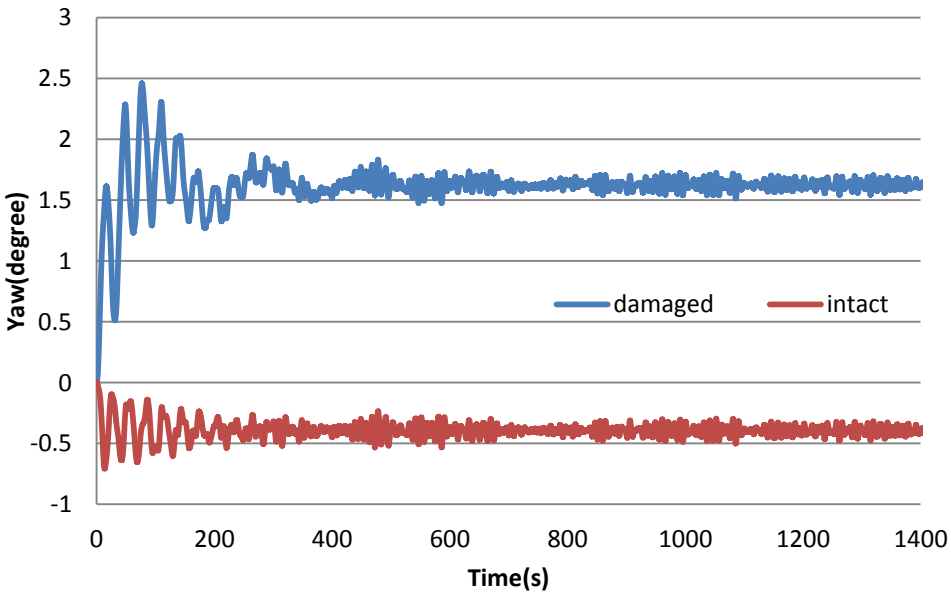

Figure 6.22 Yaw response, wave plus wind condition

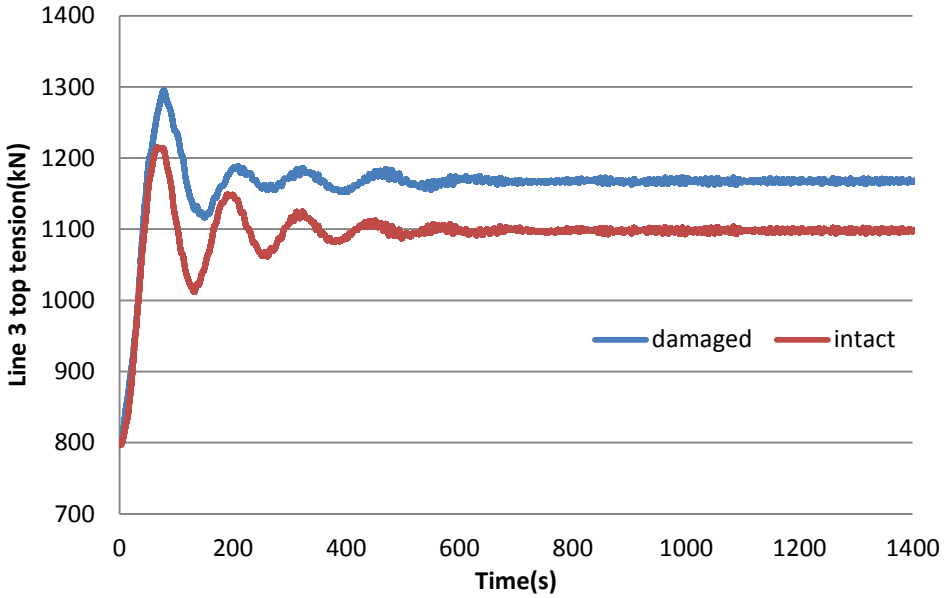

Figure 6.23 Line3 tension response, wave plus wind condition

6.6. Application II: Time-domain analysis for a taut moored Spar-type FOWT- A comparison between current method and massless spring method

6.6.1. Mooring system load-offset relationship

Mooring line layout and properties are the same as Figure 6.9 and Table 6.1. Figure 6.24 shows the surge restoring force against different initial horizontal position. From the graph we can see that the load-offset relationship is almost linear. For the linear spring method, the spring stiffness was derived from the same method- giving an initial offset and the spring stiffness was calculated with the following equation

$$K = \frac{\Delta F}{\Delta S} \tag{6.77}$$

For the linear spring method, the off-diagonal stiffness was ignored. In other words, the coupling effects (e.g. heave-pitch coupling) were not accounted for. The liner spring stiffness for surge, sway and heave are 30680.5 N/m, 29728.2 N/m and 23178 N/m, respectively.

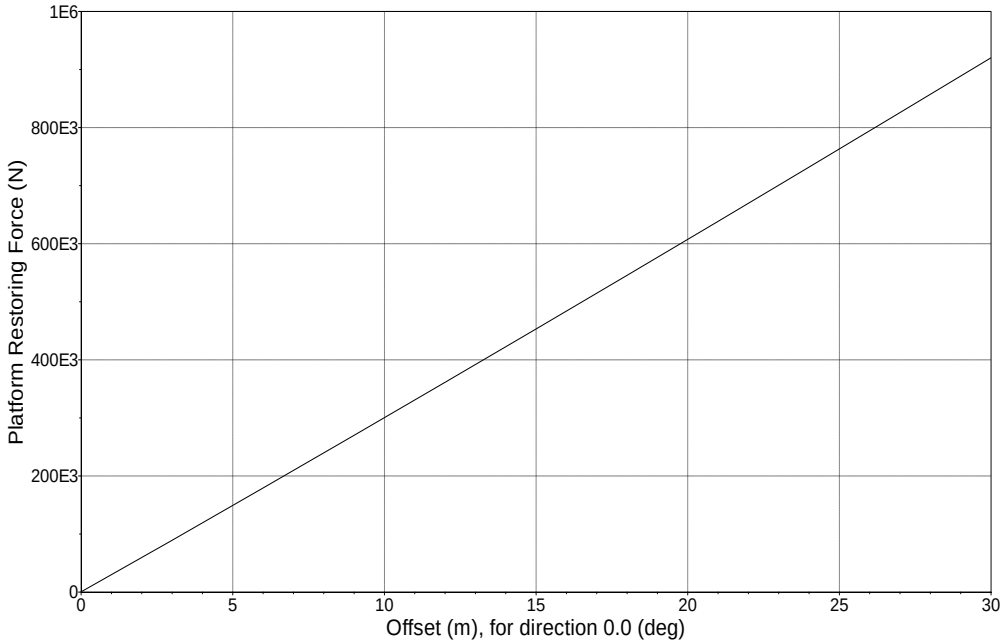

Figure 6.24 Platform surge load-offset graph (OrcaFlex)

6.6.2. Results of case studies under wave only and wave plus wind condition

Table 6.2 List of case studies, regular wave only condition

Case studies	H (m)	Frequency (rad/s)
1	2.56	0.157
2	2.56	0.185
3	2.56	0.209
4	2.56	0.242
5	2.56	0.299
6	2.56	0.483
7	2.56	0.897

Table 6.3 List of case studies, regular wave plus wind condition

Case studies	H (m)	Frequency (rad/s)	Mean wind speed (m/s)
1	2.56	0.157	11.4
2	2.56	0.185	11.4
3	2.56	0.209	11.4
4	2.56	0.242	11.4
5	2.56	0.299	11.4
6	2.56	0.483	11.4
7	2.56	0.897	11.4

- **Platform motion response**

The environmental conditions are shown in Table 6.2 and Table 6.3. The wind and wave direction are parallel to Line 1, as shown in Figure 6.9. As potential theory fails to consider viscous effects, the additional linear damping was added. The additional damping coefficients for surge, sway and heave are 100000N/ (m/s), 100000N/ (m/s) and 130000N/ (m/s), respectively (Jonkman, 2010). Figures 6.25~6.30 show the motion RAOs for the Spar under wave only and wave plus wind condition while Figures 6.31~6.42 show the time history for wave period = 7s and 26s, respectively. Under wave only condition, the amplitude of heave response is not affected by the method of analysis, but the mean heave position has seen a large difference between the two methods, as can be seen from Figure 6.38 and 6.41. Surge and pitch RAOs decrease under the wave plus wind condition, compared with wave only condition.

For the wave only condition, there is little difference between the two methods for wave frequency larger than 0.4 rad/s (e.g. Figures 6.37~6.39), except for the mean position of the heave motion. These results indicate that for the primary design of substructure of the FOWT under some survival conditions (e.g. seastate 7 or seastate 8), the linear spring method can be applied, as it gives results as accurate as the FEM method but with less running time. However, for the wave plus wind condition, although the amplitude of motion response shows little difference between the linear spring method and elastic rod theory, the mean position of surge and pitch were under-predicted by the linear spring method. Under wave only condition, the floating body oscillates about its mean position, but there is a very large mean offset (e.g. about 40m in Figures 6.34 and 6.40) when considering wave plus wind condition. Under the wave plus wind condition, the turbine thrust force is much larger than the wave forces. The turbine thrust force has little effects on the mean heave motion. However, it has an effect on the amplitude of heave motion response in lower frequencies, the same as the catenary moored FOWT (Chapter 5).

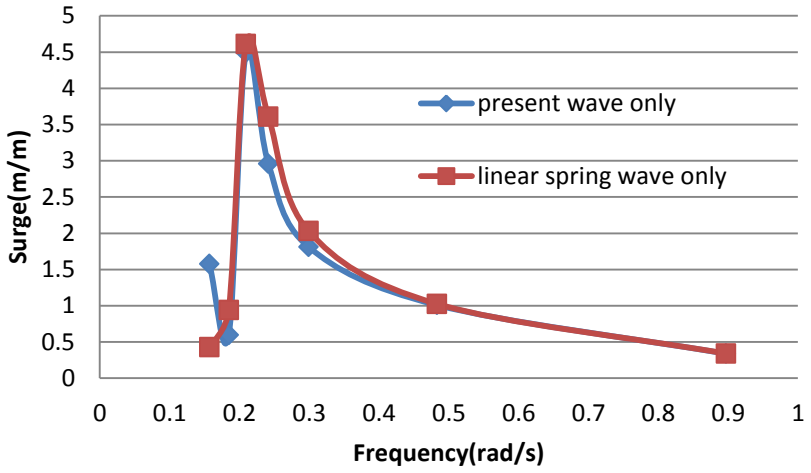

Figure 6.25 Surge RAO, wave only condition

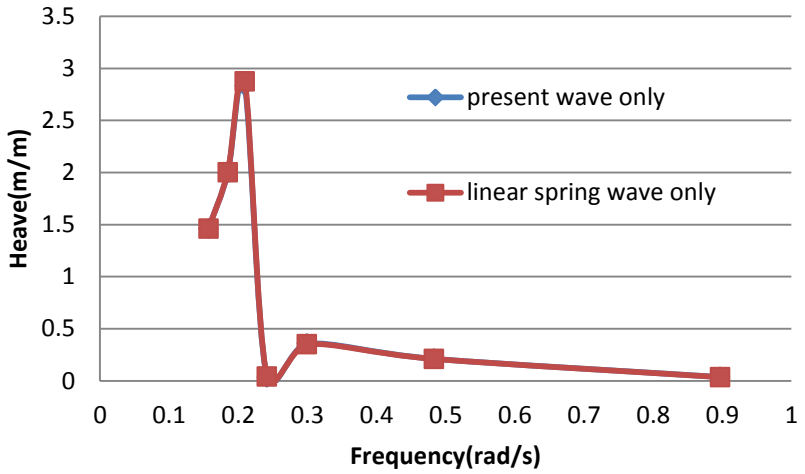

Figure 6.26 Heave RAO, wave only condition

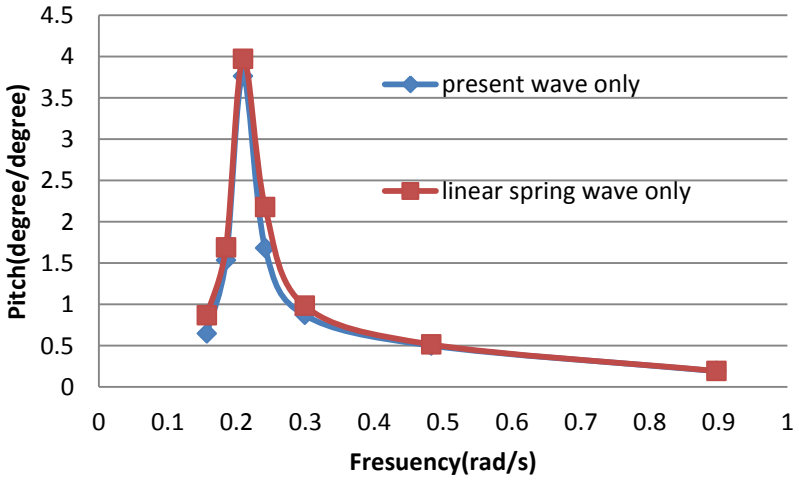

Figure 6.27 Pitch RAO, wave only condition

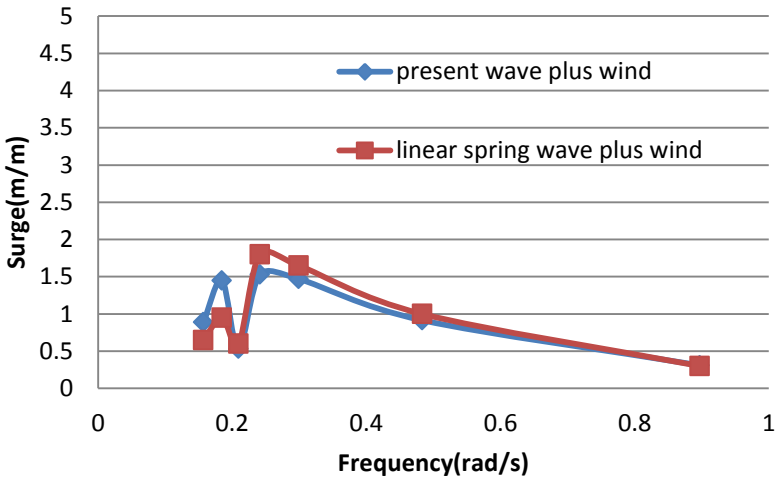

Figure 6.28 Surge RAO, wave plus wind condition

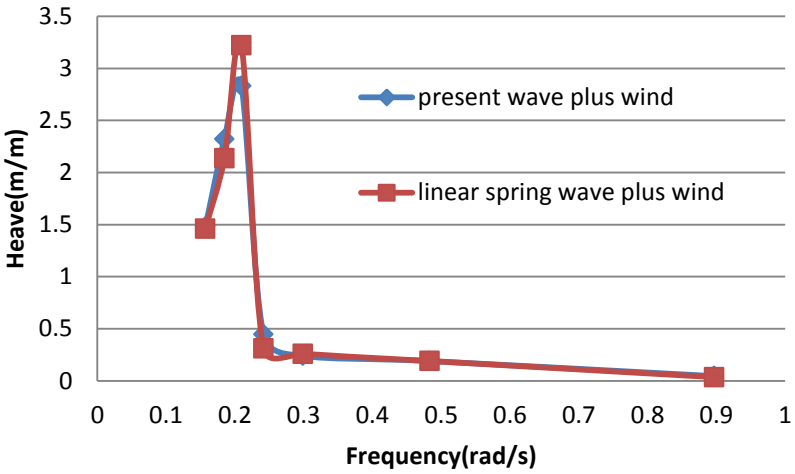

Figure 6.29 Heave RAO, wave plus wind condition

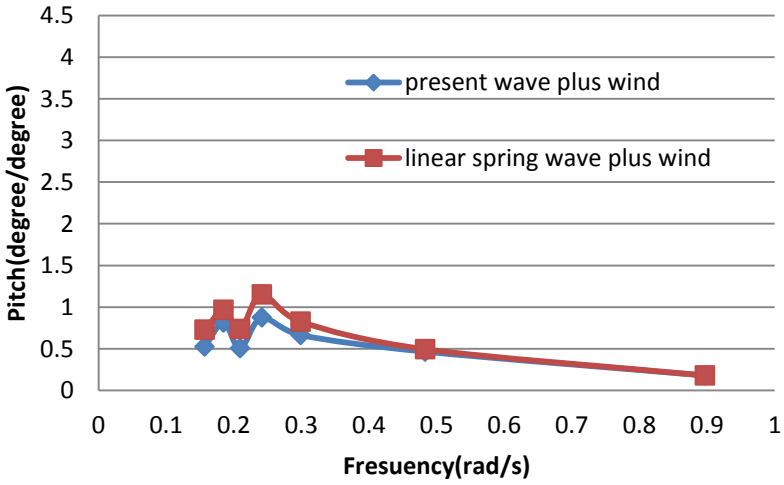

Figure 6.30 Pitch RAO, wave plus wind condition

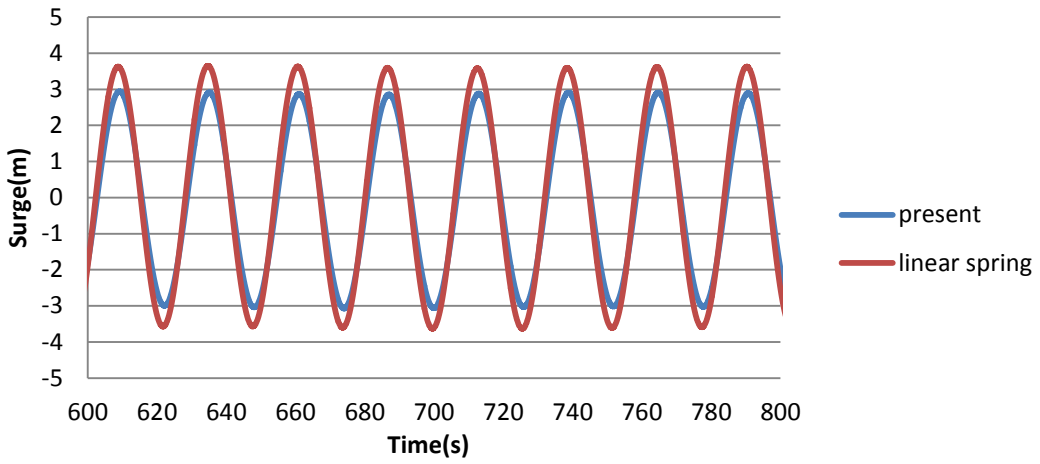

Figure 6.31 Surge time history, wave only condition T=26s

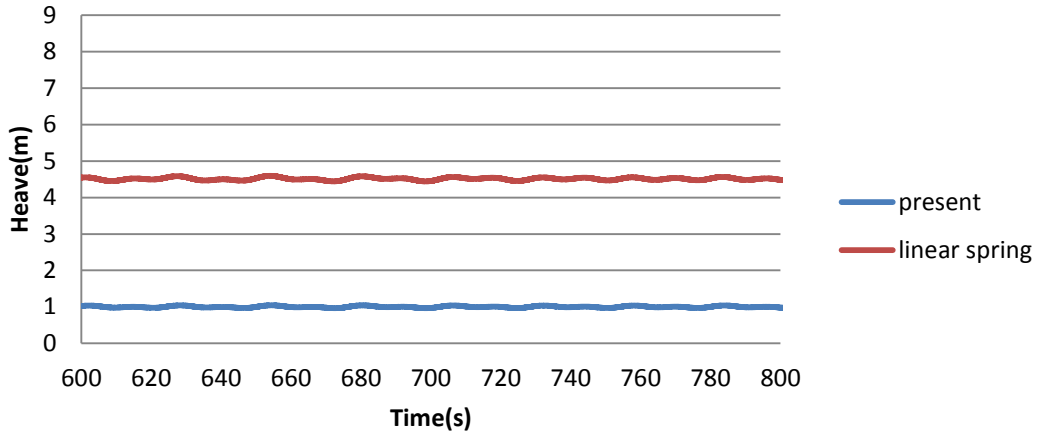

Figure 6.32 Heave time history, wave only condition T=26s

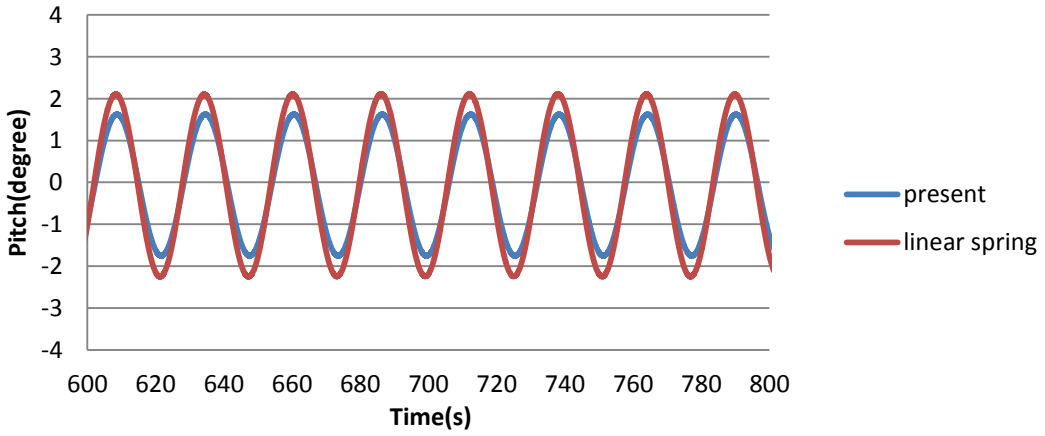

Figure 6.33 Pitch time history, wave only condition T=26s

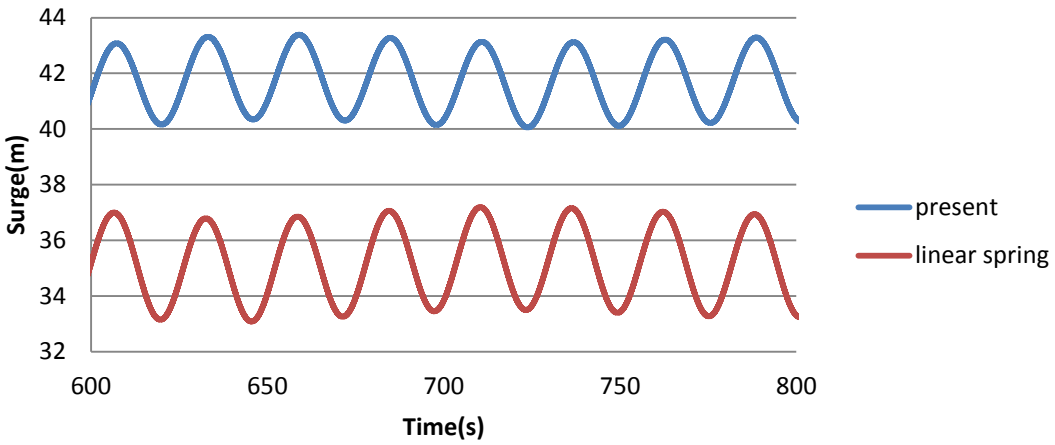

Figure 6.34 Surge time history, wave plus wind condition T=26s

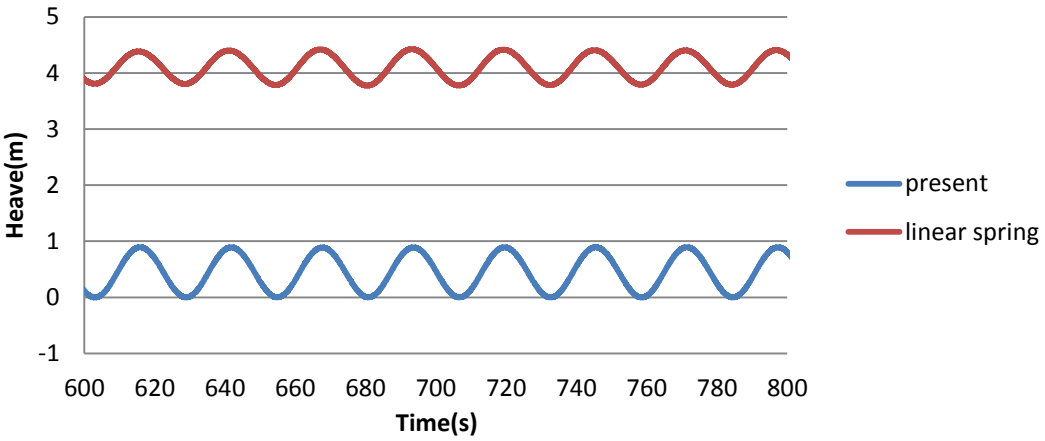

Figure 6.35 Heave time history, wave plus wind condition T=26s

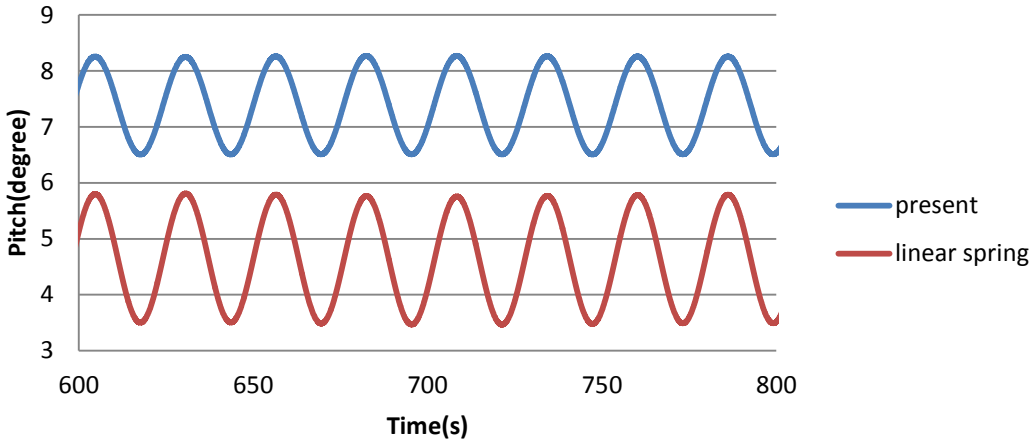

Figure 6.36 Pitch time history, wave plus wind condition T=26s

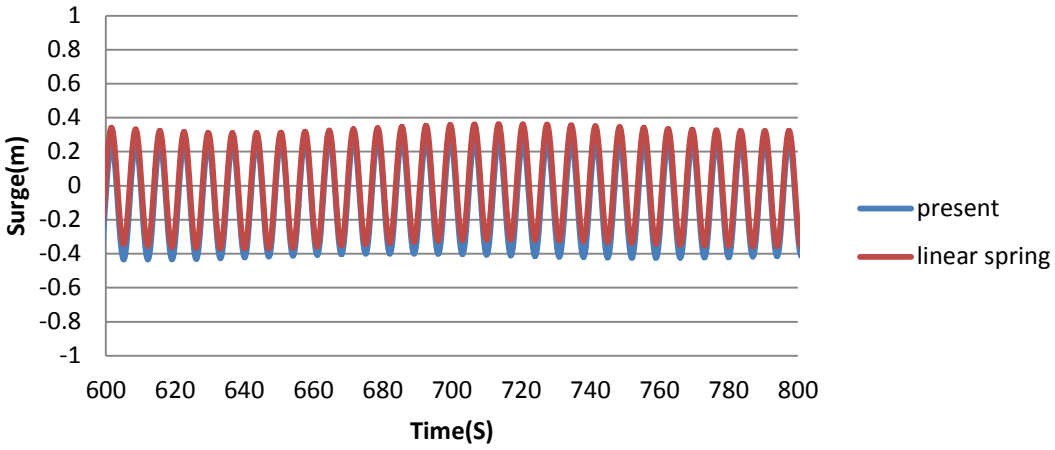

Figure 6.37 Surge time history, wave only condition T=7s

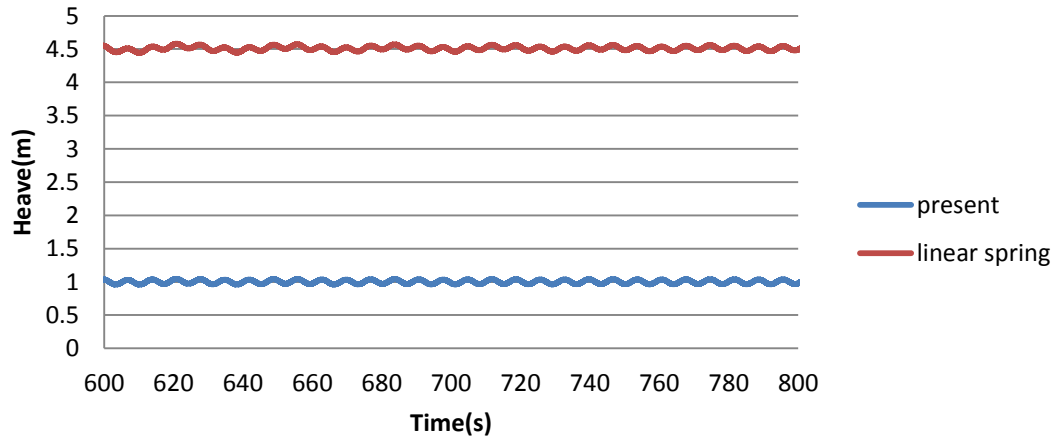

Figure 6.38 Heave time history, wave only condition T=7s

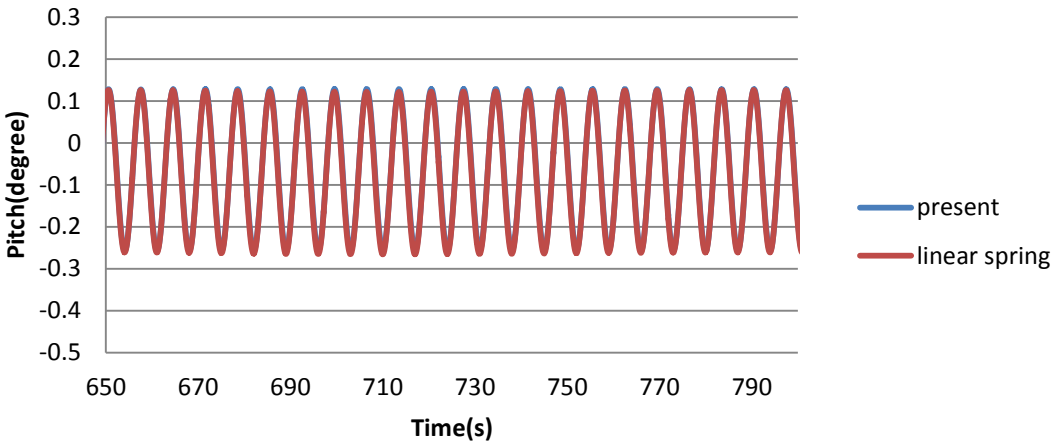

Figure 6.39 Pitch time history, wave only condition T=7s

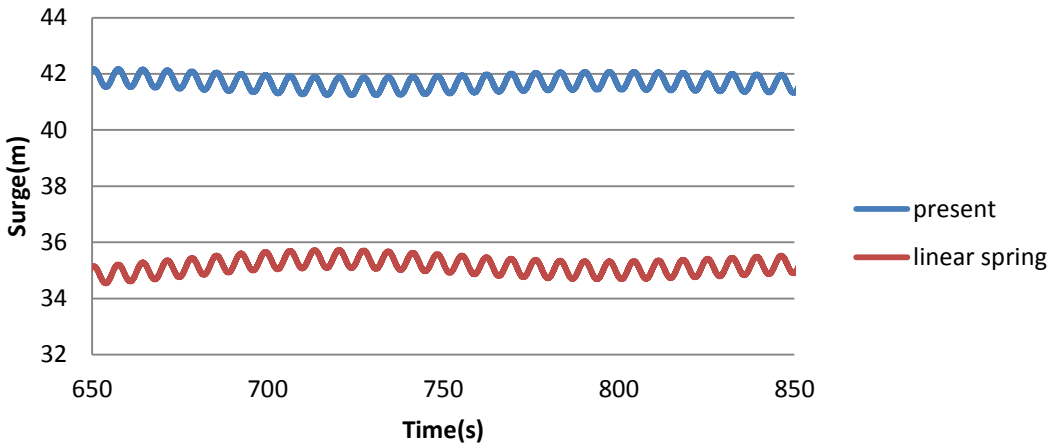

Figure 6.40 Surge time history, wave plus wind condition T=7s

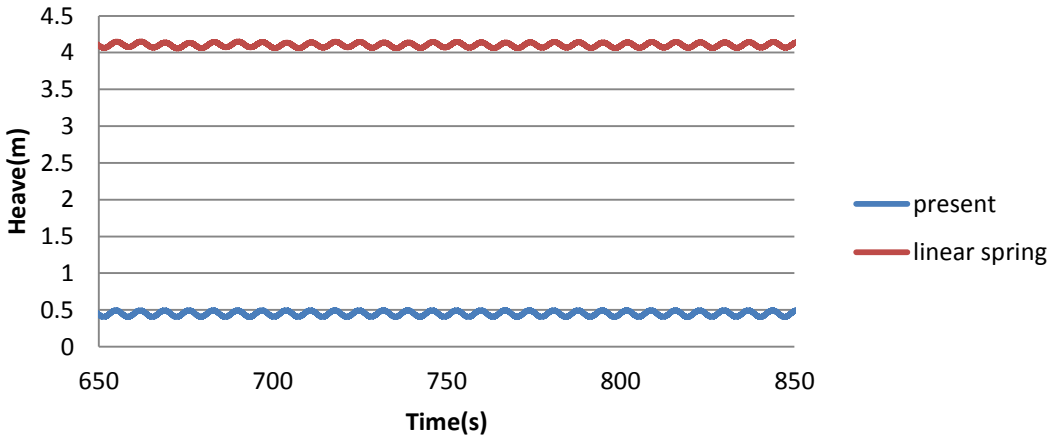

Figure 6.41 Heave time history, wave plus wind condition T=7s

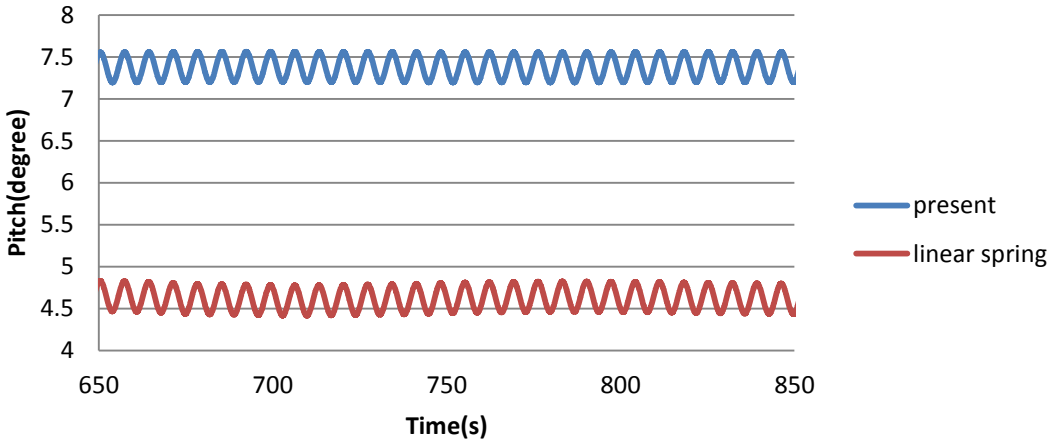

Figure 6.42 Pitch time history, wave plus wind condition T=7s

- **Turbine thrust force**

Figure 6.43 shows a comparison of mean rotor thrust force under linear spring method and present elastic rod theory. The mean thrust force is independent of wave frequency. Compared with present method, the linear spring method slightly underestimates the mean thrust force, but the difference is less than 1%.

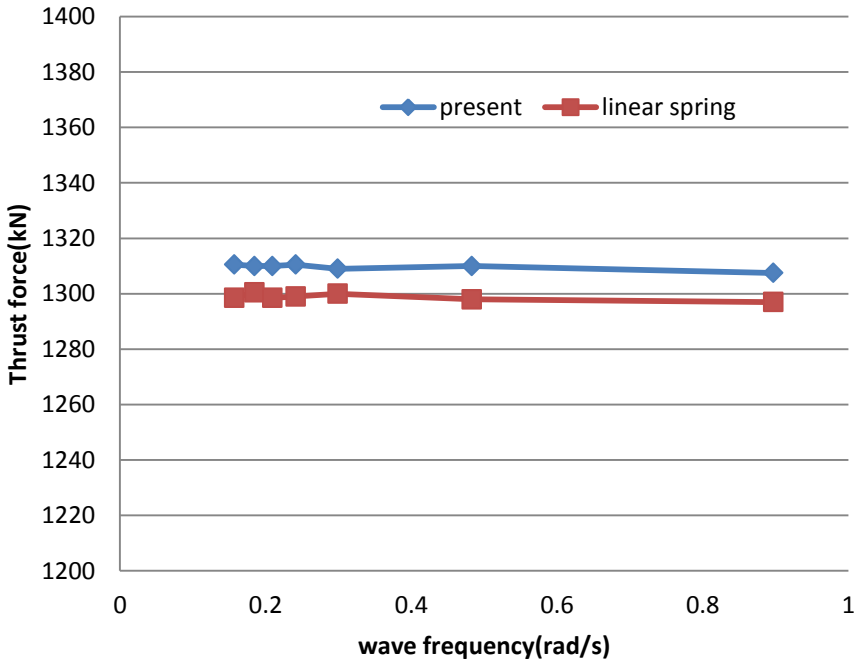

Figure 6.43 Comparison of turbine thrust force with different environmental conditions

- **Mooring line tension**

Figures 6.44 and 6.45 show the mooring line tension for both wave only and wave plus current condition. Under the wave only condition, the mooring line tension does not vary much; the floating body oscillates around its initial mean position. The reason for this phenomenon is because current modelling only included first-order wave forces. The second-order effects, as discussed in Chapter 5, are of little importance for the Spar-type wind turbine. In this chapter we mainly focused on the horizontal position of the floating body. For the wave plus wind condition, the FOWT moved to a new equilibrium position and oscillated around the new position, which results in one of the mooring lines becoming less taut. However, as discussed in previous section, the proposed method is suitable for modelling both slack and taut mooring lines.

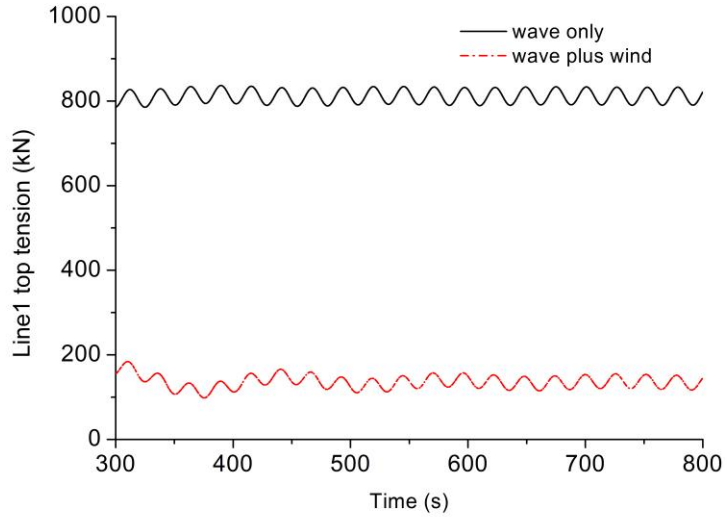

Figure 6.44 Comparison of mooring line tension (T=26s, Line1)

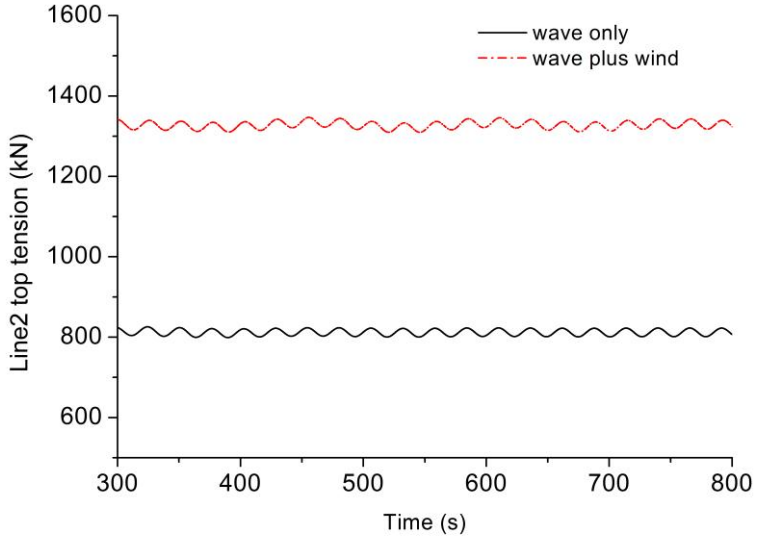

Figure 6.45 Comparison of mooring line tension (T=26s, Line2)

7. Discussion and further recommendation

7.1. General discussion

The fully coupled method has long been recognized as necessary, as least a check for some important loading cases in the design process. However, the running time is high. So for a balance between efficiency and accuracy, some simplified approaches have been proposed. For example, the coupled LF method- a hybrid method- simulates the WF response in frequency domain and LF response in time domain. The coupled LF method requires much less running time compared with the fully coupled method. For example, using a coarse mesh (30 segments for a 600m-long mooring line) the run time for a 3-hour simulation is about 20 minutes, while for the coupled LF method it is only 5 minutes.

This thesis has examined and quantified the accuracy of the coupled LF method by comparing with the fully coupled method, for a Spar platform. Low and Langley (2006) studied a spread-moored vessel in water depths of 2000m and 200m, showing that the fully coupled frequency domain method generated results as accurate as the fully coupled time domain method, provided the geometry nonlinearity is small. The geometry nonlinearity depends on the motion response, the length of mooring line/water depth and the time-dependency of the mooring line shape. When the geometric nonlinearity becomes less important, the hybrid method (simulating the WF motion response in the frequency domain and LF in the time domain) provides an accurate and efficient solution. The coupling effects between floating body WF response and mooring line are captured by a linearized mooring line drag model. The hybrid method is almost as accurate as the fully coupled time domain, but requires only one-tenth of the run time (Low and Langley, 2008).

However, in the present study for a Spar platform, the geometric nonlinearity is small, leading to a difference between the coupled LF method and fully coupled method, especially for the WF pitch motion. The difference in WF surge motion is less significant than pitch, as the total surge motion response is determined by LF response.

There are two coupling effects contribute to the difference. One is the coupling effect between the floating body and mooring line (type 1 coupling) in the WF range, as the WF response was calculated in the frequency domain without mooring line. The second is the effect between floating body WF, LF and mean position(type 2 coupling), as the interpolation of floating body WF motion response requires the instantaneous position of floating body LF response. The WF motion response is inertia dominated and it is often considered that the interaction between the floating body and mooring line is weak. However, as can be seen from the comparisons (see Figures 7.1 and 7.2, including only first-order force and motion), the discrepancy is due to the interaction between mooring line and WF motion. This phenomenon suggests that when the coupling effects are high, the coupled LF method fails to generate as accurate results as the fully coupled method, even for small geometry nonlinearity, unless the contributions from mooring lines in the WF range are accounted for.

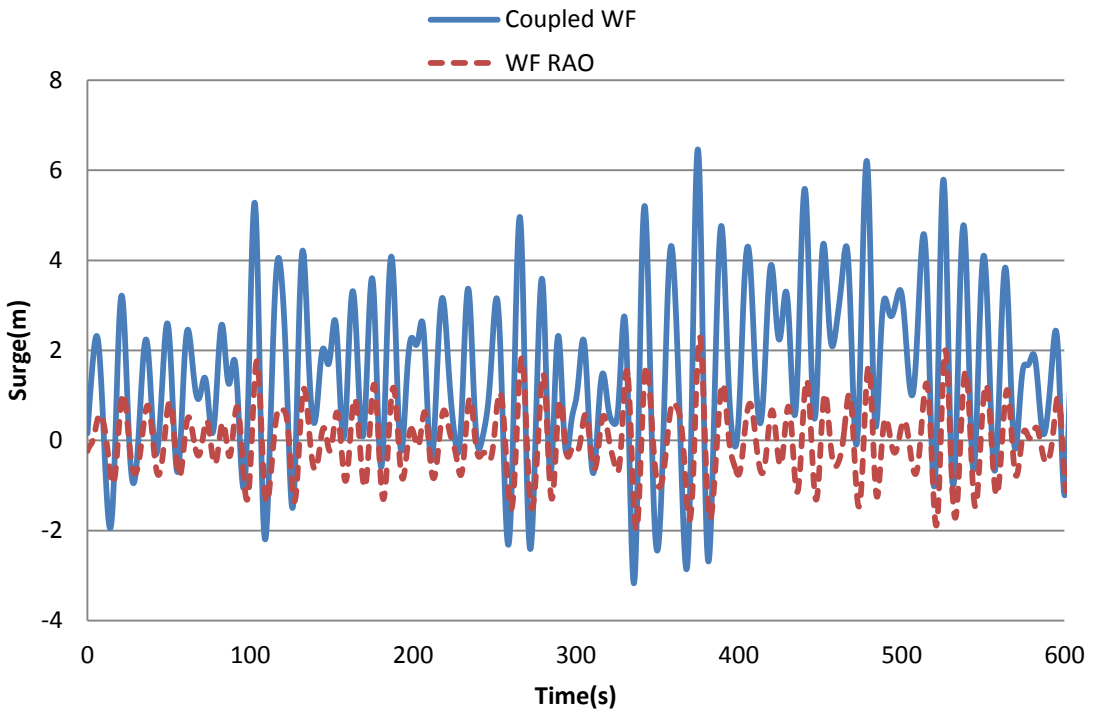

Figure 7.1 Comparison of surge motion, 318m

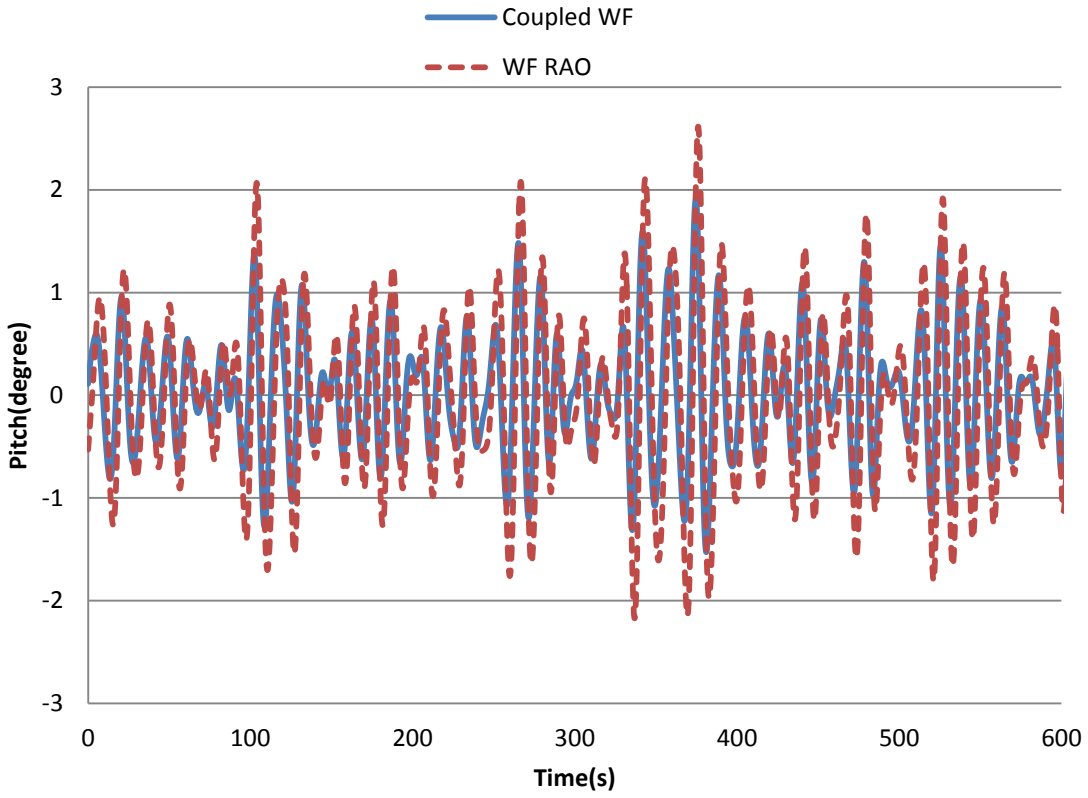

Figure 7.2 Comparison of pitch motion, 318m

The dynamic response of a catenary chain is important in deep water, as the mooring line becomes very long (Chen, 2001). In this thesis, the same results were found for the Spar platform. But for a non-slack mooring system with a multi-compound mooring line, the the WF response is significant in intermediate water depths (between 1000m and 2000m), becoming less important in ultra-deep depths (> 2000m). This is because for all water depths, the motion responses compared with the water depth/line length are small and the mooring system radius for a taut mooring line is smaller than the catenary line. Compared with a taut line, the changing of mooring line shape is more important for a catenary line (see Figures 3.1(a) and (b)), assuming the same floating body motion response. Previous researchers have not studied the effect of turbine thrust force on the dynamic response of mooring line and water depth variation is not precisely studied in the mooring system analysis of FOWT. Those studies mainly focused on the evaluation of platform motion response and the aerodynamic loading, ignoring or simplifying the mooring line modelling.

The modelling of an elastic line is complex and has not been well studied. Many attempts have been carried out on modelling of the nonlinear elongation of elastic line, but the modelling is complex and requires a large computational effort, due to the non-symmetrical tangent stiffness matrix. This thesis utilized an enhanced stiffness method to model the polyester line, focusing on the nonlinear stretch condition. The advantage of current method is the element tangent stiffness matrix remains symmetric.

7.2. Further recommendation

The present research has contributed to mooring system design with a particular focus on deep water and appropriate methods of analysis. Additionally, this research has studied the nonlinear dynamic response of polyester moorings. Based on these results, the following recommendations for future work are proposed:

- Current mooring line modelling focused the dynamic response of mooring line during intact condition and mooring line broken at time T=0, the steady state problem. It is necessary to study and modify the developed code to include the transit effect of mooring line broken during simulation.
- The effect of higher-order wave forces, which are very important for a TLP (e.g. springing and ringing phenomena).
- The present research has focused on linear incident wave, be it regular or irregular. It is necessary to study the response of a mooring system in non-linear incident waves, e.g. the set down and freak wave.

8. Conclusions

This research has focused on the analysis of deep water mooring configurations, which includes an investigation of the coupling effects between the floating body and mooring line, the coupling effects between the WF, LF and mean drift motion response and the nonlinear dynamic response of an elastic mooring line. The main contributions of the thesis can be grouped into 3 categories:

(1) For the Spar platform, three methods of analysis have been used (quasi-static, coupled LF, fully-coupled) for water depths between ~300m and 3000m. Statistical results from the fully coupled method are compared against available numerical and experimental results for validation purposes. The main results and recommendations from parametric studies indicate:

- The static method is recommended for evaluating the mean motion response - it has almost the same accuracy as the coupled LF method, but is less time consuming. The coupled LF method is also recommended for predicting the WF surge response - the total surge motion response is dominated by the LF response.
- The accuracy of the WF motion response predicted by the coupled LF method not only depends on the geometric nonlinearity, but also on the coupling effects- the coupling between WF, LF and mean drift motion response and the coupling between the floating body and mooring line in the WF range.
- For the maximum values of motion responses, a fully coupled analysis is strongly recommended.
- For the LF response of the mooring line, the coupled LF method is as accurate as the fully coupled method for the wave-only condition and for the wave-plus-current condition, regardless of the mooring line configuration.
- For a catenary chain, the WF response becomes more significant as the water depth increases (see Figs. 4.13.1~4.13.3). However, for a taut or semi-taut multi-compound mooring line, the WF response is significant in intermediate

water depths (between 1000m and 2000m), becoming less important in ultra-deep depths (> 2000m).

(2) For wind turbine mounted on a floating platform, this thesis has applied a fully coupled time-domain analysis for simulating the dynamic response of a spar-type FOWT moored with three catenary chains. Three water depths (320m, 600m and 900m) were selected as the basis of a parametric study. The main observations are:

- The drift force mainly affects the heave motion while its effect on pitch motion only appears under the shutdown condition.
- In previous study, an approximation was made by treating the turbine thrust force as an applied load on the tower. However, this approximation fails to predict the mean and maximum position of the floating body. So a coupled analysis, incorporating the dynamic turbine thrust force and motion response, is strongly recommended. A non-coupled analysis, treating the substructure and the upper structure separately, can be used for evaluating the heave motion in larger water depths, e.g. greater than 900m.
- In deep water, the (total) mooring line tension is significantly affected by the dynamic thrust force. The static thrust has little, if any, effect. However, with increasing water depth, the WF response dominates the mooring line tension, and the dynamic response of the mooring line cannot be neglected. With an increase in water depth, the dynamic thrust force increasingly affects the mooring line tension. The dynamic mooring line tension becomes more important for water depth greater than 600m, and so a fully coupled analysis is recommended.

(3) A new stiffness model has been applied for modelling the elastic line. Its accuracy has been tested numerically and the results show that the proposed model is suitable for modelling both slack and taut mooring lines. The wind turbine simulation tool FAST has been extended to allow for the simulation of a

FOWT with polyester mooring lines. The developed simulation tool has been applied to a taut-moored FOWT. Comparison was made between present developed method and the linear spring method. Although the behaviour of the mooring system's static load-offset graph was linear, the linear spring method, failed to consider the dynamics of mooring line, and under-predicted the motion response of floating body under wave plus wind condition. This under-prediction also affects maximum mooring line tension which is dependent on the instantaneous position of the floating body.

References

ABS, Global performance analysis for floating offshore wind turbine installations, February 2014

AGARWAL, A.K. and JAIN, A.K., 2003. Dynamic behavior of offshore spar platforms under regular sea waves. Ocean Engineering, 30(4), pp. 487-516.

API RP 2SK, Third Edition, October 2005. Design and analysis of stationkeeping systems for floating structures.

Aqwa Theory Manual, November 2013.ANSYS, Inc.

ARANHA, J.A.P., 1996. Second-order horizontal steady forces and moment on a floating body with small forward speed. Journal of Fluid Mechanics, 313, pp. 39-54.

ASTRUP, O.C., NESTEGÅRD, A., RONÆSS, M. and SØDAHL, N., 2001. Coupled analysis strategies for deepwater Spar platforms, Proceedings of the International Offshore and Polar Engineering Conference 2001, pp. 449-456.

BAI, W. and TENG, B., 2013. Simulation of second-order wave interaction with fixed and floating structures in time domain. Ocean Engineering, 74, pp. 168-177.

BARLTROP, N.D.P.,1998. Floating structures: a guide for design and analysis. Oilfield Publications Limited. Vol 2, pp.9-20

BARTON, Christopher M., 2014. Introduction to Deepwater Development. UH Petroleum Industry Expert Lecture Series, Petroleum Technology Program.

BATHE, K. J.,1996. Finite element procedures. Prentice Hall, Chapter 6.

ĆATIPOVIĆ, I., ČORIĆ, V. and RADANOVIĆ, J., 2011. An improved stiffness model for polyester mooring lines. Brodogradnja, 62(3), pp. 235-248.

CHARM3D USER'S MANUAL, OffshoreDynamics Inc. Address: 2207 Cypress Run Dr.SugarLand Houston, TX 77084, U.S.A.

CHEN, X., 2002. Studies on dynamic interaction between deep-water floating structures and mooring line/tendon systems. PhD, Texas A&M University.

CHEN, X., ZHANG, J. and MA, W., 2001. On dynamic coupling effects between a spar and its mooring lines. Ocean Engineering, 28(7), pp. 863-887.

CHUCHEEPSAKUL, S., SRINIL, N. and PETCHPEART, P., 2003. A variational approach for three-dimensional model of extensible marine cables with specified top tension. Applied Mathematical Modelling, 27(10), pp. 781-803.

CUMMINS,W.E.,1962. The impulse response function and ship motions. Schiffstechnik, 9, 101-109.

Deep Water- The next step for offshore wind energy, a report by the EWEA, July 2013.

DNV-OS-E301, Position mooring, October 2010.

DNV-RP-F205, Global performance analysis of deepwater floating structures, October 2010.

FALTINSEN, O.M., 1998. Sea loads on ships and offshore structures. Cambridge University Press,pp. 258-263.

FOLLEY, M., BABARIT, A., CHILD, B., FOREHAND, D., O'BOYLE, L., SILVERTHORNE, K., SPINNEKEN, J., STRATIGAKI, V. and TROCH, P., 2012. A review of numerical modelling of wave energy converter arrays, Proceedings of the International Conference on Offshore Mechanics and Arctic Engineering - OMAE 2012, pp. 535-546.

GARRETT C. J. R., 1971. Wave forces on a circular dock. Journal of Fluid Mechanics, 46, pp 129-139.

GARRETT, D.L., 1982. DYNAMIC ANALYSIS OF SLENDER RODS. J ENERGY RESOUR TECHNOL TRANS ASME, V 104(N 4), pp. 302-306.

GOODMAN, T.R. and BRESLIN, J.P., 1976. STATICS AND DYNAMICS OF ANCHORING CABLES IN WAVES. J Hydronaut, 10(4), pp. 113-120.

GOUPEE, A.J., KOO, B.J., KIMBALL, R.W., LAMBRAKOS, K.F. and DAGHER, H.J., 2014. Experimental comparison of three floating wind turbine concepts. Journal

of Offshore Mechanics and Arctic Engineering, 136(2),.

GUEDES SOARES, C., FONSECA, N. and PASCOAL, R., 2001. Experimental and Numerical Study of the Motions of a Turret Moored FPSO in Waves, Proceedings of the International Conference on Offshore Mechanics and Arctic Engineering - OMAE 2001, pp. 185-193.

ISAACSON, M. and KWOK FAI CHEUNG, 1992. Time-domain second-order wave diffraction in three dimensions. Journal of Waterway, Port, Coastal, & Ocean Engineering - ASCE, 118(5), pp. 496-516.

JONKMAN, J.M., 2007. Dynamics Modeling and Loads Analysis of an Offshore Floating Wind Turbine, Ph.D. Thesis, Department of Aerospace Engineering Sciences, University of Colorado, Boulder, CO, NREL/TP-500-41958, Golden, CO: National Renewable Energy Laboratory.

JONKMAN, J.M.; Buhl Jr., M. L., 2005. "FAST User's Guide," NREL/EL-500-29798. Golden, Colorado: National Renewable Energy Laboratory.

JONKMAN, J., 2010. Definition of the floating System for phase IV of OC3. NREL/TP-500-47535, Golden, CO: National Renewable Energy Laboratory.

JONKMAN, J.M., 2013. The new modularization framework for the FAST wind turbine CAE tool, *51st AIAA Aerospace Sciences Meeting including the New Horizons Forum and Aerospace Exposition*.

KARIMIRAD, M., 2013. Modeling aspects of a floating wind turbine for coupled wave-wind-induced dynamic analyses. Renewable Energy, 53, pp. 299-305.

KIM, B.W., SUNG, H.G., KIM, J.H. and HONG, S.Y., 2013. Comparison of linear spring and nonlinear FEM methods in dynamic coupled analysis of floating structure and mooring system. Journal of Fluids and Structures, 42, pp. 205-227.

KIM, J.W., KYOUNG, J.H. and SABLOK, A., 2010. Application of a viscoelastic model for polyester mooring, Proceedings of the International Conference on Offshore Mechanics and Arctic Engineering - OMAE 2010, pp. 19-29.

KIM, J.W., SABLOK, A., KYOUNG, J.H. and LAMBRAKOS, K., 2011. A

nonlinear viscoelastic model for polyester mooring line analysis, Proceedings of the International Conference on Offshore Mechanics and Arctic Engineering - OMAE 2011, pp. 797-803.

KIM, M.H., TAHAR, A. and KIM, Y.B., 2001a. Variability of spar motion analysis against design methodologies/parameters, Proceedings of the International Conference on Offshore Mechanics and Arctic Engineering - OMAE 2001, pp. 153-161.

KIM, M.H., TAHAR, A. and KIM, Y.B., 2001b. Variability of TLP motion analysis against various design methodologies/parameters, Proceedings of the International Offshore and Polar Engineering Conference 2001, pp. 467-473.

KIM, N.II., JEON, S.S. and KIM, M.Y., 2004. Nonlinear finite element analysis of ocean cables. China Ocean Engineering, 18(4), pp. 537-550.

KIM, S. and SCLAVOUNOS, P.D., 2001. Fully coupled response simulations of theme offshore structures in water depths of up to 10,000 feet, Proceedings of the International Offshore and Polar Engineering Conference 2001, pp. 457-466.

KREUZER, E. and WILKE, U., 2002. Mooring systems - A multibody dynamic approach. Multibody System Dynamics, 8(3), pp. 279-297.

KURIAN, V.J., YASSIR, M.A. and HARAHAP, I.S., 2010. Nonlinear coupled dynamic response of a semi-submersible platform, Proceedings of the International Offshore and Polar Engineering Conference 2010, pp. 492-499.

LEE, C.-H. and SCLAVOUNOS, P.D., 1989. Removing the irregular frequencies from integral equations in wave-body interactions. Journal of Fluid Mechanics, 207, pp. 393-418.

LEE, W.T., Bales, W. L., and Stowby, S. E., 1985. Standardized wind and wave environments for North Pacific Ocean areas. (Research Report, R/SPD-0919–02), David W. Taylor Naval Ship Research and Development Center, Washington, DC.

LEONARD, J.W. and NATH, J.H., 1981. Comparison of finite element and lumped parameter methods for oceanic cables. Engineering Structures, 3(3), pp. 153-167.

LIU, Y. and BERGDAHL, L., 1997. Influence of current and seabed friction on mooring cable response: Comparison between time-domain and frequency-domain analysis. Engineering Structures, 19(11), pp. 945-953.

LOVE, A.E.H.,2003. A treatise on the mathematical theory of elasticity. 4th Edition. Dover Publications New York .

LOW Y. M., 2006. Efficient methods for the dynamic analysis of deepwater offshore production systems. PhD, University of Cambridge.

LOW, Y.M. and LANGLEY, R.S., 2008. A hybrid time/frequency domain approach for efficient coupled analysis of vessel/mooring/riser dynamics. Ocean Engineering, 35(5-6), pp. 433-446.

LOW, Y.M. and LANGLEY, R.S., 2006. Time and frequency domain coupled analysis of deepwater floating production systems. Applied Ocean Research, 28(6), pp. 371-385.

LUO, Y. and BAUDIC, S., 2003. Predicting FPSO responses using model tests and numerical analysis, Proceedings of the International Offshore and Polar Engineering Conference 2003, pp. 167-174.

MA, W. & WEBSTER, W.C.,1994. An analytical approach to cable dynamics: theory and user manual. SEA GRANT PROJECT R/OE-26 Department of NAOE, UCB.

MACCAMY RC, FUCHS RA.,1954. Wave forces on piles: a diffraction theory. Tech. Memo No. 69, U.S. Army Corps of Engrs, Washington D.C, USA

MASCIOLA, M., ROBERTSON, A., JONKMAN, J., COULLING, A. and GOUPEE, A., 2013. Assessment of the importance of mooring dynamics on the global response of the DeepCwind floating semisubmersible offshore wind turbine, Proceedings of the International Offshore and Polar Engineering Conference 2013, pp. 359-368.

MEI, C.C., 1978. Numerical methods in water-wave diffraction and radiation. Annu Rev Fluid Mech, 10, pp. 393-416.

MERCIER, Rick. Technology Issues with Deepwater Wind Energy Systems. OTRC.

MCCAUL, James R. President Growing Requirement for Floating Production Systems (2006)

MOLIN, B., 1979. Second-order diffraction loads upon three-dimensional bodies. Applied Ocean Research, 1(4), pp. 197-202.

MORISON JR, O'Brien MR, Johnson JW, Schaaf SA.,1950. The forces exerted by surface waves on piles. Petroleum Transactions, AIME189, 149–154.

NAVA, V., RAJIC, M. and SOARES, C.G., 2013. Effects of the mooring line configuration on the dynamics of a point absorber, Proceedings of the International Conference on Offshore Mechanics and Arctic Engineering - OMAE 2013.

NEWMAN, J.N., 1974. SECOND-ORDER, SLOWLY-VARYING FORCES ON VESSELS IN IRREGULAR WAVES. , pp. APRIL 2-5, 1974.

NORDGREN, R.P., 1974. ON COMPUTATION OF THE MOTION OF ELASTIC RODS. Journal of Applied Mechanics, Transactions ASME, 41 Ser E(2), pp. 777-780.

NWTC Computer-Aided Engineering Tools (FAST by Jason Jonkman, Ph.D.). http://wind.nrel.gov/designcodes/simulators/fast/. Last modified 2-July-2014; accessed 1-September-2014.

NWTC Computer-Aided Engineering Tools (MAP by Marco D. Masciola, Ph.D.). http://wind.nrel.gov/designcodes/simulators/map/. Last modified 17-July-2014; accessed 31-August-2014.

NWTC Information Portal (HydroDyn). https://nwtc.nrel.gov/HydroDyn. Last modified 25-March-2015 ; Accessed 06-April-2015

OGILVIE T.F.,1983. Second-order hydrodynamic effects on ocean platforms.Proc. Int Workshop on Ship and Platform Motions, 205-265, Berkley.

OrcaFlex user manual Version 9.7a. Orcina Ltd. Daltongate, Ulverston Cumbria. LA12 7AJ, UK

ORMBERG, H. and LARSEN, K., 1998. Coupled analysis of floater motion and mooring dynamics for a turret-moored ship. Applied Ocean Research, 20(1-2), pp. 55-

67.

ORMBERG, H., SODAHL, N. and STEINKJER, O., 1998. Efficient analysis of mooring systems using de-coupled and coupled analysis, Proceedings of the International Conference on Offshore Mechanics and Arctic Engineering - OMAE 1998.

PAULING, J. R., WEBSTER, W.C.,1986. A consistent large amplitude analysis of the coupled response of a TLP and tendon system. Proceedings of the International Conference on Offshore Mechanics and Arctic Engineering OMAE Vol 3, p 126

QIAO, D., OU, J. and WU, F., 2012. Design selection analysis for mooring positioning system of deepwater semi-submersible platform, Proceedings of the International Offshore and Polar Engineering Conference 2012, pp. 1099-1106.

RAN, Z.,2000. Coupled dynamic analysis of floating structures in waves and currents, PhD, Texas A&M University

RENZI, E., ABDOLALI, A., BELLOTTI, G. and DIAS, F., 2014. Wave-power absorption from a finite array of oscillating wave surge converters. Renewable Energy, 63, pp. 55-68.

ROALD, L., JONKMAN, J., ROBERTSON, A. and CHOKANI, N., 2013. The effect of second-order hydrodynamics on floating offshore wind turbines, Energy Procedia 2013, pp. 253-264.

SANNASIRAJ, S.A., SUNDAR, V. and SUNDARAVADIVELU, R., 1998. Mooring forces and motion responses of pontoon-type floating breakwaters. Ocean Engineering, 25(1), pp. 27-48.

Sesam User Manual-DeepC Theory,June,2005. DNV.

Spar Model Test Joint Industry Project, Final Report, 1995, Deep Oil Technology, Inc. 2182 DuPont Drive, Irvine, CA 92715pp. 5-21.

TAHAR, A. and KIM, M.H., 2003. Hull/mooring/riser coupled dynamic analysis and sensitivity study of a tanker-based FPSO. Applied Ocean Research, 25(6), pp. 367-382.

TAHAR, A., 2001. Hull/mooring/riser coupled dynamic analysis of a deepwater floating platform with polyester mooring lines. PhD , Texas A&M University.

TAHAR, A. and SIDARTA, D., 2013. Dual stiffness approach for polyester mooring line analysis in time domain - Semisubmersible case, Proceedings of the International Conference on Offshore Mechanics and Arctic Engineering - OMAE 2013.

TAHAR, A., SIDARTA, D. and RAN, A., 2012. Dual stiffness approach for polyester mooring line analysis in time domain, Proceedings of the International Conference on Offshore Mechanics and Arctic Engineering - OMAE 2012, pp. 513-521

TAO, L., SONG, H. and CHAKRABARTI, S., 2009. Scaled boundary FEM model for interaction of short-crested waves with a concentric porous cylindrical structure. Journal of Waterway, Port, Coastal and Ocean Engineering, 135(5), pp. 200-212.

TJAVARAS, A.A., ZHU, Q., LIU, Y., TRIANTAFYLLOU, M.S. and YUE, D.K.P., 1998. The mechanics of highly-extensible cables. Journal of Sound and Vibration, 213(4), pp. 709-734.

VAN DEN BOOM, H.J.J., 1985. Dynamic behaviour of mooring lines. IN: BEHAVIOUR OF OFFSHORE STRUCTURES, PROC.4TH INT.CONF., BOSS '85, pp359-368.

WALTON, THOMAS S. & POLACHEK, HARRY, 1959. Calculation of nonlinear transient motion of cables. David Taylor Model Basin. Washington, D.C.

WAMIT User's manual, versions 7.0.,2013. Wamit Inc. and Department of Ocean Engineering, Massachusetts Institute of Technology, Cambridge, Mass., USA.

WEHMEYER,C and Rasmussen, J,H, Mooring Response of a Floating Offshore Wind Turbine in Nonlinear Irregular Waves, Journal of Ocean and Wind Energy, Vol. 2, No. 1, February 2015, pp. 37–44

WICHERS, J.E.W. and DEVLIN, P.V., 2001. Effect of coupling of mooring lines and risers on the design values for a turret moored FPSO in deep water of the Gulf of Mexico, Proceedings of the International Offshore and Polar Engineering Conference 2001, pp. 480-487.

YANG, M., TENG, B., NING, D. and SHI, Z., 2012. Coupled dynamic analysis for wave interaction with a truss spar and its mooring line/riser system in time domain. Ocean Engineering, 39, pp. 72-87.

Appendices

Appendix 1. Catenary Equation

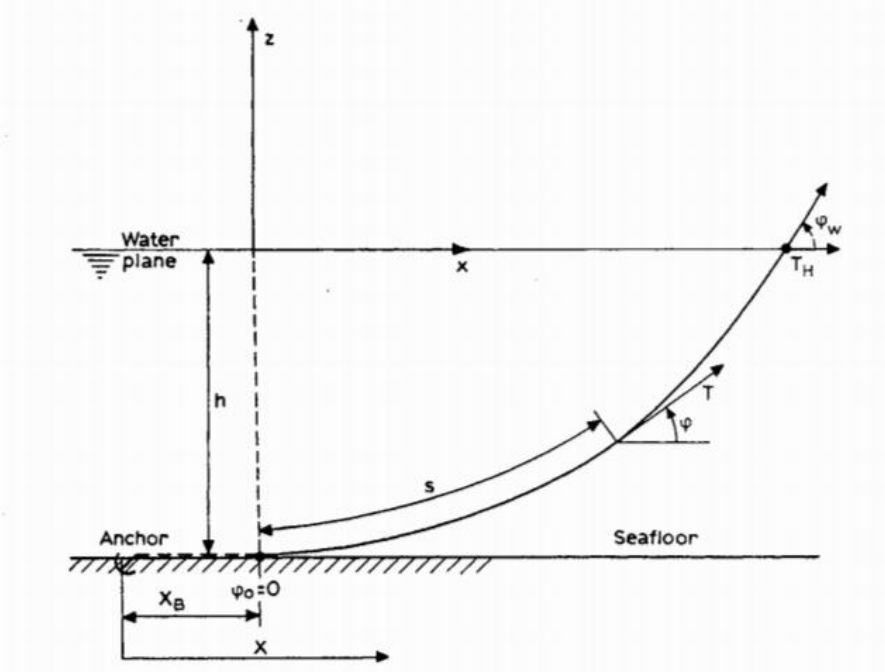

Figure 1.1 Cable line with symbols (Faltinsen, 1998)

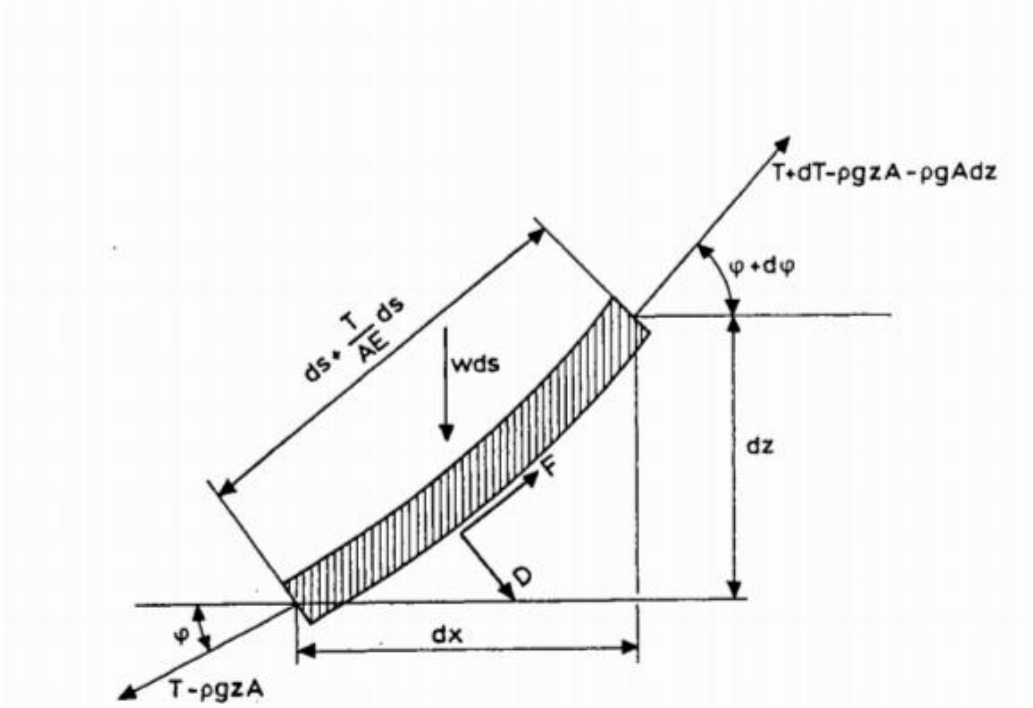

Figure 1.2 Force acting an element of an anchor line (Faltinsen, 1998)

The following derivations are from Faltinsen (1998).Considering a two-dimensional problem, as illustrated Figure 1.1, we will show the formulations of the catenary equation. The dynamic response of the line is ignored. Figure 1.2 shows the forces acting on a line element. In order to study the relationship between vessel offset and horizontal distance *X*, from Figure 1.2 we have

$$\begin{cases} dT - \rho g A dz = [w\sin\phi - F(1+\frac{T}{AE})]ds \\ Td\phi - \rho g A z d\phi = [w\cos\phi - D(1+\frac{T}{AE})]ds \end{cases} \tag{1.1}$$

w is mass per unit in water, without buoyancy force. But at both ends of the element, there is no buoyancy force. So we can write the correction of line tension

$$T' = T - \rho g z A \tag{1.2}$$

Ignoring the current force *F* and *D*, we have

$$\begin{cases} dT' = \omega\sin\phi ds \\ T'd\phi = \omega\cos\phi ds \end{cases} \tag{1.3}$$

By dividing the above two equations and integrating we can see that

$$T' = T_0'\frac{\cos\phi_0}{\cos\phi} \tag{1.4}$$

By integrating $T'd\phi = \omega\cos\phi$, we have

$$s - s_0 = \frac{1}{\omega}\int_{\phi_0}^{\phi}\frac{T_0'}{\cos\theta}\frac{\cos\phi_0}{\cos\theta}d\theta = \frac{T_0'\cos\phi_0}{\omega}(\tan\phi - \tan\phi_0) \tag{1.5}$$

Where s is un-stretched length of the line

To find the relationship between the angle Φ and x-, z-coordinates respectively, two types of relationship are given as follows:

$$\frac{dx}{ds} = \cos\phi, \frac{dz}{ds} = \sin\phi$$

So we can write

$$x - x_0 = \frac{1}{\omega}\int_{\phi_0}^{\phi} T_0' \frac{\cos\phi_0}{\cos\theta} d\theta = \frac{T_0' \cos\phi_0}{\omega}[\log(\frac{1}{\cos\phi} + \tan\phi) - \log(\frac{1}{\cos\phi_0} + \tan\phi_0)] \quad (1.6)$$

$$z - z_0 = \frac{1}{\omega}\int_{\phi_0}^{\phi} T_0' \frac{\cos\phi_0 \sin\theta}{\cos^2\theta} d\theta = \frac{T_0' \cos\phi_0}{\omega}(\frac{1}{\cos\phi} - \frac{1}{\cos\phi_0}) \quad (1.7)$$

By integrating from the touchdown to mean water plane, choosing the coordinate system $x_0 = 0$ $z_0 = -h$ and $s_0 = 0$, $\phi_0 = 0$ we have

$$T' = \frac{T_0'}{\cos\phi} \Rightarrow T_0' = T_H \quad (1.8)$$

$$s = \frac{T_H}{\omega}\tan\phi \quad (1.9)$$

$$x = \frac{T_H}{\omega}\log(\frac{1}{\cos\phi} + \tan\phi) \quad (1.10)$$

$$z + h = \frac{T_H}{\omega}\frac{1}{\cos\phi} \quad (1.11)$$

From (1.10) we have

$$\frac{x\omega}{T_H} = \log(\frac{1}{\cos\phi} + \tan\phi) \quad (1.12)$$

By introducing

$$y = \log(\frac{1}{\cos\phi} + \tan\phi) = \log(\frac{1+\sin\phi}{\cos\phi})$$
$$\sinh y = \frac{e^{y} - e^{-y}}{2} = \frac{1}{2}(\frac{1+\sin\phi}{\cos\phi} - \frac{\cos\phi}{1+\sin\phi}) = \tan\phi \quad (1.13)$$
$$\cosh y = \frac{e^{y} + e^{-y}}{2} = \frac{1}{2}(\frac{1+\sin\phi}{\cos\phi} + \frac{\cos\phi}{1+\sin\phi}) = \frac{1}{\cos\phi}$$

$$\text{i.e.} \quad \begin{matrix} \sinh\frac{x\omega}{T_H} = \tan\phi \\ \cosh\frac{x\omega}{T_H} = \frac{1}{\cos\phi} \end{matrix} \quad (1.14)$$

So we can write

$$s = \frac{T_H}{\omega}\sinh\frac{x\omega}{T_H} \quad (1.15)$$

$$z + h = \frac{T_H}{\omega}[\cosh(\frac{\omega x}{T_H}) - 1] \quad (1.16)$$

From (1.2) we can write the line tension

$$T = T' + \rho zA = \frac{T_H}{\cos\phi} + \rho zAz \quad (1.17)$$

Since, $z + h = \frac{T_H}{\omega}(\frac{1}{\cos\phi} - 1)$ i.e. $\frac{1}{\cos\phi} = \frac{\omega(z+h)}{T_H} + 1$, we can write the line tension

$$T = T_H + \omega(z+h) + \rho zAz \quad (1.18)$$

Vertical line tension

$$T_z = T\sin\phi = \frac{T_H}{\cos\phi}\sin\phi = T_H\tan\phi = T_H\frac{\omega s}{T_H} = \omega s \quad (1.19)$$

Applying (1.15), (1.16) and (1.18) to the top end of the line, we can write the relationship between minimum line length, maximum line tension, water depth and x-coordinate

$$T_{\max} = T_H + \omega h \tag{1.20}$$

$$l_s = a \sinh \frac{x}{a}, a = \frac{T_H}{\omega} \tag{1.21}$$

$$h = a[\cosh(\frac{x}{a}) - 1], a = \frac{T_H}{\omega} \tag{1.22}$$

So we can write the horizontal distance X

$$\begin{aligned} X &= l - l_s + x \\ &= l - h\sqrt{1 + 2\frac{a}{h}} + a \cosh^{-1}(1 + \frac{h}{a}) \end{aligned} \tag{1.23}$$

Appendix 2. 3-D Wave-rigid body interaction using boundary element method

Using Green's theorem, the diffraction potential φ_d and radiation $\varphi_j\ (j=1\sim 6)$ potential satisfy the following integral equations, respectively

$$\begin{aligned} &2\pi\varphi_j(X)+\iint_{s_b}\frac{\partial G(\xi,X)}{\partial n_\xi}\varphi_j(\xi)d\xi \\ &=\iint_{s_b} n_j G(\xi,X)d\xi \end{aligned} \quad \text{for radiation potential} \tag{2.1}$$

$$\begin{aligned} &2\pi\varphi_s(X)+\iint_{s_b}\frac{\partial G(\xi,X)}{\partial n_\xi}\varphi_s(\xi)d\xi \\ &=-\iint_{s_b}\frac{\partial\varphi_0(\xi)}{\partial n}G(\xi,X)d\xi \end{aligned} \quad \text{for diffraction potential} \tag{2.2}$$

The free surface Green function applied here for infinite water depth is

$$G(\xi,X)=\frac{1}{r}+\frac{1}{r'}+\frac{2K}{\pi}\int_0^\infty dk\,\frac{e^{k(z+\zeta)}}{k-K}J_0(kR) \tag{2.3}$$

$$r^2=(x-x_o)\xi^2+(y-\eta)^2+(z-\zeta)^2 \tag{2.4}$$

$$r'^2=(x-x_o)\xi^2+(y-\eta)^2+(z+\zeta)^2 \tag{2.5}$$

where $J_0(x)$ is the zero order Bessel function

The free surface green function applied here for finite water depth is

$$G(X,\xi)=\frac{1}{r}+\frac{1}{r''}+2\int_0^\infty dk\,\frac{(K+k)\cosh k(z+H)\cosh k(\zeta+H)}{k\sinh kH-K\cosh kH}e^{-kH}J_0(kR) \tag{2.6}$$

$$(r'')^2=(x-\xi)\xi^2+(y-\eta)^2+(z+\zeta+2H)^2 \tag{2.7}$$

Appendix 3. Discretization of the integral equations with the higher-order method

In the higher-order method, body surface is first divided into patches with smooth continuous surfaces. On each patch, the velocity potential is represented by a B-spline basis functions $U(u)$ and $V(v)$. By applying the discretization described above, the integral equation has the following form

$$\begin{aligned} &2\pi\sum_{m=1}^{M_v}\sum_{l=1}^{M_u}(\phi_j)_k U_k(u_f)+\sum_{n=1}^{N_P}\iint du\sum_{m=1}^{M_v}\sum_{l=1}^{M_u}(\phi_j)_k U_k(u)\frac{\partial G\left(u,u_f\right)}{\partial n(u)}J(u) \\ &=\sum_{n=1}^{N_P}\iint du\frac{\partial \phi_j}{\partial n}(u)G\left(u,u_f\right)J(u) \end{aligned} \tag{3.1}$$

where

$$U_k = U_l(U)V_m(v) \tag{3.2}$$

$$\iint du = \int_{-1}^{1} dv \int_{-1}^{1} du \tag{3.3}$$

Reference of appendices

FALTINSEN, O.M., 1998. Sea loads on ships and offshore structures. Cambridge University Press,pp. 258-263.

WAMIT User's manual, versions 7.0.,2013. Wamit Inc. and Department of Ocean Engineering, Massachusetts Institute of Technology, Cambridge, Mass., USA.

LEE, C.H.,1995. WAMIT Theory Manual, MIT Report 95-2, Dept. Of Ocean Eng., MIT.